

Contents lists available at ScienceDirect

# Journal of Computational Physics

www.elsevier.com/locate/jcp



# New 25-point stencils with optimal accuracy for 2-D heat transfer problems. Comparison with the quadratic isogeometric elements



A. Idesman\*, B. Dev

Department of Mechanical Engineering, Texas Tech University, Lubbock, TX 79409-1021, USA

#### ARTICLE INFO

# Article history: Received 29 October 2019 Received in revised form 31 May 2020 Accepted 3 June 2020 Available online 9 June 2020

Keywords:
Heat equation
Poisson equation
High-order isogeometric elements
Local truncation error
Increase in the order of accuracy

#### ABSTRACT

A new approach for the increase in the order of accuracy of high order elements used for the time dependent heat equation and for the time independent Poisson equation has been suggested on uniform square and rectangular meshes. It is based on the optimization of the coefficients of the corresponding discrete stencil equation with respect to the local truncation error. By a simple modification of the coefficients of 25-point stencils, the new approach exceeds the accuracy of the quadratic isogeometric elements by four orders for the heat equation and by twelve orders for the Poisson equation. Despite the significant increase in accuracy, the computational costs of the new technique are the same as those for the conventional quadratic isogeometric elements on a given mesh. The numerical examples are in a good agreement with the theoretical results for the new approach and also show that the new approach is much more accurate than the conventional isogeometric elements at the same number of degrees of freedom. Hybrid methods that combine the new stencils with the conventional isogeometric and finite elements and can be applied to irregular domains are also presented.

© 2020 Elsevier Inc. All rights reserved.

#### 1. Introduction

In this paper we will show that the accuracy of high-order numerical techniques for the heat and Poisson equations used in many applications (computational physics, computational mechanics and others; e.g. see [1–4] and many others) can be significantly improved compared to the known numerical approaches. For many problems, high-order finite element techniques have advantages compared to the linear finite elements due to a higher order of accuracy of these techniques; e.g., see [5–7] and others. However, the conventional derivation of the discrete equations for finite element techniques (e.g., based on the Galerkin approaches) does not lead to the optimal accuracy of the discrete equations. This is known for many years for the linear finite elements applied to the wave equation for which different techniques have been developed for the increase in accuracy of the discrete equations; e.g., see [8–15] and many others. Their extension to high-order elements is not straightforward. For example, the dispersion reduction technique for the high-order finite elements have been suggested in [16] for acoustic waves. This technique is based on the calculation of the mass matrix **M** in Eq. (3) as a weighted average of the consistent and lumped mass matrices for the high-order finite elements. It was also shown in [16] that the same results can be obtained with the modified integration rule for the mass matrix. With this technique, the dispersion error

<sup>\*</sup> Corresponding author.

E-mail address: alexander.idesman@ttu.edu (A. Idesman).

is improved from the order 2p to the order 2p + 2 (p is the order of polynomial approximations). However, even for the quadratic elements, the modified stencil equation derived in [16] in the 1-D case is based on the replacement of the midside degree of freedom by the degrees of freedom related to the nodes located at the ends of the element (it seems that such a replacement is impossible in the 2-D or 3-D cases due to the belonging of the same mid-side degree of freedom to different elements).

The modification of the non-diagonal mass matrix in [17,18] for the high-order isogeometric elements allows the increase in the order of the dispersion error from the order 2p to the order 2p + 2 in the 1-D case and for one specific direction of harmonic waves in the 2-D case (however, this technique does not improve the order of the dispersion error in the general 2-D case). The issues with the application of such a technique to a general multidimensional case has been resolved in the latest papers [19-22].

Recently, we have improved the accuracy of high-order isogeometric elements from the order 2p to the order 4p for the scalar wave equation in the general multidimensional case; see [23,24]. This increase in the order of accuracy is much higher than that in the above-mentioned papers [16–20]. In contrast to the high-order finite and spectral elements, the stencil equation for the isogeometric elements on uniform meshes is the same for all internal degrees of freedom (for the high-order finite and spectral elements there are several stencil equations with different structures depending on the location of nodes). This simplifies the analysis of the numerical dispersion error for the isogeometric elements. The improvement of accuracy in [23,24] is based on the optimization of the order of the numerical dispersion error and on the existence of the exact harmonic solutions to the wave equation with zero loading function for an infinite domain. This approach cannot be applied to the heat equation due to the absence of exact harmonic solutions to the heat equation even with zero heat source. However, using the local truncation error, we are able to significantly increase the accuracy of the high-order isogeometric elements from the order 2p to the order 4p for the time dependent heat equation and even to a much higher order of accuracy for the isogeometric elements applied to the time-independent Poisson equation.

In our recent papers [25,26] we have shown that the local truncation error can be used for the increase in accuracy of the linear finite elements for the heat and Poisson equation as well as of the high-order isogeometric elements for the wave and heat equations. In contrast to the new linear elements in [25], the new stencils developed in this paper yield a much higher order of accuracy (much greater than the difference in the orders of accuracy between the conventional linear and quadratic finite elements). The improvement of accuracy of the global system of the semidiscrete equations for the high-order elements applied to the time-dependent heat and wave equations with zero right-hand side has been shortly considered in our paper [26] with the help of the local truncation error. The determination of the elemental matrices for the isogeometric elements has not been considered in [26]. In this paper we show how to calculate the elemental matrices for the new technique as well as we extend the new approach to the heat equation with non-zero heat source (i.e., to a new class of problems). Moreover, in contrast to [26], we have also developed new stencils for the time independent Poisson equation with zero and non-zero heat source. We should mention that for the Poisson equation, the accuracy of the quadratic isogeometric elements is improved by twelve orders (from the sixth order for the conventional elements to the eighteenth order for the new stencils). The accuracy of the new 25-point stencils are also twelve orders higher compared to the 9-point stencils of the new linear finite elements developed in [25]. We have never seen such a huge increase in the order of accuracy without additional computational costs.

Heat transfer in an isotropic homogeneous medium is described by the heat equation in domain  $\Omega$ :

$$\frac{\partial u}{\partial t} - a\nabla^2 u = f \tag{1}$$

for transient problems and by the Poisson equation:

$$\nabla^2 u = f \tag{2}$$

for steady-state problems with the boundary conditions  $\mathbf{n} \cdot \nabla u = g_1$  on  $\Gamma^t$  and  $u = g_2$  on  $\Gamma^u$ , and the initial conditions  $u(\mathbf{x},t=0)=g_3$  in  $\Omega$  (the initial conditions are given for the transient problems only). Here, u is the temperature, f is a given heat source that may depend on the space coordinates and time for the transient problems and on the space coordinates for the Poisson equation,  $\nabla^2$  is the Laplace operator ( $\nabla^2 u = \frac{\partial^2 u}{\partial x^2} + \frac{\partial^2 u}{\partial y^2}$  in the 2-D case), a is the thermal diffusivity (e.g., for homogeneous isotropic materials  $a = k/(c\rho)$ , where k is the conductivity coefficient,  $\rho$  is the density and c is the capacitance), t is the time,  $\Gamma^t$  and  $\Gamma^u$  denote the natural and essential boundaries,  $g_i$  (i = 1, 2, 3) are the given functions,  $\mathbf{n}$  is the outward unit normal on  $\Gamma^t$ . Other boundary conditions (e.g., convective heat exchange or radiation heat exchange and others) can be also formulated. The application of the continuous Galerkin approach and the space discretization (e.g., the finite elements, spectral elements, isogeometric elements; see [6,27,28] and others) to Eqs. (1) and (2) leads to a system of ordinary differential equations in time for transient problems:

$$\mathbf{M}\,\dot{\mathbf{U}} + a\,\mathbf{K}\,\mathbf{U} = \mathbf{R} \tag{3}$$

and to a system of algebraic equations for steady-state problems:

$$KU = R \tag{4}$$

with

$$\mathbf{M} = \sum_{e} \mathbf{M}^{e}, \qquad \mathbf{K} = \sum_{e} \mathbf{K}^{e}, \tag{5}$$

where U(t) is the vector of the nodal temperatures, R is the right-hand side vector, the global M and K matrices have a banded structure and are obtained by the summation of the corresponding local (element  $\Omega^e$ ) matrices  $M^e$  and  $K^e$ :

$$\mathbf{M}^{e} = \int_{\Omega^{e}} \mathbf{N}^{T} \mathbf{N} d\Omega^{e} , \qquad \mathbf{K}^{e} = \int_{\Omega^{e}} \mathbf{B}^{T} \mathbf{B} d\Omega^{e} . \tag{6}$$

Here, N and  $B = \frac{\partial N}{\partial x}$  are the shape matrix and its derivative with respect to the physical coordinate x; see [6,7,29]. In Section 2.1 we consider the improvement of the order of the local truncation error by the optimization of the coefficients of the 25-point stencil equation for the quadratic isogeometric elements applied to the time dependent heat equation with zero heat source in the 2-D case. In Section 2.2 we extend these results to the 2-D time independent Poisson equation. The numerical examples showing the accuracy and the convergence rate of the conventional quadratic isogeometric elements and the new 25-point stencils are presented in Section 3. Currently, the new high-order technique has been developed for uniform square and rectangular meshes. However, in Section 3.3 we show that this technique can be easily combined with the conventional isogeometric or finite elements and form a hybrid method. The hybrid method can be easily applied to irregular domains. In Appendix B we extend the results to non-zero heat source. The computational program "Mathematica" has been used for the derivation of many analytical expressions. Some long formulas from the paper (see Eqs. (21), (40), (46), (B.4) and (B.5) below) are also given as a Mathematica file in Appendix H.

#### 2. Local truncation error in space for discretized equations

In the analysis of the local truncation error considered below, the stencil equation of the discretized global system of equations, Eq. (3), for transient problems can be written as

$$h^2 m_i \dot{u}_i^{num} + ak_j u_j^{num} - \bar{f} = 0. \tag{7}$$

Here,  $u_j^{num}$  and  $\dot{u}_i^{num}$  are the nodal values of function u and its first time derivative in the numerical solution,  $\bar{f}$  is calculated with the help of the heat source (e.g., see Appendix B), coefficients  $m_i$  and  $k_j$  for the conventional isogeometric elements are calculated with the help of Eqs. (3) - (6), h is the element size (e.g., along the x-axis); the summation over the repeated indexes is assumed in Eq. (7). The examples of the coefficients  $m_i$  and  $k_j$  can be found below in the following sections. The substitution of the exact solution of the heat equation, Eq. (1), for function  $u_i$  and its first time derivative  $\dot{u}_i$  at nodes into Eq. (7) will lead to the residual of this equation called the local truncation error e of the semidiscrete equation (7):

$$e = h^2 m_i \dot{u}_i + a k_i u_j - \bar{f} . \tag{8}$$

Calculating the difference between Eqs. (8) and (7) we can get

$$e = h^2 m_i [\dot{u}_i - \dot{u}_i^{num}] + a k_j [u_j - u_j^{num}] = h^2 m_i \bar{e}_i^{\nu} + a k_j \bar{e}_j,$$
(9)

where  $\bar{e}_j = u_j - u_i^{num}$  and  $\bar{e}_i^v = \dot{u}_i - \dot{u}_i^{num}$  are the errors of function u and its first time derivative at nodes j and i. As can be seen from Eq. (9), the local truncation error e is a linear combination of the errors in the function u and its first time derivative at nodes i which are included into the stencil equation. The local truncation error e for Eq. (4) can be obtained from Eqs. (7)-(9) with  $m_i = 0$  and a = 1. The derivations in Section 2 are based on zero heat source  $f(\mathbf{x}, t) = \overline{f} = 0$ . The extension to non-zero heat source is considered in Appendix B.

# 2.1. Transient problems with zero heat source ( $f(\mathbf{x}, t) = \bar{f} = 0$ )

The calculation of the conventional  $M^e$  and  $K^e$  matrices of the isogeometric elements is based on the univariate B-spline basis functions; see [27,30]. In the 1-D case they are defined recursively starting with p=0

$$N_{i,p}(\xi) = \begin{cases} 1, & \text{if } \xi_i \le \xi < \xi_{i+1}. \\ 0, & \text{otherwise.} \end{cases}$$
 (10)

For p > 1:

$$N_{i,p}(\xi) = \frac{\xi - \xi_i}{\xi_{i+p} - \xi_i} N_{i,p-1}(\xi) + \frac{\xi_{i+p+1} - \xi}{\xi_{i+p+1} - \xi_{i+1}} N_{i+1,p-1}(\xi),$$
(11)

where a knot vector  $\{\xi_1 = 0, ..., \xi_i, ..., \xi_{n+p+1} = 1\}$  is a set of non-decreasing real numbers representing coordinates in the parametric space of the curve, p is the order of the B-spline, n is the number of the basis functions, i = 1, 2, ..., n + p + 1. In the 2-D case the basis functions can be constructed with the help of the tensor product as follows:

$$M_{ii}^{pq}(\xi,\eta) = N_{i,p}(\xi) N_{j,q}(\eta) , \qquad (12)$$

where  $N_{i,p}(\xi)$  and  $N_{j,q}(\eta)$  are the basis functions of order p and q given by Eq. (11). Below the 2-D basis functions of the same order in the  $\xi$  and  $\eta$  directions (p = q) are used.

The  $M^e$  and  $K^e$  matrices of a typical interior rectangular quadratic isogeometric element in Eq. (6) are (see also [17]):

$$\boldsymbol{M}^{e} = \frac{b_{y}h^{2}}{14400} \begin{pmatrix} 36 & 78 & 6 & 78 & 169 & 13 & 6 & 13 & 1 \\ 78 & 324 & 78 & 169 & 702 & 169 & 13 & 54 & 13 \\ 6 & 78 & 36 & 13 & 169 & 78 & 1 & 13 & 6 \\ 78 & 169 & 13 & 324 & 702 & 54 & 78 & 169 & 13 \\ 169 & 702 & 169 & 702 & 2916 & 702 & 169 & 702 & 169 \\ 13 & 169 & 78 & 54 & 702 & 324 & 13 & 169 & 78 \\ 6 & 13 & 1 & 78 & 169 & 13 & 36 & 78 & 6 \\ 13 & 54 & 13 & 169 & 702 & 169 & 78 & 324 & 78 \\ 1 & 13 & 6 & 13 & 169 & 78 & 6 & 78 & 36 \end{pmatrix},$$

$$(13)$$

$$\boldsymbol{K}^{e} = \frac{1}{720by} \begin{bmatrix} 12\left(b_{y}^{2}+1\right) & 26-6b_{y}^{2} & 2-6b_{y}^{2} & 26b_{y}^{2}-6 & -13\left(b_{y}^{2}+1\right) & -13b_{y}^{2}-1 & 2\left(b_{y}^{2}-3\right) & -b_{y}^{2}-13 & -b_{y}^{2}-1 \\ 26-6b_{y}^{2} & 12\left(b_{y}^{2}+9\right) & 26-6b_{y}^{2} & -13\left(b_{y}^{2}+1\right) & 26b_{y}^{2}-54 & -13\left(b_{y}^{2}+1\right) & -b_{y}^{2}-13 & 2\left(b_{y}^{2}-27\right) & -b_{y}^{2}-13 \\ 2-6b_{y}^{2} & 26-6b_{y}^{2} & 12\left(b_{y}^{2}+1\right) & -13b_{y}^{2}-1 & -13\left(b_{y}^{2}+1\right) & 26b_{y}^{2}-6 & -b_{y}^{2}-1 & -b_{y}^{2}-13 & 2\left(b_{y}^{2}-27\right) & -b_{y}^{2}-13 \\ 26b_{y}^{2}-6 & -13\left(b_{y}^{2}+1\right) & -13b_{y}^{2}-1 & 12\left(9b_{y}^{2}+1\right) & 26-54b_{y}^{2} & 26-54b_{y}^{2} & 26b_{y}^{2}-6 & -13\left(b_{y}^{2}+1\right) & -13b_{y}^{2}-1 \\ -13\left(b_{y}^{2}+1\right) & 26b_{y}^{2}-54 & -13\left(b_{y}^{2}+1\right) & 26-54b_{y}^{2} & 108\left(b_{y}^{2}+1\right) & 26-54b_{y}^{2} & -13\left(b_{y}^{2}+1\right) & 26b_{y}^{2}-54 & -13\left(b_{y}^{2}+1\right) \\ -13b_{y}^{2}-1 & -13\left(b_{y}^{2}+1\right) & 26b_{y}^{2}-6 & 2-54b_{y}^{2} & 26-54b_{y}^{2} & 12\left(9b_{y}^{2}+1\right) & -13b_{y}^{2}-1 & -13\left(b_{y}^{2}+1\right) & 26b_{y}^{2}-6 \\ 2\left(b_{y}^{2}-3\right) & -b_{y}^{2}-13 & -b_{y}^{2}-1 & 26b_{y}^{2}-6 & -13\left(b_{y}^{2}+1\right) & -13b_{y}^{2}-1 & 12\left(b_{y}^{2}+1\right) & 26-6b_{y}^{2} & 2-6b_{y}^{2} \\ -b_{y}^{2}-13 & 2\left(b_{y}^{2}-27\right) & -b_{y}^{2}-13 & -13\left(b_{y}^{2}+1\right) & 26b_{y}^{2}-54 & -13\left(b_{y}^{2}+1\right) & 26-6b_{y}^{2} & 26-6b_{y}^{2} \\ -b_{y}^{2}-1 & -b_{y}^{2}-13 & 2\left(b_{y}^{2}-3\right) & -13b_{y}^{2}-1 & -13\left(b_{y}^{2}+1\right) & 26b_{y}^{2}-6 & 2-6b_{y}^{2} \\ -b_{y}^{2}-1 & -b_{y}^{2}-13 & 2\left(b_{y}^{2}-3\right) & -13b_{y}^{2}-1 & -13\left(b_{y}^{2}+1\right) & 26b_{y}^{2}-6 & 2-6b_{y}^{2} \\ -b_{y}^{2}-1 & -b_{y}^{2}-13 & 2\left(b_{y}^{2}-3\right) & -13b_{y}^{2}-1 & -13\left(b_{y}^{2}+1\right) & 26b_{y}^{2}-6 \\ -b_{y}^{2}-1 & -b_{y}^{2}-13 & 2\left(b_{y}^{2}-3\right) & -13b_{y}^{2}-1 & -13\left(b_{y}^{2}+1\right) & 26b_{y}^{2}-6 \\ -b_{y}^{2}-1 & -b_{y}^{2}-13 & 2\left(b_{y}^{2}-3\right) & -13b_{y}^{2}-1 & -13\left(b_{y}^{2}+1\right) & 26b_{y}^{2}-6 & 2-6b_{y}^{2} & 26-6b_{y}^{2} \\ -b_{y}^{2}-1 & -b_{y}^{2}-13 & 2\left(b_{y}^{2}-3\right) & -13b_{y}^{2}-1 & -13\left(b_{y}^{2}+1\right) & 26b_{y}^{2}-6 & 2-6b_{y}^{2} & 26-6b_{y}^{2} & 26-6b_{y}^{2} \\$$

where the sequence of uniformly spaced control points in the x and y directions with  $x_A = hA$  and  $y_B = b_y hB$  is used.

Considering the discretized heat equation (Eq. (3)) on an infinite plane with the sequence of uniformly spaced control points in the x and y directions, the 25-point stencil equation for the degree of freedom  $u_{A,B}$  can be calculated with the help of Eqs. (3), (5), (13) and (14) for  $3 \times 3 = 9$  neighboring elements. It includes 25 degrees of freedom  $u_{i,j}$  (i = A-2, A-1, A, A+1, A+2 and j = B-2, B-1, B, B+1, B+2) which are close to the degree of freedom  $u_{A,B}$  (see Fig. 11 in the Appendix A) and has the following form:

$$\begin{split} h^2\{m_1\dot{u}_{A,B}^{num} + m_2[\dot{u}_{(A-1),(B+1)}^{num} + \dot{u}_{(A+1),(B-1)}^{num} + \dot{u}_{(A+1),(B+1)}^{num} + \dot{u}_{(A-1),(B-1)}^{num}] \\ + m_3[\dot{u}_{A,(B+1)}^{num} + \dot{u}_{A,(B-1)}^{num}] + m_4[\dot{u}_{(A-2),(B-2)}^{num} + \dot{u}_{(A+2),(B+2)}^{num} + \dot{u}_{(A-2),(B+2)}^{num} + \dot{u}_{(A+2),(B+2)}^{num}] \\ + m_5[\dot{u}_{(A+2),(B-1)}^{num} + \dot{u}_{(A-2),(B+1)}^{num} + \dot{u}_{(A-2),(B-1)}^{num} + \dot{u}_{(A+1),(B+2)}^{num}] + m_6[\dot{u}_{A,(B+2)}^{num} + \dot{u}_{A,(B-2)}^{num}] \\ + m_7[\dot{u}_{(A-1),B}^{num} + \dot{u}_{(A+1),B}^{num}] + m_8[\dot{u}_{(A-1),(B-2)}^{num} + \dot{u}_{(A+1),(B+2)}^{num} + \dot{u}_{(A-1),(B+2)}^{num} + \dot{u}_{(A+1),(B-2)}^{num}] \\ + m_9[\dot{u}_{(A-2),B}^{num} + \dot{u}_{(A+2),B}^{num}] \\ + a\{k_1u_{A,B}^{num} + k_2[u_{(A-1),(B+1)}^{num} + u_{(A+1),(B-1)}^{num} + u_{(A+1),(B+1)}^{num} + u_{(A-1),(B-1)}^{num}] \\ + k_3[u_{A,(B+1)}^{num} + u_{A,(B-1)}^{num}] + k_4[u_{(A-2),(B-2)}^{num} + u_{(A+2),(B+2)}^{num} + u_{(A-2),(B+2)}^{num} + u_{A,(B-2)}^{num}] \\ + k_5[u_{(A+2),(B-1)}^{num} + u_{(A-2),(B+1)}^{num} + u_{(A-2),(B-1)}^{num} + u_{(A+1),(B+2)}^{num} + u_{A,(B-2)}^{num}] \\ + k_7[u_{(A-1),B}^{num} + u_{(A+1),B}^{num}] + k_8[u_{(A-1),(B-2)}^{num} + u_{(A+1),(B+2)}^{num} + u_{(A+1),(B+2)}^{num} + u_{(A+1),(B-2)}^{num}] \\ + k_9[u_{(A-2),B}^{num} + u_{(A+1),B}^{num}] + k_8[u_{(A-1),(B-2)}^{num} + u_{(A+1),(B+2)}^{num} + u_{(A+1),(B-2)}^{num}] \\ + k_9[u_{(A-2),B}^{num} + u_{(A+2),B}^{num}] + u_{(A+2),B}^{num}] = 0, \end{split}$$

where the coefficients  $m_j$  and  $k_j$  (j=1,2,3,...,9) for the conventional quadratic isogeometric elements are given in Table 1. For the derivation of the new technique with improved accuracy let us assume that similar to the conventional elements the 25-point stencil equation for the degree of freedom  $u_{A,B}$  can be also represented by Eq. (15) with unknown coefficients  $m_j$  and  $k_j$  (j=1,2,3,...,9) before each degree of freedom. Similar to the conventional isogeometric elements, the symmetry for coefficients  $m_j$  and  $k_j$  in the stencil equation (15) is assumed for the degrees of freedom  $u_{j,l}$  (j=A-2,A-1,A,A+1,A+2 and l=B-2,B-1,B,B+1,B+2) symmetrically located with respect to the degree of freedom  $u_{A,B}$ ; see Fig. 11 in the Appendix A.

**Table 1**The coefficients of the stencil equation for the conventional Q9\_IGE quadratic isogeometric elements used for the heat equation and for the Poisson equation in the 2-D case.

Coefficients	Q9_IGE	Coefficients	Q9_IGE
$m_1$	$121b_y$	$k_1$	$11(1+b_y^2)$
	400		$20b_y$
$m_2$	$169b_{y}$	$k_2$	$13(1+b_y^2)$
	3600		$-\frac{180b_{y}}{}$
$m_3$	$\frac{143b_y}{}$	$k_3$	$13 - 11b_y^2$
	1200		$60b_y$
$m_4$	$b_{y}$	$k_4$	$1 + b_y^2$
	14400		$-\frac{720b_{y}}{720b_{y}}$
$m_5$	$13b_y$	$k_5$	$13 + b_y^2$
	7200		$-{360b_{y}}$
$m_6$	$11b_y$	$k_6$	$1 - 11b_y^2$
	2400		$120b_y$
$m_7$	143b <sub>y</sub>	$k_7$	$-11 + 13b_y^2$
	1200		$60b_y$
$m_8$	13b <sub>y</sub>	k <sub>8</sub>	$1 + 13b_y^2$
	7200		$-{360b_{y}}$
$m_9$	$11b_y$	k <sub>9</sub>	$-11 + b_y^2$
	2400		$120b_y$

For the derivation of the stencil equation of the new approach we do not use the basis functions. We just assume that similar to the conventional isogeometric elements, the 25-point stencil equation for the new approach, Eq. (15), is a linear combination of degrees of freedom  $u_{i,j}^{num}$ . Therefore, we can also treat these degrees of freedom as the values of function u at the nodes (similar to the conventional finite elements).

Remark. If for some approaches the stencil equations are given in terms of other variables that are not the values of function u at the nodes, then a linear transformation of these variables to the values of function u at the nodes of a grid can be used for the modification of the stencil equation.

For the calculation of the local truncation error, let us expand the exact solution  $u_{j,l}$  and  $\dot{u}_{j,l}$  (j = A - 2, A - 1, A, A + 1, A + 2 and l = B - 2, B - 1, B, B + 1, B + 2) to the heat equation into a Taylor series at small  $h \ll 1$  as follows:

$$u_{A\pm i,B\pm j} = u_{A,B} + \frac{\partial u_{A,B}}{\partial x}(\pm ih) + \frac{\partial u_{A,B}}{\partial y}(\pm jb_yh) + \frac{\partial^2 u_{A,B}}{\partial x^2} \frac{(\pm ih)^2}{2!} + \frac{\partial^2 u_{A,B}}{\partial x \partial y} \frac{(\pm ih)(\pm jb_yh)}{2!} + \frac{\partial^2 u_{A,B}}{\partial y^2} \frac{(\pm jb_yh)^2}{2!} + \dots$$

$$(16)$$

$$\dot{u}_{A\pm i,B\pm j} = \dot{u}_{A,B} + \frac{\partial \dot{u}_{A,B}}{\partial x}(\pm ih) + \frac{\partial \dot{u}_{A,B}}{\partial y}(\pm jb_yh) + \frac{\partial^2 \dot{u}_{A,B}}{\partial x^2} \frac{(\pm ih)^2}{2!} + \frac{\partial^2 \dot{u}_{A,B}}{\partial x \partial y} \frac{(\pm ih)(\pm jb_yh)}{2!} + \frac{\partial^2 \dot{u}_{A,B}}{\partial y^2} \frac{(\pm jb_yh)^2}{2!} + \dots$$
(17)

with i, j = 0, 1, 2. The exact solution  $u_{A,B}$  to Eq. (1) at  $x = x_A$  and  $y = y_B$  meets the following equations:

$$\frac{\partial u_{A,B}}{\partial t} - a\nabla^2 u_{A,B} = 0, \tag{18}$$

$$\frac{\partial^{(2i+2j+1)} u_{A,B}}{\partial x^{2i} \partial y^{2j} \partial t} - a \frac{\partial^{(2i+2j)} \nabla^2 u_{A,B}}{\partial x^{2i} \partial y^{2j}} = 0 \tag{19}$$

with  $i, j = 0, 1, 2, 3, 4, \dots$  Here, Eq. (19) is directly obtained by the differentiation of Eq. (18) with respect to x and y. Similar to Eq. (8), inserting Eqs. (16) - (19) with the exact solution to the heat equation, Eq. (1), into the stencil equation (15) we will get the following local truncation error in space e:

$$e = a\{b_1 u_{A,B} + h^2 [b_2 \frac{\partial^2 u_{A,B}}{\partial x^2} + b_3 \frac{\partial^2 u_{A,B}}{\partial y^2}] + \frac{h^4}{12} [b_4 \frac{\partial^4 u_{A,B}}{\partial x^4} + b_5 \frac{\partial^4 u_{A,B}}{\partial y^4} + b_6 \frac{\partial^4 u_{A,B}}{\partial x^2 \partial y^2}]$$

$$+\frac{h^{6}}{360}\left[b_{7}\frac{\partial^{6}u_{A,B}}{\partial x^{6}}+b_{8}\frac{\partial^{6}u_{A,B}}{\partial y^{6}}+b_{9}\frac{\partial^{6}u_{A,B}}{\partial x^{4}\partial y^{2}}+b_{10}\frac{\partial^{6}u_{A,B}}{\partial x^{2}\partial y^{4}}\right]$$

$$+\frac{h^{8}}{20160}\left[b_{11}\frac{\partial^{8}u_{A,B}}{\partial x^{8}}+b_{12}\frac{\partial^{8}u_{A,B}}{\partial y^{8}}+b_{13}\frac{\partial^{8}u_{A,B}}{\partial x^{6}\partial y^{2}}+b_{14}\frac{\partial^{8}u_{A,B}}{\partial x^{4}\partial y^{4}}+b_{15}\frac{\partial^{8}u_{A,B}}{\partial x^{2}\partial y^{6}}\right]$$

$$+\frac{h^{10}}{1814400}\left[b_{16}\frac{\partial^{10}u_{A,B}}{\partial x^{10}}+b_{17}\frac{\partial^{10}u_{A,B}}{\partial y^{10}}+b_{18}\frac{\partial^{10}u_{A,B}}{\partial x^{8}\partial y^{2}}\right]$$

$$+b_{19}\frac{\partial^{10}u_{A,B}}{\partial x^{6}\partial y^{4}}+b_{20}\frac{\partial^{10}u_{A,B}}{\partial x^{4}\partial y^{6}}+b_{21}\frac{\partial^{10}u_{A,B}}{\partial x^{2}\partial y^{8}}\right]\}+O(h^{12})$$

$$(20)$$

with the coefficients  $b_n(p=1,2,3,...,21)$  given in Appendix C; see Eq. (C.1).

The use of Eqs. (18) and (19) are partly based on the ideas of the Lax-Wendroff method related to the replacement of the time derivative by the spatial derivative according to the governing partial differential equation, Eq. (1). Therefore, Eq. (20) does not include the time derivatives. In order to improve the order of the local truncation error in Eq. (20) at small  $h \ll 1$ , we can equate to zero the coefficients  $b_p$  in Eq. (20) that are expressed in terms of the 18 unknown coefficients  $m_i$  and  $k_i$  (i=1,2,...,9); see Eq. (C.1). For example, for the 10-th order or 12-th order of the local truncation error, the first 15 or 21 coefficients  $b_p$  in Eq. (20) should be zero, respectively. As can be seen, for the 12-th order of the local truncation error the 18 unknown coefficients  $m_i$  and  $k_i$  (i=1,2,...,9) are insufficient for meeting the 21 equations  $b_p=0$  (i=1,2,...,21). Therefore, the maximum possible order of the local truncation error for the stencil equation, Eq. (15), with the 18 unknown coefficients  $m_i$  and  $k_i$  (i=1,2,...,9) is 10; i.e., the maximum possible order of the local truncation error is defined by the number of the unknown coefficients  $m_i$  and  $k_i$  in the stencil equation. Equating to zero the first 15 coefficients  $b_p$  in Eq. (20), we get the corresponding system of linear algebraic equations  $b_p=0$  (i=1,2,...,15) with respect to the unknown coefficients  $m_i$  and  $k_i$  (i=1,2,...,9). Solving these equations  $b_p=0$  (p=1,2,...,15), we can find the coefficients  $m_i$  and  $k_i$  (i=1,2,...,9) for the new approach i=1,2,...,9 for the new approach i=1,2,...,9 for the earbitrary coefficients i=1,2,...,9 and i=1,2,...,9 for the new approach i=1,2,...,9 for the earbitrary coefficients i=1,2,...,9 and i=1,2,...,9

$$\begin{split} m_1 &= \frac{b_y^4(2220a_1 - 4677a_2 + 4016a_3) + 5b_y^2(-2334a_1 + 3537a_2 - 596a_3) + 2850a_1}{5x_1}\,, \\ m_2 &= \frac{b_y^4(8880a_1 - 3567a_2 - 424a_3) + b_y^2(19227a_2 - 8(5835a_1 + 257a_3)) + 11400a_1}{45x_1}\,, \\ m_3 &= \frac{b_y^4(-2960a_1 - 2397a_2 + 5416a_3) + b_y^2(15560a_1 + 3537a_2 - 1736a_3) - 3800a_1}{10x_1}\,, \\ m_4 &= \frac{b_y^4(2220a_1 + 69a_2 - 832a_3) + b_y^2(-11670a_1 + 1011a_2 + 92a_3) + 2850a_1}{180x_1}\,, \\ m_5 &= \frac{b_y^4(-8880a_1 - 1311a_2 + 2488a_3) + 5b_y^2(9336a_1 + 543a_2 - 184a_3) - 11400a_1}{180x_1}\,, \\ m_7 &= \frac{b_y^4(-2960a_1 - 2397a_2 + 5416a_3) + b_y^2(15560a_1 + 3537a_2 - 1736a_3) - 3800a_1}{10x_1}\,, \\ m_8 &= \frac{b_y^4(-8880a_1 - 1311a_2 + 2488a_3) + 5b_y^2(9336a_1 + 543a_2 - 184a_3) - 11400a_1}{180x_1}\,, \\ m_8 &= \frac{b_y^4(-8880a_1 - 1311a_2 + 2488a_3) + 5b_y^2(9336a_1 + 543a_2 - 184a_3) - 11400a_1}{5x_1}\,, \\ k_1 &= -\frac{6(b_y^2 + 1)(3a_2(583b_y^2 - 2358) + a_3(1097 - 1222b_y^2))}{5x_1}\,, \\ k_2 &= \frac{8(b_y^2 + 1)(a_2(73b_y^2 + 187) + 8a_3(8 - 43b_y^2))}{5x_1}\,, \\ k_3 &= \frac{2(3a_2(773b_y^4 - 3855b_y^2 + 142) - 8a_3(109b_y^4 - 520b_y^2 + 91))}{5x_1}\,, \\ k_4 &= \frac{(b_y^2 + 1)(a_2(46b_y^2 - 341) + a_3(62b_y^2 + 23))}{10x_1}\,, \\ k_5 &= \frac{a_2(-23b_y^4 + 845b_y^2 - 1922) - 216a_3(b_y^4 - 1)}{5x_1}\,, \\ \end{split}$$

$$k_{6} = \frac{609a_{2}(b_{y}^{4} - 1) + a_{3}(-1922b_{y}^{4} + 845b_{y}^{2} - 23)}{5x_{1}},$$

$$k_{7} = \frac{128a_{3}(43b_{y}^{4} - 25b_{y}^{2} + 22) - 18a_{2}(106b_{y}^{4} - 305b_{y}^{2} + 1179)}{5x_{1}},$$

$$k_{8} = a_{2}, \qquad k_{9} = a_{3},$$
(21)

where  $x_1 = 74b_y^4 - 389b_y^2 + 95$ . Inserting the coefficients  $m_j$  and  $k_j$  (j = 1, 2, 3, ..., 9) for the new stencils with improved accuracy and for the conventional elements into Eq. (20), we will get the local truncation errors in space e for the new approach and the conventional elements. They are

$$e_{impr}^{quad} = \frac{ab_y^2 h^{10}}{25200(b_y^2 - 5)(74b_y^2 - 19)} \{-316(3(b_y^2 - 3)a_2 - 4b_y^2 a_3 + 2a_3)(\frac{\partial^{10} u_{A,B}}{\partial x^{10}} + b_y^8 \frac{\partial^{10} u_{A,B}}{\partial y^{10}}) + b_y^2 [7(37b_y^4 (69a_2 - 392a_3 + 1200a_1) + b_y^2 (10611a_2 + 2392a_3 - 233400a_1) + 57000a_1)(\frac{\partial^{10} u_{A,B}}{\partial y^4 \partial x^6} + \frac{\partial^{10} u_{A,B}}{\partial y^6 \partial x^4}) - ((3657b_y^2 - 36549)a_2 + 8(1333b_y^2 + 184)a_3)(\frac{\partial^{10} u_{A,B}}{\partial y^2 \partial x^8} + b_y^4 \frac{\partial^{10} u_{A,B}}{\partial y^8 \partial x^2})]\} + O(h^{12})$$

$$(22)$$

for the new 25-point stencils with improved accuracy and

$$e_{conv}^{quad} = -\frac{b_y a h^6}{720} \left( b_y^4 \frac{\partial^6 u_{A,B}}{\partial v^6} + \frac{\partial^6 u_{A,B}}{\partial x^6} \right) + O(h^8)$$
 (23)

for the conventional quadratic isogeometric elements; i.e., the new approach improves the local truncation error in space by four orders compared to that for the quadratic isogeometric elements (similar to the improvement of the order of the numerical dispersion error for the quadratic isogeometric elements with reduced dispersion that are used for the scalar wave equation; see [23,24]).

Remark. Three arbitrary coefficients  $a_1$ ,  $a_2$  and  $a_3$  are used for the calculations of the coefficients  $m_i$  and  $k_i$  (i = 1, 2, ..., 9) for the new stencils. These coefficients  $a_i$  (i = 1, 2, 3) do not affect the order of the local truncation error but contribute to the leading terms of the local truncation error in Eq. (22) that include the mixed tenth order derivatives of the exact solution; see Eq. (22). We can use two of coefficients  $a_i$  (i = 1, 2, 3) to simplify the leading terms of the local truncation error in Eq. (22). For example, equating to zero two coefficients  $b_{17}$  and  $b_{18}$  (along with the first 15 coefficients  $b_p$  (p = 1, 2, ..., 15)) in Eq. (20), we can express the coefficients  $a_2$  and  $a_3$  in terms of just one coefficient  $a_1$  as follows:

$$a_2 = -\frac{40(1333b_y^2 + 184)a_1}{9039b_y^2}, \qquad a_3 = \left(\frac{265}{131} - \frac{465}{23b_y^2}\right)a_1. \tag{24}$$

In this case the error in Eq. (22) is simplified as follows:

$$e_{impr}^{quad} = \frac{23889600aa_1h^{10}}{3013} \left( \frac{\partial^{10}u_{A,B}}{\partial x^{10}} + b_y^8 \frac{\partial^{10}u_{A,B}}{\partial y^{10}} \right) + O(h^{12}). \tag{25}$$

Below we show that the new approach can be also implemented similar to the isogeometric elements with the elemental  $\mathbf{M}^e$  and  $\mathbf{K}^e$  matrices. Let us find the elemental  $\mathbf{M}^e$  and  $\mathbf{K}^e$  matrices that yield the stencil equation (15) with the coefficients  $m_j$  and  $k_j$  (j=1,2,...,9) for the new approach  $Q_{QOPT}$  given by Eq. (21) (it is assumed that the stencil equation for the new elements is calculated similar to the conventional isogeometric elements according to Eq. (5). The new elemental  $\mathbf{M}^e$  and  $\mathbf{K}^e$  matrices are assumed to have the same form as that for the conventional elemental matrices with unknown coefficients  $d_i$  and  $d_i$  (i=1,2,3,...,17):

$$\mathbf{M}^{e} = h^{2} \begin{pmatrix} d_{1} & d_{5} & d_{2} & d_{8} & d_{9} & d_{6} & d_{4} & d_{7} & d_{3} \\ d_{5} & d_{10} & d_{5} & d_{11} & d_{13} & d_{11} & d_{7} & d_{12} & d_{7} \\ d_{2} & d_{5} & d_{1} & d_{6} & d_{9} & d_{8} & d_{3} & d_{7} & d_{4} \\ d_{8} & d_{11} & d_{6} & d_{14} & d_{16} & d_{15} & d_{8} & d_{11} & d_{6} \\ d_{9} & d_{13} & d_{9} & d_{16} & d_{17} & d_{16} & d_{9} & d_{13} & d_{9} \\ d_{6} & d_{11} & d_{8} & d_{15} & d_{16} & d_{14} & d_{6} & d_{11} & d_{8} \\ d_{4} & d_{7} & d_{3} & d_{8} & d_{9} & d_{6} & d_{1} & d_{5} & d_{2} \\ d_{7} & d_{12} & d_{7} & d_{11} & d_{13} & d_{11} & d_{5} & d_{10} & d_{5} \\ d_{3} & d_{7} & d_{4} & d_{6} & d_{9} & d_{8} & d_{2} & d_{5} & d_{1} \end{pmatrix},$$

$$(26)$$

$$\mathbf{K}^{e} = \begin{pmatrix} f_{1} & f_{5} & f_{2} & f_{8} & f_{9} & f_{6} & f_{4} & f_{7} & f_{3} \\ f_{5} & f_{10} & f_{5} & f_{11} & f_{13} & f_{11} & f_{7} & f_{12} & f_{7} \\ f_{2} & f_{5} & f_{1} & f_{6} & f_{9} & f_{8} & f_{3} & f_{7} & f_{4} \\ f_{8} & f_{11} & f_{6} & f_{14} & f_{16} & f_{15} & f_{8} & f_{11} & f_{6} \\ f_{9} & f_{13} & f_{9} & f_{16} & f_{17} & f_{16} & f_{9} & f_{13} & f_{9} \\ f_{6} & f_{11} & f_{8} & f_{15} & f_{16} & f_{14} & f_{6} & f_{11} & f_{8} \\ f_{4} & f_{7} & f_{3} & f_{8} & f_{9} & f_{6} & f_{1} & f_{5} & f_{2} \\ f_{7} & f_{12} & f_{7} & f_{11} & f_{13} & f_{11} & f_{5} & f_{10} & f_{5} \\ f_{3} & f_{7} & f_{4} & f_{6} & f_{9} & f_{8} & f_{2} & f_{5} & f_{1} \end{pmatrix},$$

$$(27)$$

where the symmetry of the coefficients of the  $M^e$  and  $K^e$  matrices for the degrees of freedom contributing to these matrices is used; see Appendix A. In this case the matrices  $M^e$  and  $K^e$  depend on the 34 unknown terms  $d_j$  and  $f_j$  (j = 1, 2, ..., 17). Considering  $3 \times 3 = 9$  elements that contribute to the stencil equation for the degree of freedom  $u_{A,B}$  according to Eq. (5), the coefficients of the stencil equation (15) can be expressed in terms of the coefficients of the matrices  $M^e$  and  $K^e$  as follows:

$$m_{1} = 4d_{1} + 2d_{10} + 2d_{14} + d_{17}, m_{2} = 2(d_{11} + d_{9}), m_{3} = 2(d_{16} + 2d_{5}), m_{4} = d_{3},$$

$$m_{5} = 2d_{7}, m_{6} = d_{15} + 2d_{2}, m_{7} = 2(d_{13} + 2d_{8}), m_{8} = 2d_{6}, m_{9} = d_{12} + 2d_{4},$$

$$k_{1} = 4f_{1} + 2f_{10} + 2f_{14} + f_{17}, k_{2} = 2(f_{11} + f_{9}), k_{3} = 2(f_{16} + 2f_{5}), k_{4} = f_{3},$$

$$(28)$$

$$k_5 = 2f_7$$
,  $k_6 = f_{15} + 2f_2$ ,  $k_7 = 2(f_{13} + 2f_8)$ ,  $k_8 = 2f_6$ ,  $k_9 = f_{12} + 2f_4$ . (29)

Solving simultaneously a system of linear algebraic equations (28), (29) with the coefficients  $m_j$  and  $k_j$  (j=1,2,...,9) for the new approach given by Eq. (21), the coefficients  $d_j$  and  $f_j$  (j=1,2,...,17) of the  $M^e$  and  $K^e$  matrices in Eqs. (26) and (27) for the 2-D quadratic isogeometric elements with improved accuracy can be found; see Eqs. (D.1) and (D.2) in Appendix D. In Eqs. (D.1) and (D.2)  $a_j$  (j=1,2,...,16) are sixteen arbitrary coefficients that do not affect the stencil equation (15) (the first three coefficients  $a_j$  (j=1,2,3) are the same as those used in Eq. (21) for  $m_j$  and  $k_j$  (j=1,2,...,9) of the new approach). For example, these coefficients can be used for the minimization of the error in the case of the combination of the different order elements (this will be studied in the future). The order of the local truncation error is independent of the values of these coefficients. At the derivation of Eqs. (D.1) and (D.2) the following additional algebraic equations (see Eqs. (30) and (31) below) have been also used. Because the M and K matrices for the wave equation and the heat equation are the same then let us use some terminology related to the wave equation in order to normalize the elemental  $M^e$  and  $K^e$  matrices. Let us assume that the velocity  $\mathbf{v}(\mathbf{x},t) = \dot{\mathbf{u}}(\mathbf{x},t) = \mathbf{v}_0$  is the same for the entire domain. In this case the kinetic energy for one rectangular element can be calculated with the help of the mass matrix and by the analytical formula for the considered rectangular element. Equating these two expressions we get

$$\mathbf{V}_{0}^{T}\mathbf{M}^{e}\mathbf{V}_{0} = v_{0}^{2}b_{y}h^{2}, \tag{30}$$

$$K^e U_0 = \mathbf{0}, \tag{31}$$

Let us consider the lumped matrix  $\mathbf{M}$  with zero coefficients  $m_j=0$  (j=2,3,...,9) except  $m_1$ . In this case Eq. (20) can be also used for the calculation of the local truncation error of the conventional elements (using the coefficients  $k_j$  for the conventional isogeometric elements in Table 1) as well as of the new approach with the coefficients  $m_1$  and  $k_j$  obtained by the minimization of the order of the local truncation error. For example, equating to zero the first 6 coefficients  $b_p$  (p=1,2,...,6), we will get the corresponding system of linear algebraic equations. Solving these equations  $b_p=0$  (p=1,2,...,6) in the case of the lumped matrix  $\mathbf{M}$  ( $m_j=0,\ j=2,3,...,9$ ), we can find the following coefficients  $m_1$  and  $k_i$  (i=1,2,3,...,9):

$$m_1 = a_1, \qquad m_2 = m_3 = \dots = m_9 = 0,$$
 
$$k_1 = \frac{5a_1}{2} - 2(a_3 + a_4), \qquad k_2 = -\frac{2a_1}{3b_y^2} - a_2 - \frac{a_4}{2},$$
 
$$k_3 = \frac{1}{12}(16(\frac{1}{b_y^2} - 1)a_1 + 18a_2 + 16a_3 + 13a_4), \qquad k_4 = \frac{b_y^2(-6a_2 + 4a_3 + a_4) + a_1}{24b_y^2},$$

$$k_{5} = \frac{1}{24}(6a_{2} - 16a_{3} - a_{4}), \qquad k_{6} = \frac{(b_{y}^{2} - 1)a_{1} - b_{y}^{2}(18a_{2} + 4a_{3} + a_{4})}{12b_{y}^{2}},$$

$$k_{7} = a_{4}, \qquad k_{8} = a_{2}, \qquad k_{9} = a_{3}$$
(32)

for the new approach  $(a_1, a_2, a_3)$  and  $a_4$  are four arbitrary coefficients). Inserting the coefficients  $m_1$  and  $k_j$  from Eq. (32) obtained by the minimization of the order of the local truncation error and the coefficients  $k_j$  for the conventional quadratic isogeometric elements (see Table 1) into Eq. (20), we will get the local truncation errors in space e for the two approaches with the lumped matrix  $\mathbf{M}$ . They are:

$$e_{impr}^{quad-lump} = \frac{ah^{6}}{360} \left[ 4b_{y}^{4} a_{1} \frac{\partial^{6} u_{A,B}}{\partial y^{6}} + 15b_{y}^{2} \frac{\partial^{6} u_{A,B}}{\partial y^{4} \partial x^{2}} \left( 3b_{y}^{2} (a_{4} - 6a_{2}) + 4a_{1} \right) + 60 \frac{\partial^{6} u_{A,B}}{\partial y^{2} \partial x^{4}} \left( b_{y}^{2} (4a_{3} + a_{4}) + a_{1} \right) + 4a_{1} \frac{\partial^{6} u_{A,B}}{\partial x^{6}} \right] + O(h^{8})$$
(33)

for the new approach with the coefficients given by Eq. (32) and

$$e_{conv}^{quad-lump} = a(m_1 - b_y)h^2(\frac{\partial^2 u_{A,B}}{\partial x^2} + \frac{\partial^2 u_{A,B}}{\partial y^2}) - \frac{ab_y h^4}{4}[\frac{\partial^4 u_{A,B}}{\partial x^4} + b_y^2 \frac{\partial^4 u_{A,B}}{\partial y^4} + (1 + b_y^2) \frac{\partial^4 u_{A,B}}{\partial y^2 \partial x^2}] + O(h^6)$$
 (34)

for the conventional elements with the lumped matrix M; i.e., for the lumped matrix M, the new approach improves the local truncation error by two orders compared to that for the conventional isogeometric elements. It is interesting to mention that Eq. (34) for the local truncation error of the conventional isogeometric elements allows to find the optimal value of the diagonal terms of the lumped matrix M. It follows from Eq. (34) that  $m_1 = b_y$  minimizes the order of the local truncation error.

# 2.2. Steady-state problems (Poisson equation with zero heat source $f(\mathbf{x}) = \bar{f} = 0$ )

In the case of the time independent Poisson equation (Eq. (2)), the 25-point stencil equation for the degree of freedom  $u_{A,B}^{num}$  for a structured rectangular mesh with the quadratic isogeometric elements can be represented as follows (it can be also obtained from Eq. (15) with a = 1 and  $m_j = 0$  for j = 1, 2, 3, ..., 9):

$$k_{1}u_{A,B}^{num} + k_{2}[u_{(A-1),(B+1)}^{num} + u_{(A+1),(B-1)}^{num} + u_{(A+1),(B+1)}^{num} + u_{(A-1),(B-1)}^{num}]$$

$$+k_{3}[u_{A,(B+1)}^{num} + u_{A,(B-1)}^{num}] + k_{4}[u_{(A-2),(B-2)}^{num} + u_{(A+2),(B+2)}^{num} + u_{(A-2),(B+2)}^{num} + u_{(A+2),(B-2)}^{num}]$$

$$+k_{5}[u_{(A+2),(B-1)}^{num} + u_{(A-2),(B+1)}^{num} + u_{(A-2),(B-1)}^{num} + u_{(A+2),(B+1)}^{num}] + k_{6}[u_{A,(B+2)}^{num} + u_{A,(B-2)}^{num}]$$

$$+k_{7}[u_{(A-1),B}^{num} + u_{(A+1),B}^{num}] + k_{8}[u_{(A-1),(B-2)}^{num} + u_{(A+1),(B+2)}^{num} + u_{(A+1),(B-2)}^{num}]$$

$$+k_{9}[u_{(A-2),B}^{num} + u_{(A+2),B}^{num}] = 0,$$

$$(35)$$

where the coefficients  $k_j$  (j=1,2,3,...,9) can be expressed in terms of the elemental  $\mathbf{K}^e$  matrices for the conventional quadratic isogeometric elements and are the same as those for the 2-D heat equation; see Table 1. For the new approach, the same structure of the 25-point stencil equation as that for the conventional elements is assumed and the optimal coefficients  $k_j$  are calculated by the minimization of the order of the local truncation error (these coefficients can be used for the modification of the elemental  $\mathbf{K}^e$  matrices); see below. The 25-point stencil equation (35) also includes the symmetry of coefficients  $k_j$  for the degrees of freedom  $u_{j,l}^{num}$  (j=A-2,A-1,A,A+1,A+2 and l=B-2,B-1,B,B+1,B+2) symmetrically located with respect to the degree of freedom  $u_{A,B}^{num}$ . The exact solution  $u_{A,B}$  to the Poisson equation, Eq. (2), at  $x=x_A$  and  $y=y_B$  meets the following equations:

$$\frac{\partial^2 u_{A,B}}{\partial x^2} = -\frac{\partial^2 u_{A,B}}{\partial y^2},\tag{36}$$

$$\frac{\partial^{(i+2j)}u_{A,B}}{\partial v^i \partial x^{2j}} = (-1)^j \frac{\partial^{(i+2j)}u_{A,B}}{\partial v^{(i+2j)}},\tag{37}$$

$$\frac{\partial^{(i+2j-1)} u_{A,B}}{\partial y^i \partial x^{(2j-1)}} = (-1)^j \frac{\partial^{(i+2j-1)} u_{A,B}}{\partial y^{(i+2j-2)} \partial x}$$
(38)

with i = 0, 1, 2, 3, ... and j = 1, 2, 3, ... The right-hand sides of Eqs. (37) and (38) are obtained by the replacement of the second x-derivative in the left-hand sides of Eqs. (37) and (38) by the second y-derivative using Eq. (36). For the calculation of the local truncation error, we also use Eq. (16). Inserting Eqs. (16), (36) - (38) into the stencil equation (35) we will get the following local truncation error in space e:

$$e = b_{1}u_{A,B} + h^{2}b_{2}\frac{\partial^{2}u_{A,B}}{\partial y^{2}} + \frac{h^{4}b_{3}}{12}\frac{\partial^{4}u_{A,B}}{\partial y^{4}} + \frac{h^{6}b_{4}}{360}\frac{\partial^{6}u_{A,B}}{\partial y^{6}} + \frac{h^{8}b_{5}}{20160}\frac{\partial^{8}u_{A,B}}{\partial y^{8}} + \frac{h^{10}b_{6}}{1814400}\frac{\partial^{10}u_{A,B}}{\partial y^{10}} + \frac{h^{12}b_{7}}{239500800}\frac{\partial^{10}u_{A,B}}{\partial y^{12}} + \frac{h^{14}b_{8}}{43589145600}\frac{\partial^{14}u_{A,B}}{\partial y^{14}} + \frac{h^{16}b_{9}}{10461394944000}\frac{\partial^{16}u_{A,B}}{\partial y^{16}} + \frac{h^{18}b_{10}}{3201186852864000}\frac{\partial^{18}u_{A,B}}{\partial y^{18}} + \frac{h^{20}b_{11}}{1216451004088320000}\frac{\partial^{20}u_{A,B}}{\partial y^{20}} + O(h^{22})$$

$$(39)$$

with the coefficients  $b_p(p=1,2,...,11)$  given in Appendix E; see Eq. (E.1). Due to the use of the Poisson equation, Eqs. (36) - (38), the local truncation error, Eq. (39), doe not include the partial derivatives with respect to x.

To improve the order of the local truncation error in Eq. (39) at small  $h \ll 1$ , we equate to zero the first 8 coefficients  $b_p$  (p=1,2,3,...,8). This allows us to find the 9 unknown coefficients  $k_i$  (i=1,2,...,9) of the stencil equation, Eq. (35) (equating to zero the first 9 coefficients  $b_p$  (p=1,2,3,...,9) leads to the solution  $k_i=0$  (i=1,2,3,...,9) that is inappropriate; i.e., equating to zero the first 8 coefficients  $b_p$  yields the maximum possible order of the local truncation error in Eq. (39)). Solving these equations  $b_p=0$  (p=1,2,3,...,8), we can find the coefficients  $k_i$  (i=1,2,3,...,9) for the new approach  $Q9_0PT_1$  in terms of one arbitrary coefficient  $a_1$ :

$$k_1 = a_1, \\ k_2 = \frac{16a_1(b_y^2 + 4)(4b_y^2 + 1)}{9y_1} [598096b_y^{12} - 6291208b_y^{10} + 26094929b_y^8 - 47431534b_y^6 \\ + 26094929b_y^4 - 6291208b_y^2 + 598096], \\ k_3 = -\frac{8a_1(b_y^2 + 1)(b_y^2 + 4)}{3y_1} [14572244b_y^{12} - 105226995b_y^{10} + 247191783b_y^8 - 129893985b_y^6 \\ + 30238377b_y^4 - 4502520b_y^2 + 598096], \\ k_4 = \frac{a_1(b_y^2 + 1)^2(b_y^2 + 4)}{36y_1} [176656b_y^{10} - 892136b_y^8 + 1284013b_y^6 - 556778b_y^4 \\ - 57419b_y^2 + 44164], \\ k_5 = -\frac{4a_1(b_y^2 + 1)(b_y^2 + 4)}{9y_1} [44164b_y^{12} - 1132795b_y^{10} + 5767943b_y^8 - 12208585b_y^6 + 12056297b_y^4 \\ - 4480120b_y^2 + 598096], \\ k_6 = \frac{a_1}{6y_1} [58288976b_y^{16} - 481727600b_y^{14} + 1456399991b_y^{12} - 1756955850b_y^{10} + 1159844496b_y^8 \\ - 441576750b_y^6 + 83309881b_y^4 - 4919800b_y^2 + 176656], \\ k_7 = -\frac{8a_1(b_y^2 + 1)}{3y_1} [2392384b_y^{14} - 17411984b_y^{12} + 116450988b_y^{10} - 489337563b_y^8 + 858873147b_y^6 \\ - 173716197b_y^4 - 46938019b_y^2 + 14572244], \\ k_8 = -\frac{4a_1(b_y^2 + 1)}{9y_1} [2392384b_y^{14} - 17322384b_y^{12} + 43745068b_y^{10} - 36778043b_y^8 + 10863187b_y^6 \\ + 1236763b_y^4 - 956139b_y^2 + 44164], \\ k_9 = \frac{a_1}{6y_1} [176656b_y^{16} - 4919800b_y^{14} + 83309881b_y^{12} - 441576750b_y^{10} + 1159844496b_y^8 \\ - 1756955850b_y^6 + 1456399991b_y^4 - 481727600b_y^2 + 58288976],$$
 (40)

with

$$y_1 = 58288976b_y^{16} - 12041600b_y^{14} - 1112834229b_y^{12} + 805729100b_y^{10} + 7325265506b_y^{8} + 805729100b_y^{6} - 1112834229b_y^{4} - 12041600b_y^{2} + 58288976.$$

$$(41)$$

Inserting the coefficients  $k_j$  for the new approach and for conventional isogeometric elements into Eq. (39), we will get the local truncation errors in space e for the new stencils with improved accuracy and for the conventional isogeometric elements. They are:

$$e_{impr} = \frac{a_1 y_2 h^{16}}{169827840 y_1} \frac{\partial^{16} u_{A,B}}{\partial y^{16}} + O(h^{18})$$
(42)

with

$$y_2 = b_y^4 (b_y^2 + 1)^2 (791104b_y^{20} - 6526608b_y^{18} + 7168588b_y^{16} + 81226757b_y^{14} - 288383192b_y^{12} \\ + 409496702b_y^{10} - 288383192b_y^8 + 81226757b_y^6 + 7168588b_y^4 - 6526608b_y^2 + 791104)$$

and

$$e_{impr}(b_y = 1) = -\frac{a_1 h^{16}}{148132333440} \frac{\partial^{16} u_{A,B}}{\partial v^{16}} + O(h^{18})$$
(43)

for the new Q9\_OPT\_1 stencils with improved accuracy on rectangular (Eq. (42)) and square (Eq. (43)) meshes and

$$e_{conv} = -\frac{b_y (b_y^4 - 1)h^6}{720} \frac{\partial^6 u_{A,B}}{\partial y^6} - \frac{b_y (b_y^4 + 1)(b_y^4 - 8b_y^2 + 1)h^8}{20160} \frac{\partial^8 u_{A,B}}{\partial y^8} + O(h^{10})$$
(44)

and

$$e_{conv}(b_y = 1) = \frac{h^8}{1680} \frac{\partial^8 u_{A,B}}{\partial v^8} + O(h^{10})$$
(45)

for the conventional quadratic rectangular (Eq. (44)) and square (Eq. (45)) isogeometric elements; i.e., the new approach  $Q ext{ 9}\_O PT\_1$  improves the local truncation error in space by ten orders for rectangular elements and by eight orders for square elements. These different improvements in accuracy are explained by the fact (see Eqs. (42)-(45)) that the orders of accuracy are the same for the new  $Q ext{ 9}\_O PT\_1$  stencils on rectangular and square meshes but they are different for the conventional rectangular and square isogeometric elements (the conventional square elements are more accurate compared to the conventional rectangular elements). It is interesting to note that it is possible to develop more accurate 25-point stencils on square meshes. In order to improve the order of the local truncation error in Eq. (39) on square meshes at small  $h \ll 1$ , we equate to zero the first 7 coefficients  $b_p = 0$  (p = 1, 2, 3, ..., 7) and the coefficient  $b_9 = 0$ . In this case for square meshes ( $b_y = 1$ ), the coefficient  $b_8$  will be also zero after the solution of the corresponding system of equations for the coefficients  $k_i$  (i = 1, 2, 3, ..., 9); see below. The solution of the 8 linear algebraic equations  $b_p = 0$  (p = 1, 2, 3, ..., 7, 9) provides the following coefficients  $k_i$  (i = 1, 2, 3, ..., 9) for the new approach  $Q ext{ 9}\_O PT\_2$  on square meshes (in terms of one arbitrary coefficient  $a_1$ ):

$$k_2 = \frac{32a_1(b_y^2 + 4)(4b_y^2 + 1)}{9y_3}[6835568b_y^{16} - 98357880b_y^{14} + 569516043b_y^{12} - 1642477120\\b_y^{10} + 2351066778b_y^8 - 1642477120b_y^6 + 569516043b_y^4 - 98357880b_y^2 + 6835568],\\k_3 = -\frac{8a_1(b_y^2 + 1)(b_y^2 + 4)}{3y_3}[380494644b_y^{16} - 3950564583b_y^{14} + 15033132452b_y^{12}\\-24170522596b_y^{10} + 17293159050b_y^8 - 5959344309b_y^6 + 1165078718b_y^4\\-158704512b_y^2 + 13671136],\\k_4 = \frac{a_1(b_y^2 + 1)^2(b_y^2 + 4)}{36y_3}[3115216b_y^{14} - 26043688b_y^{12} + 75055561b_y^{10} - 95771520b_y^8\\+52708230b_y^6 - 6382196b_y^4 - 3590407b_y^2 + 778804],\\k_5 = -\frac{4a_1(b_y^2 + 1)(b_y^2 + 4)}{9y_3}[778804b_y^{16} - 24576363b_y^{14} + 190632612b_y^{12} - 654628796b_y^{10}\\+1186108650b_y^8 - 1172018969b_y^6 + 602568798b_y^4 - 146695872b_y^2 + 13671136],\\k_6 = \frac{a_1}{6y_3}[1521978576b_y^{20} - 17351608272b_y^{18} + 76872755327b_y^{16} - 164715787152b_y^{14}\\+193939316847b_y^{12} - 137578948912b_y^{10} + 60627164237b_y^8 - 15793920632b_y^6\\+2089789797b_y^4 - 107855032b_y^2 + 3115216],\\k_7 = -\frac{8a_1(b_y^2 + 1)}{3y_3}[54684544b_y^{18} - 621146912b_y^{16} + 4501610360b_y^{14}$$

$$-22672298518b_{y}^{12} + 63213291891b_{y}^{10} - 79388931334b_{y}^{8} + 35962007212b_{y}^{6} - 769125880b_{y}^{4}$$

$$-2428586007b_{y}^{2} + 380494644],$$

$$k_{8} = -\frac{4a_{1}(b_{y}^{2} + 1)}{9y_{3}} [54684544b_{y}^{18} - 573112352b_{y}^{16} + 2263579320b_{y}^{14} - 4085507078b_{y}^{12}$$

$$+3572415631b_{y}^{10} - 1432406534b_{y}^{8} + 107901652b_{y}^{6} + 92327160b_{y}^{4} - 21461147b_{y}^{2} + 778804],$$

$$k_{9} = \frac{a_{1}}{6y_{3}} [3115216b_{y}^{20} - 107855032b_{y}^{18} + 2089789797b_{y}^{16} - 15793920632b_{y}^{14} + 60627164237b_{y}^{12}$$

$$-137578948912b_{y}^{10} + 193939316847b_{y}^{8} - 164715787152b_{y}^{6}$$

$$+76872755327b_{y}^{4} - 17351608272b_{y}^{2} + 1521978576] \tag{46}$$

with

$$y_{3} = 1521978576b_{y}^{20} - 5139284512b_{y}^{18} - 28549593453b_{y}^{16} + 109395021498b_{y}^{14}$$

$$+127446304877b_{y}^{12} - 454742253972b_{y}^{10} + 127446304877b_{y}^{8} + 109395021498b_{y}^{6}$$

$$-28549593453b_{y}^{4} - 5139284512b_{y}^{2} + 1521978576.$$

$$(47)$$

Inserting the coefficients  $k_j$  (j = 1, 2, 3, ..., 9) for the new approach (Eq. (46)) into Eq. (39), we will get the following local truncation error in space e for the new  $Q9_0PT_2$  stencils with improved accuracy:

$$e_{impr} = \frac{a_1(b_y - 1)y_4h^{14}}{505440y_3} \frac{\partial^{14}u_{A,B}}{\partial y^{14}} + \frac{a_1(b_y - 1)y_5h^{18}}{952734182400y_3} \frac{\partial^{18}u_{A,B}}{\partial y^{18}} + \frac{a_1y_6h^{20}}{760281877555200y_3} \frac{\partial^{20}u_{A,B}}{\partial y^{20}} + O(h^{18})$$
 (48)

with

$$\begin{aligned} y_4 &= -b_y^4 (b_y + 1)(b_y^2 + 1)^2 (b_y^2 + 4)(4b_y^2 + 1)(98888(2b_y^2 - 25)b_y^{14} + 12101221b_y^{12} \\ &- 28651300b_y^{10} + 37571006b_y^8 - 28651300b_y^6 + 12101221b_y^4 - 2472200b_y^2 + 197776) \,, \\ y_5 &= b_y^4 (b_y + 1)(b_y^2 + 1)^2 (b_y^2 + 4)(4b_y^2 + 1)(625634704b_y^{20} - 11413084680b_y^{18} + 83518306213b_y^{16} \\ &- 313824069580b_y^{14} + 668108180083b_y^{12} - 853151497480b_y^{10} + 668108180083b_y^8 - 313824069580b_y^6 \\ &+ 83518306213b_y^4 - 11413084680b_y^2 + 625634704) \,, \\ y_6 &= b_y^4 (b_y^2 + 1)^2 (73997862272b_y^{28} - 1339004858400b_y^{26} + 8192438210104b_y^{24} - 11647076272678b_y^{22} \\ &- 82420844080219b_y^{20} + 446001505501362b_y^{18} - 1015267660872157b_y^{16} + 1312698369019432b_y^{14} \\ &- 1015267660872157b_y^{12} + 446001505501362b_y^{10} - 82420844080219b_y^8 - 11647076272678b_y^6 \\ &+ 8192438210104b_y^4 - 1339004858400b_y^2 + 73997862272) \end{aligned}$$

for the new Q9\_OPT\_2 stencils on rectangular meshes and

$$e_{impr}(b_y = 1) = \frac{a_1 h^{20}}{75077835408576} \frac{\partial^{20} u_{A,B}}{\partial v^{20}} + O(h^{22}), \tag{49}$$

for the new  $Q9\_OPT\_2$  stencils on square meshes. As can be seen, the new  $Q9\_OPT\_2$  stencils are less accurate compared to the new  $Q9\_OPT\_1$  stencils in the case of rectangular meshes and are more accurate compared to the new  $Q9\_OPT\_1$  stencils in the case of square meshes. The new  $Q9\_OPT\_2$  stencils on square meshes improve the local truncation error in space by twelve orders compared to that for the conventional square isogeometric elements and yield the maximum order of accuracy among all 25-point stencils (independent of the method used for their derivation).

Let us find the elemental  $K^e$  matrix (see Eq. (27)) that yields the stencil equation (35) with the coefficients  $k_j$  (j = 1, 2, ..., 9) given by Eqs. (40) and (46) for the new  $Q9\_OPT\_1$  and  $Q9\_OPT\_2$  stencils. Similar to the previous section, solving simultaneously a system of linear algebraic equations (29) with the coefficients  $k_j$  (j = 1, 2, ..., 9) for the new  $Q9\_OPT\_1$  and  $Q9\_OPT\_2$  stencils, the coefficients  $f_j$  (j = 1, 2, ..., 17) of the  $K^e$  matrix in Eq. (27) can be found. They are shown in Appendix F and Appendix G, respectively; see Eqs. (E.2) and (G.1).

In Eqs. (F.2) and (G.1)  $a_j$  (j = 1, 2, ..., 6) are six arbitrary coefficients (the first coefficient  $a_1$  is the same as that used in Eqs. (40) and (46) for  $k_j$  (j = 1, 2, ..., 9) of the new approach). The order of the local truncation error is independent of the values of these coefficients. At the derivation of Eqs. (F.2) and (G.1) the additional algebraic equations (31) have been also used.

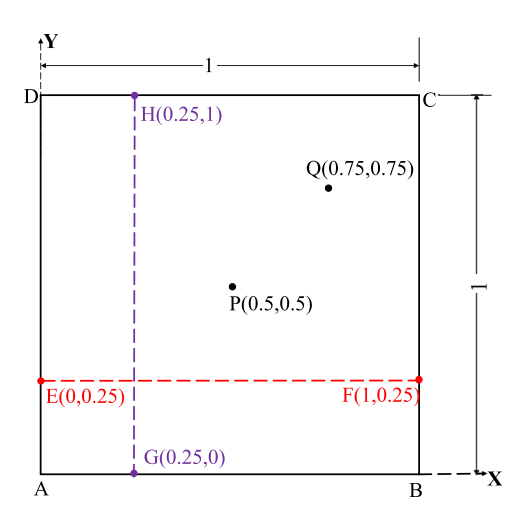


Fig. 1. A plate used for the heat equation and for the Poisson equation in the 2-D case.

#### 3. Numerical examples

In this section the computational efficiency of the 2-D numerical techniques based on the conventional  $Q9\_IGE$  quadratic isogeometric elements with 25-point stencils, the  $Q4\_MIR$  linear finite elements with 9-point stencils based on the MIR technique (e.g., see [12]), the new  $Q9\_OPT$ ,  $Q9\_OPT$ \_1 and  $Q9\_OPT$ \_2 25-point stencils with the optimal order of accuracy will be compared. The test problems with the following analytical solutions u to the heat equation (Eq. (1)):

$$u(x, y, t) = e^{\alpha_2 y - a(\alpha_1^2 - \alpha_2^2)t} \sin(\alpha_1 x)$$
(50)

without heat source,

$$u(x, y, t) = e^{\alpha_2 y + \alpha_3 t} \sin(\alpha_1 x) \quad \text{with} \quad f(x, y, t) = (\alpha_3 - a(\alpha_2^2 - \alpha_1^2))e^{\alpha_2 y + \alpha_3 t} \sin(\alpha_1 x)$$
 (51)

with the heat source, the following analytical solutions u to the Poisson equation (Eq. (2)):

$$u(x, y) = e^{\alpha y} \sin(\alpha x) \tag{52}$$

without heat source and

$$u(x, y) = e^{\alpha_2 y} \sin(\alpha_1 x) \quad \text{with} \quad f(x, y) = (\alpha_2^2 - \alpha_1^2) e^{\alpha_2 y} \sin(\alpha_1 x) \tag{53}$$

with the heat source will be solved in the 2-D case.  $\alpha$ ,  $\alpha_1$ ,  $\alpha_2$  and  $\alpha_3$  in Eqs. (50) - (53) are arbitrary constants which will be defined later and the heat sources f in Eqs. (51) and (53) are obtained by the substitution of the analytical solutions in the corresponding partial differential equations.

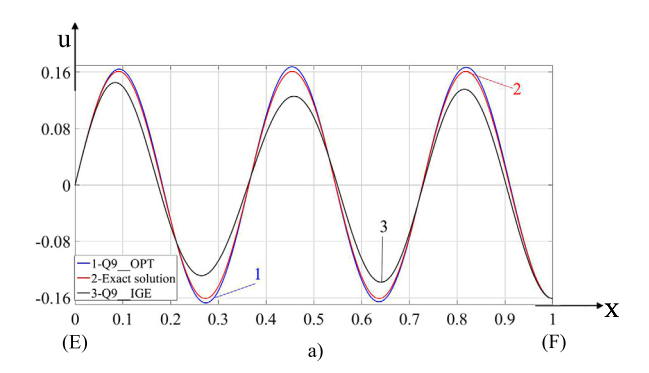
In the numerical examples solved below on meshes with uniformly spaced control points along the x- and y-axes, the element size h is defined as the distance between two consecutive control points along the largest side of 2-D rectangular elements. This means that at the same element aspect ratios, the same sizes h of the linear finite elements and the quadratic isogeometric elements correspond to the same number of degrees of freedom. The high-order boundary conditions developed in [26] are used.

The backward difference method is used for the time integration of the heat equation. A sufficiently small size of time increments is used in calculations. In this case the error in time can be neglected and the numerical error is related to the spatial error.

#### 3.1. 2-D heat equation

Let us consider a square plate *ABCD* of length  $1 \times 1$ ; see Fig. 1. The problem without heat source and the exact solution given by Eq. (50) with a=100,  $\alpha_1=\frac{11\pi}{2}$  and  $\alpha_2=4$  as well as the problem with heat source and the exact solution given by Eq. (51) with a=100,  $\alpha_1=5\pi$ ,  $\alpha_2=4$  and  $\alpha_3=\pi$  are considered. The time intervals are  $0=t_0 \le t \le t_f=0.0001$  and  $0=t_0 \le t \le t_f=1$  for the heat equation without and with heat sources, where  $t_0$  and  $t_f$  are the initial and final times. For these problems, the initial conditions at the corresponding initial times and the boundary conditions in terms of the function u at the boundary are calculated using the exact solutions Eqs. (50) and (51).

Figs. 2 and 3 represent the numerical results obtained by the different techniques on square and rectangular ( $b_y = dy/dx = 0.5$ ) uniform meshes for the heat equation without heat source. The distribution of u at the final time  $t_f$  along



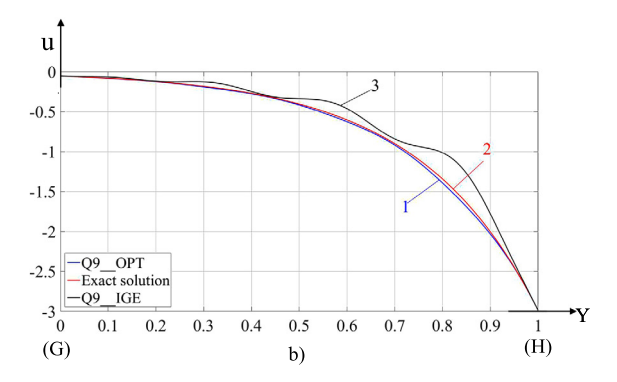


**Fig. 2.** The distribution of u at the final time  $t_f$  along lines EF (a) and GH (b) for the heat equation without heat source; see Fig. 1 for the locations of lines EF and GH. A uniform square mesh with  $9 \times 9 = 81$  degrees of freedom is used. Curve 2 corresponds to the exact solution. Curves 1 and 3 correspond to the numerical results obtained by the new  $Q9_OPT$  stencils and by the conventional  $Q9_IGE$  quadratic isogeometric elements, respectively.

lines EF and GH (see Fig. 1 for the locations of the lines EF and GH) obtained by the different techniques on a square mesh with  $9 \times 9 = 81$  degrees of freedom is shown in Fig. 2. As can be seen from Fig. 2, the new  $Q9\_OPT$  stencils yield much more accurate results than those obtained by the conventional  $Q9\_IGE$  quadratic isogeometric elements; compare curves 1 and 3 with the exact solution, curve 2 in Fig. 2.

In order to compare the accuracy of the different techniques at mesh refinement, Fig. 3 shows the maximum error  $e_{max}$ , the error  $e_P$  at point P and the error  $e_Q$  at point Q (see Fig. 1 for the locations of the points P and Q) as a function of the element size P in the logarithmic scale on square and rectangular uniform meshes. These errors are defined as follows:

$$e_P = |u_P^{num} - u_P^{exact}|; \qquad e_Q = |u_Q^{num} - u_Q^{exact}|; \qquad e_{max} = \max_i |u_i^{num} - u_i^{exact}|, \qquad i = 1, 2, ..., N,$$
 (54)

where  $u_{P(Q)}^{num}$  and  $u_{P(Q)}^{exact}$  are the numerical and exact solutions at point P(Q),  $u_i^{num}$  and  $u_i^{exact}$  are the numerical and exact solutions at the ith control point, and N is the total number of control points. It can be seen from Fig. 3 that the numerical results obtained by the new  $Q9\_OPT$  stencils are much more accurate than those obtained by the  $Q4\_MIR$  linear finite elements and by the conventional  $Q9\_IGE$  quadratic isogeometric elements on square or rectangular uniform meshes with the same element size h; compare curves 1, 2 and 3 in Fig. 3 at the same h. It can be also seen from Fig. 3 that the conventional  $Q9\_IGE$  quadratic elements yield slightly more accurate results than those obtained by the  $Q4\_MIR$  linear elements on square or rectangular uniform meshes with the same element size h.

The orders of accuracy for the techniques considered here are determined by the slope of the curves at small h in Fig. 3. As can be seen from Fig. 3, the  $Q9\_IGE$  and  $Q4\_MIR$  elements show the 4th order of accuracy on square and rectangular uniform meshes; see the slope of the curves 2 and 3 in Fig. 3 at small h. On the other hand, the new  $Q9\_OPT$  stencils show the 8th order of accuracy on square and rectangular uniform meshes as predicted in section 2.1; see curve 1 in Fig. 3. It is interesting to mention that a uniform refinement in one direction (i.e., the transformation of square elements into smaller rectangular elements) does not improve the accuracy for any numerical technique considered here. For example, a uniform refinement in one direction with the new  $Q9\_OPT$  stencils leads to slightly less accurate results; compare curves 1 and 4 in Fig. 3d-f at the same h. However, at the same h the rectangular meshes in Fig. 3 include twice as many degrees of freedom as those for the square meshes. Therefore, it can be concluded that at the same number of degrees of freedom, all the elements considered here yield more accurate results on uniform square meshes compared with those on uniform rectangular meshes.

In order to study the convergence of the new  $Q ext{ 9\_OPT}$  stencils in more detail, Fig. 4 analyzes the convergence of the new approach (curves 1 in Fig. 3a, d) at the gradual decrease of the mesh size  $h = 1/(N_x - 1)$  of the Cartesian grids where  $N_x = 9$ , 10, ..., 33 is the number of the grid points along the x-axis (curve 1 and 2 in Fig. 4 correspond to curve 1 in Fig. 3a and 3d). As can be seen, the results obtained by the new  $Q ext{ 9\_OPT}$  stencils show monotone convergence with the gradual decrease in the mesh size. We should also mention that the detailed study of convergence of the new technique (similar to that in Fig. 4) was also applied to all numerical examples considered in this paper and showed that the new technique yields stable and convergent results.

Similar to the heat equation without heat source, the new  $Q9\_OPT$  stencils for the heat equation with heat source show the 8th order of accuracy on square and rectangular uniform meshes and yield much more accurate results than those obtained by the  $Q4\_MIR$  linear finite elements and by the conventional  $Q9\_IGE$  quadratic isogeometric elements on the same uniform meshes; see curves 1, 2 and 3 in Fig. 5. It can be also seen from Fig. 5 that a uniform refinement in one direction does not improve the accuracy of the numerical results obtained by any numerical technique considered here; compare curves 2 and 3 in Figs. 5a-c and 5d-f as well as curves 1 and 4 in Fig. 5d-f at the same h.

It can be concluded that at the same number of degrees of freedom, the new  $Q \, 9\_O \, PT$  stencils are the most accurate among all the numerical techniques considered and show the 8th order of accuracy on square and rectangular uniform meshes for the 2-D heat equation.

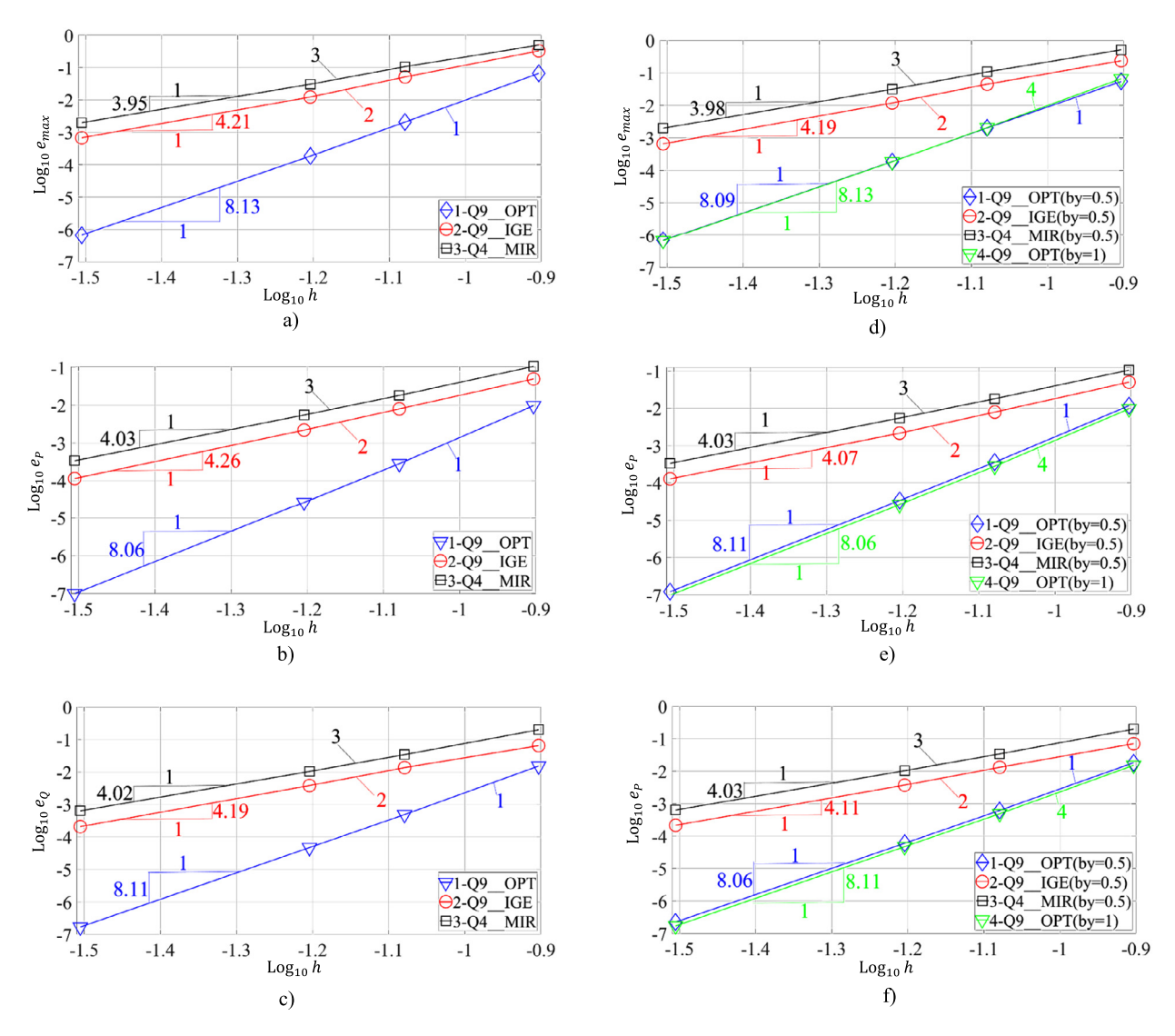


**Fig. 3.** The maximum error  $e_{max}$  (a, d), the error  $e_P$  at point P (b, e) and the error  $e_Q$  at point Q (c, f) as a function of the element size h in the logarithmic scale for the heat equation without heat source; see Fig. 1 for the locations of the points P and Q and Eq. (54) for the definitions of these errors. Curves 1, 2 and 3 correspond to the numerical results on square (a, b, c) and rectangular (d, e, f) uniform meshes with the new  $Q9\_OPT$  stencils, the conventional  $Q9\_IGE$  quadratic isogeometric elements and the  $Q4\_MIR$  linear finite elements, respectively. Rectangular meshes with the aspect ratio  $b_y = 0.5$  are used in (d, e, f). Curve 4 in (d, e, f) corresponds to curve 1 in (a, b, c) for the numerical results obtained by the new  $Q9\_OPT$  stencils on uniform square meshes. Symbols  $\nabla$ ,  $\bigcirc$ ,  $\diamond$  and  $\square$  correspond to the results on the uniform meshes used in calculations.

#### 3.2. 2-D Poisson equation

The same 2-*D* plate from Section 3.1 is considered; see Fig. 1. The problem without heat source and the exact solution given by Eq. (52) with  $\alpha = 5\pi$  as well as the problem with heat source and the exact solution given by Eq. (53) with  $\alpha_1 = \frac{17}{2}\pi$  and  $\alpha_2 = 6\pi$  are numerically solved. The boundary conditions are calculated in terms of *u* using the exact solutions, Eqs. (52) and (53).

Figs. 6-8 represent the numerical results obtained by the different techniques on uniform square and rectangular  $(b_y = dy/dx = 0.5)$  meshes for the Poisson equation without heat source. Fig. 6 shows the distribution of u along lines EF (Fig. 6a, b) and GH (Fig. 6c, d) obtained by the new  $Q9_OPT_2$  stencils and the conventional  $Q9_IGE$  quadratic isogeometric elements on a uniform square mesh with  $5 \times 5 = 25$  degrees of freedom; see Fig. 1 for the locations of the line lines EF and GH. As can be seen from Fig. 6 the results obtained by the conventional  $Q9_IGE$  isogeometric elements are very inaccurate; compare curves 2 and 3 in Fig. 6a, c. On the other hand, the new  $Q9_OPT_2$  stencils yield accurate results. In order to show the difference between the results obtained by the new  $Q9_OPT_2$  stencils and the exact solution, Fig. 6b, d does not include the results obtained by the conventional  $Q9_IGE$  isogeometric elements. It can be seen that even for this

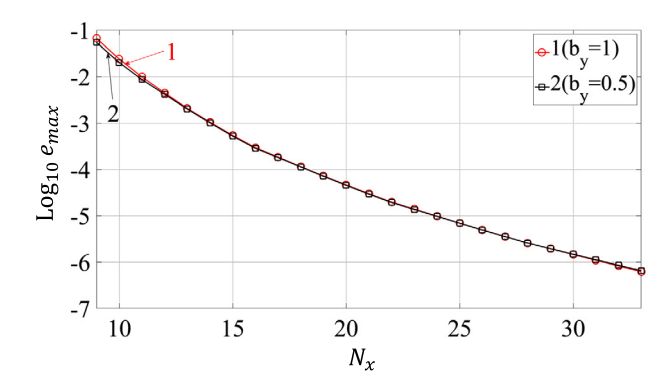


**Fig. 4.** The maximum error  $e_{max}$  in the logarithmic scale at the final time T = 0.0001 as a function of the number  $N_x$  of the grid points along the x-axis  $(N_x = 9, 10, ..., 33)$ . The numerical solutions of the 2-D heat equation with zero heat source are obtained by the new  $Q.9_OPT$  stencils on uniform square (curve 1) and rectangular (curve 2) Cartesian meshes. Symbols  $\bigcirc$  and  $\square$  correspond to the results on the uniform meshes used in calculations.

coarse mesh, the results obtained by the new  $Q9_0PT_2$  stencils are close to the exact solution; compare curves 1 and 2 in Fig. 6b, d.

Similar to the Section 3.1, the maximum error  $e_{max}$ , the error  $e_P$  at point P and the error  $e_Q$  at point Q (see Fig. 1 for the locations of the points P and Q and Eq. (54) for the definitions of these errors) are shown in Fig. 7. The slope of the curves in Figs. 7 and 8 at small h is related to the order accuracy of the corresponding numerical techniques. It can be seen that the order of accuracy is six for the  $Q4\_MIR$  linear finite elements and the  $Q9\_IGE$  quadratic isogeometric elements on uniform square meshes and it is four for these elements on uniform rectangular meshes; see the slope of the curves 3 and 4 at small h in Fig. 7. As can be seen from Fig. 7 the new  $Q9\_OPT\_1$  stencils show the 14th order of accuracy on square and rectangular uniform meshes. On the other hand, the new  $Q9\_OPT\_2$  stencils show the 18th order of accuracy on uniform square meshes. The accuracy reduces to the 12th order on uniform rectangular meshes for the new  $Q9\_OPT\_2$  stencils; see the slope of the curve 2 at small h in Fig. 7. These observations are in agreement with the theoretical results obtained in Section 2.2.

The results obtained by the Q4\_MIR linear finite elements are slightly more accurate than those obtained by the Q9\_IGE quadratic isogeometric elements on uniform square meshes; see curves 3 and 4 in Fig. 7a-c as well as curves 1 and 2 in Fig. 8b. On uniform square meshes the results obtained by the new  $Q9_OPT_1$  stencils are less accurate than those obtained by the new Q9\_OPT\_2 stencils, however, they are much more accurate than those obtained by the Q4\_MIR linear finite elements and by the conventional  $Q9\_IGE$  quadratic elements; compare curves 1-4 in Fig. 7a-c at the same h. From the above observation it can be concluded that the new Q9\_OPT\_2 stencils yield the most accurate results among all the numerical techniques considered on uniform square meshes. A uniform refinement in one direction does not improve the accuracy of the results for any numerical technique considered here. For example, the results obtained by the new  $Q9_{-}OPT_{-}1$  stencils on square and rectangular uniform meshes are practically same at mesh refinement; compare curves 1 and 3 at small h in Fig. 8a. However, at the same element size h, the rectangular meshes include twice as many degrees of freedom as those for the square meshes. Therefore, it can be concluded that at the same number of degrees of freedom, uniform square meshes yield more accurate results than those on uniform rectangular meshes for any numerical technique considered here. It is interesting to note that the results obtained by the conventional Q9\_IGE quadratic isogeometric elements are slightly more accurate than those obtained by the Q 4\_MIR linear finite elements on uniform rectangular meshes; see curves 3 and 4 in Fig. 7d-f as well as curves 3 and 4 in Fig. 8b. In contrast to the results on the uniform square meshes, the results obtained by the new  $Q = QPT_2$  stencils on the uniform rectangular meshes with the aspect ratio  $b_v = 0.5$ are less accurate than those obtained by the new Q9\_OPT\_1 stencils; compare curves 1 and 2 in Fig. 7d-f at the same h. However, these results are much more accurate than those obtained by the Q4\_MIR linear finite elements and by the conventional  $Q9\_IGE$  quadratic isogeometric elements; compare curves 2-4 in Fig. 7d-f at the same h.

Similar numerical results have been obtained for the Poisson equation with heat source; see Fig. 9. At any element size h, the new  $Q ext{ 9_O} PT ext{ 2}$  stencils yield the most accurate results on uniform square meshes while the new  $Q ext{ 9_O} PT ext{ 1}$  stencils can yield the most accurate results on uniform rectangular meshes with the selected aspect ratio  $b_y = 0.5$  among all the numerical techniques considered; compare curves 1, 2 and 3 in Fig. 9. It can be also seen from Fig. 9 that the orders of accuracy for the considered techniques are same for zero and non-zero heat source; see the slope of the curves at small h in Figs. 7 and 9.

It can be concluded that among all the numerical techniques considered the new  $Q9\_OPT\_2$  stencils are the most accurate on uniform square meshes and yield the 18th order of accuracy. However, the order of accuracy of these elements is significantly lower on rectangular meshes and is twelve (it is still much higher than that for the conventional  $Q9\_IGE$  quadratic isogeometric elements on the square meshes). The new  $Q9\_OPT\_1$  stencils show the 14th order of accuracy on square and rectangular uniform meshes. It is interesting to mention that if the aspect ratio differs significantly from unity, then the new  $Q9\_OPT\_1$  stencils may yield more accurate results than those obtained by the new  $Q9\_OPT\_2$  stencils on the same rectangular meshes. However, at the same number of degrees of freedom, the new  $Q9\_OPT\_2$  stencils on uniform

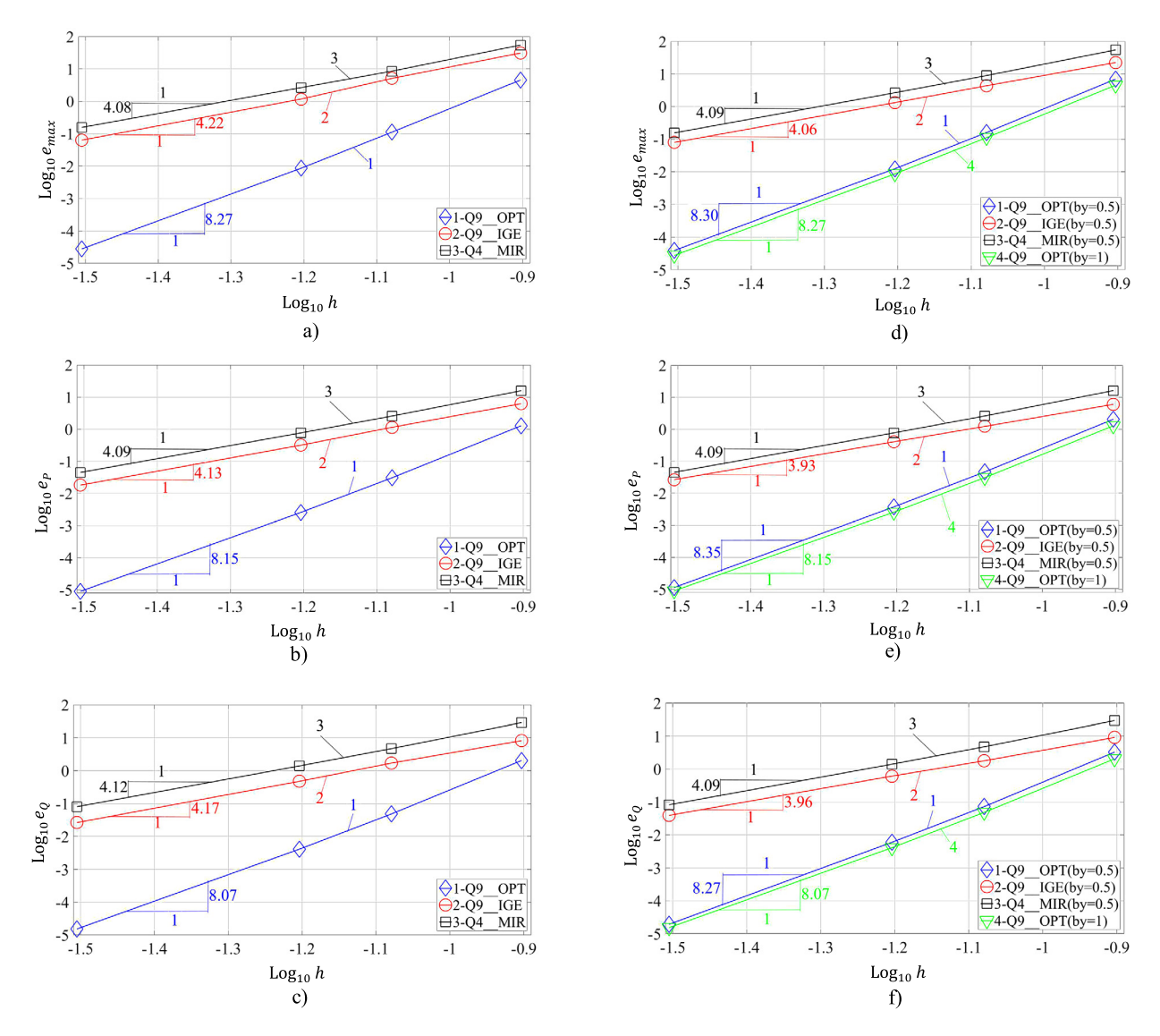


**Fig. 5.** The maximum error  $e_{max}$  (a, d), the error  $e_P$  at point P (b, e) and the error  $e_Q$  at point Q (c, f) as a function of the element size h in the logarithmic scale for the heat equation with heat source; see Fig. 1 for the locations of the points P and Q and Eq. (54) for the definitions of these errors. Curves 1, 2 and 3 correspond to the numerical results on square (a, b, c) and rectangular (d, e, f) uniform meshes with the new  $Q9\_OPT$  stencils, the conventional  $Q9\_IGE$  quadratic isogeometric elements and the  $Q4\_MIR$  linear finite elements, respectively. Rectangular meshes with the aspect ratio  $b_y = 0.5$  are used in (d, e, f). Curve 4 in (d, e, f) corresponds to curve 1 in (a, b, c) for the numerical results obtained by the new  $Q9\_OPT$  stencils on uniform square meshes. Symbols  $\nabla$ ,  $\bigcirc$ ,  $\diamond$  and  $\square$  correspond to the results on the uniform meshes used in calculations.

square meshes yield more accurate results than those obtained by the new  $Q9\_OPT\_1$  stencils on square or rectangular uniform meshes.

#### 3.3. A hybrid method: the combination of the conventional quadratic isogeometric or finite elements with the new 25-point stencils

In this section we will show that the new 25-point stencils developed in the paper can be easily combined with the conventional quadratic isogeometric or finite elements and form a hybrid method. The hybrid method can be applied to irregular domains using special meshes. For example, an irregular domain can be partly discretized by Cartesian meshes located far from the boundary of the irregular domain and by the conventional irregular isogeometric or finite element meshes located close to the boundary. Because our Matlab code does not have mesh generators for irregular domains, we will show the application of the hybrid method on a regular domain. Its application on irregular domains with the special meshes is trivial as described above.

Let us consider a square plate  $1 \times 1$  shown in Fig. 10. Here, we solve the heat equation with the exact solution given by Eq. (50) and the Poisson equation with the exact solution given by Eq. (52). These problems are solved by the conventional quadratic isogeometric and finite elements and by two hybrid methods on square Cartesian meshes. The hybrid method

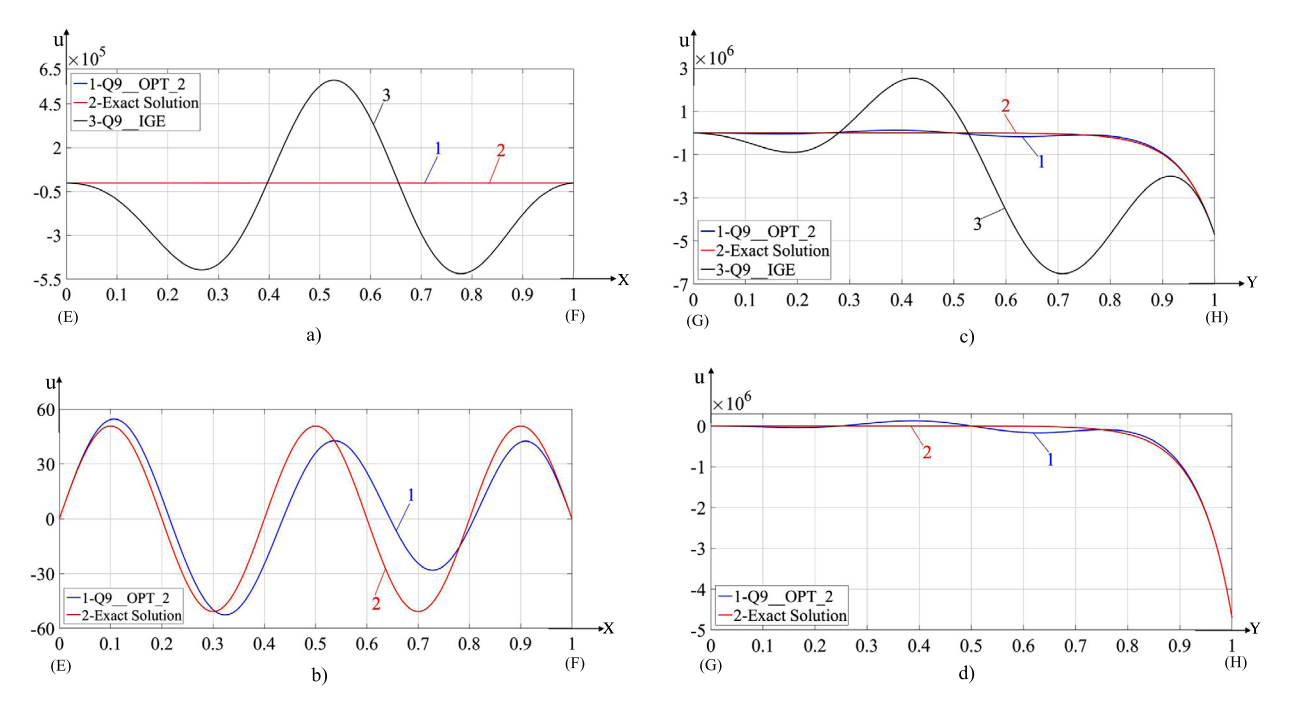


**Fig. 6.** The distribution of u along lines EF (a, b) and GH (c, d) for the Poisson equation without heat source; see Fig. 1 for the locations of lines EF and GH. A uniform square mesh with  $5 \times 5 = 25$  degrees of freedom is used. Curve 2 corresponds to the exact solution. Curves 1 and 3 correspond to the numerical results obtained by the new  $Q9_OPT_2$  stencils and the conventional  $Q9_IGE$  quadratic isogeometric elements, respectively. (b, d) zoom (a, c) along the y-axis and do not include curve 3.

**Table 2**The comparison of the maximum errors  $e_{max}$  obtained by the conventional quadratic isogeometric and finite elements and by the hybrid methods for the heat equation.

h	$e_{max}$		Accuracy $e_{max}$ increase by a		nax	Accuracy increase by a
	Quadratic IGE	Hybrid method I	factor of	Quadratic FE	Hybrid method II	factor of
1/8	0.3292	0.0661	4.98	3.2062	0.4217	7.59
1/16	0.0123	0.0018	6.83	0.1259	0.0183	6.88
1/32	6.7867e-04	1.0213e-04	6.65	0.0099	0.0015	6.6

**Table 3** The comparison of the maximum errors  $e_{max}$  obtained by the conventional quadratic isogeometric and finite elements and by the hybrid methods for the Poisson equation.

h	$e_{max}$		Accuracy $e_{max}$ increase by a		nax	Accuracy
n	Quadratic IGE	Hybrid method I	factor of	Quadratic FE	Hybrid method II	factor of
1/8	9.2532e+04	35.2808	2622	1.6496e+06	654.1970	2521
1/16	1.1367e+03	0.4703	2417	6.5433e+04	30.7845	2125
1/32	12.1263	0.0066	1837	3.9793e+03	2.5227	1577

I combines the new 25-point stencils with the conventional quadratic isogeometric elements while the hybrid method II combines the new 25-point stencils with the conventional quadratic finite elements. The hybrid methods can be easily constructed as follows. First we form the semidiscrete (Eq. (3) for the heat equation) or discrete (Eq. (4) for the Poisson equation) global equations for the conventional isogeometric or finite elements. Then, we replace the stencils equations of the conventional elements for the grid points in the upper half of the plate  $(0.5 < y \le 1)$  by the new 25-point stencils; see Fig. 10b, d. The new  $Q9_OPT_2$  stencils are used in the hybrid methods for the Poisson equation because they have the optimal 18th order of accuracy on square Cartesian meshes.

The accuracy of the results obtained by the conventional quadratic isogeometric and finite elements as well as by the hybrid methods I and II are reported in Table 2 for the heat equation and in Table 3 for the Poisson equation. As can be seen, the use of the hybrid methods for the heat equation reduces the maximum error  $e_{max}$  by a factor of 5 and more compared

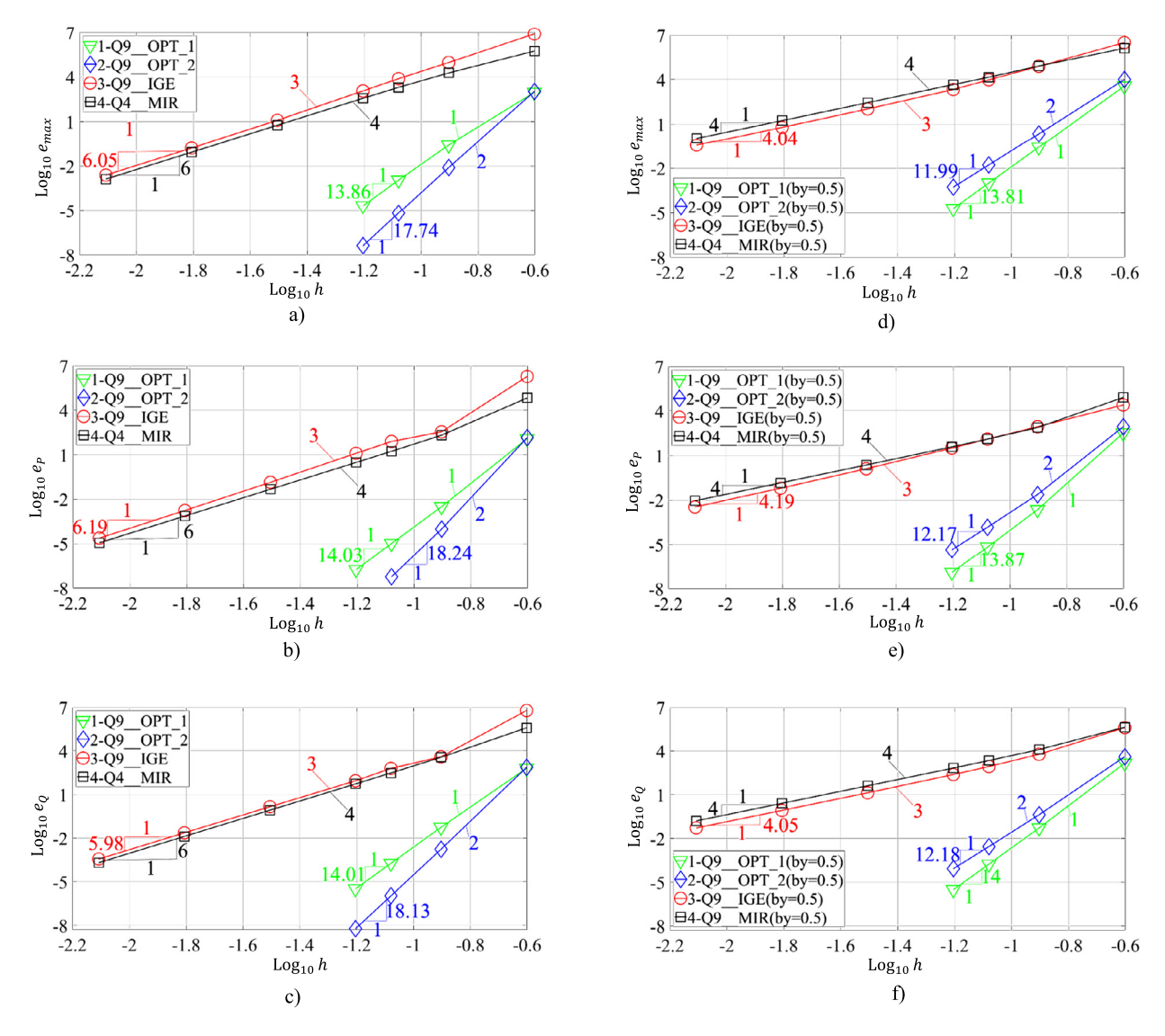


**Fig. 7.** The maximum error  $e_{max}$  (a, d), the error  $e_P$  at point P (b, e) and the error  $e_Q$  at point Q (c, f) as a function of the element size h in the logarithmic scale for the Poisson equation without heat source; see Fig. 1 for the locations of the points P and Q and Eq. (54) for the definitions of these errors. Curves 1, 2, 3 and 4 correspond to the numerical results on square (a, b, c) and rectangular (d, e, f) uniform meshes with the new  $Q9_OPT_1$  and  $Q9_OPT_2$  stencils and the conventional  $Q9_IGE$  quadratic isogeometric elements and the  $Q4_MIR$  linear finite elements, respectively. Rectangular meshes with the aspect ratio  $b_y = 0.5$  are used in (d, e, f). Symbols  $\nabla$ ,  $\bigcirc$ ,  $\diamond$  and  $\square$  correspond to the results on the uniform meshes used in calculations.

to that for the conventional isogeometric or finite elements for all considered meshes; see the accuracy improvement in Table 2. In the case of the Poisson equation, the reduction of the maximum error  $e_{max}$  obtained by the hybrid methods is more than 1000 times; see Table 3. This means that the hybrid methods with the new 25-point stencils can significantly improve the accuracy of numerical solutions. For the considered problems, the maximum error for the solutions obtained by the conventional quadratic isogeometric elements or by the conventional quadratic finite elements occurs in the upper part of the domain. Therefore, the use of the hybrid method with highly accurate stencils in the upper part of the domain is partly similar to the improvement in accuracy due to p-refinement.

#### 4. Concluding remarks

The new findings of the paper can be summarized as follows:

• A new approach for the increase in the order of accuracy of the 25-point stencils used for the time dependent heat equation and for the time independent Poisson equation has been suggested. It is based on the optimization of the coefficients of the corresponding discrete stencil equation with respect to the local truncation error. The accuracy of the conventional quadratic isogeometric elements is improved by four orders for the heat equation and by twelve orders for

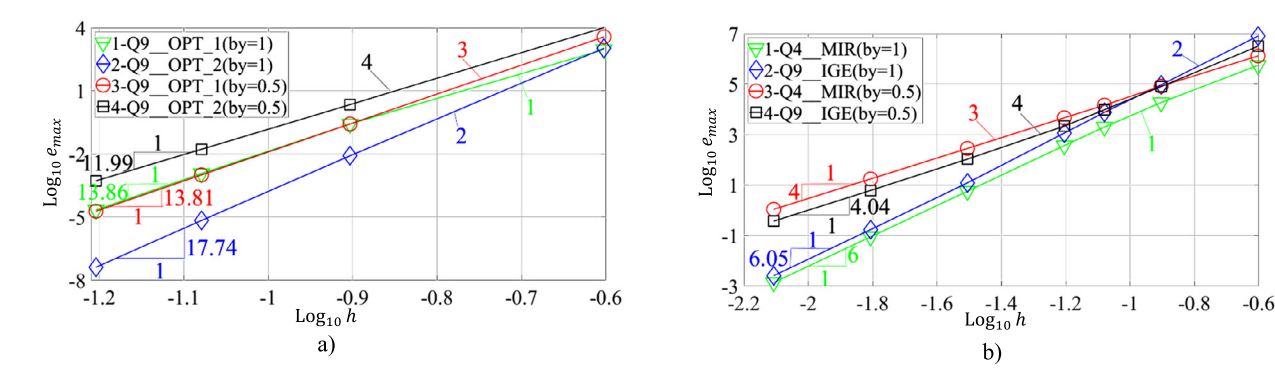


**Fig. 8.** The comparison of the maximum error  $e_{max}$  on square and rectangular uniform meshes using the curves from Fig. 7a, d. Curves (1, 2) and (3,4) correspond to the numerical results on the square and rectangular ( $b_y = 0.5$ ) uniform meshes. Curves (1, 3) and (2, 4) in (a) correspond to the new  $Q9\_OPT\_1$  and  $Q9\_OPT\_2$  stencils, respectively. Curves (1, 3) and (2, 4) in (b) correspond to the  $Q4\_MIR$  linear finite elements and the conventional  $Q9\_IGE$  quadratic isogeometric elements, respectively.

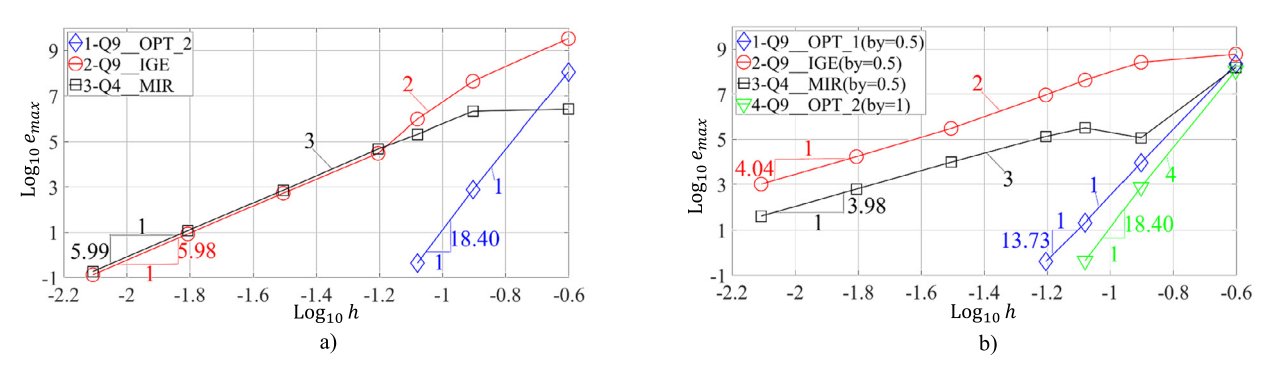


**Fig. 9.** The maximum error  $e_{max}$  as a function of the element size h in the logarithmic scale for the Poisson equation with heat source; see Eq. (54) for the definition of  $e_{max}$ . Curves 2 and 3 correspond to the numerical results on the square (a) and rectangular (b) uniform meshes with the conventional  $Q9\_IGE$  quadratic isogeometric elements and the  $Q4\_MIR$  linear finite elements, respectively. Curves 1 in (a) and 4 in (b) are the same and correspond to the numerical results on uniform square meshes with the new  $Q9\_OPT\_2$  stencils. Curve 1 in (b) corresponds to the numerical results on uniform rectangular meshes with the new  $Q9\_OPT\_1$  stencils. Rectangular meshes with the aspect ratio  $b_y = 0.5$  are used in (b). Symbols  $\nabla$ ,  $\bigcirc$ ,  $\diamond$  and  $\square$  correspond to the results on the uniform meshes used in calculations.

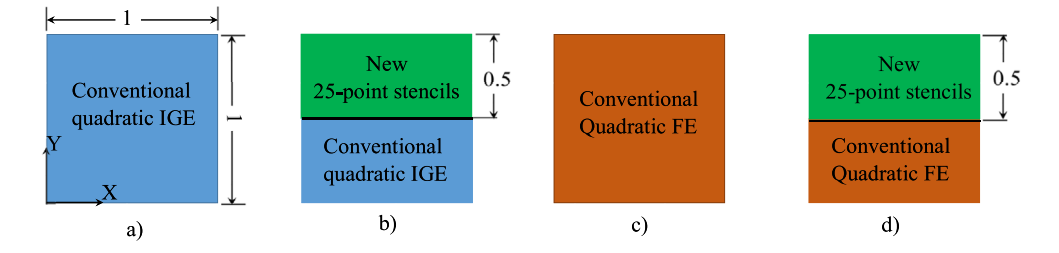


**Fig. 10.** The conventional and hybrid methods applied to the solution of the heat and Poisson equations for a plate. (a) the conventional quadratic isogeometric elements, (b) the hybrid method I, (c) the conventional quadratic finite elements, (d) the hybrid method II.

the Poisson equation. This increase in the order of accuracy of the 25-point stencils is optimal. The new approach yields the maximum possible order of accuracy among all numerical techniques with the same 25-point stencil equations independent of the method used for the derivation of discrete or semidiscrete equations. This optimal order of accuracy cannot be improved without changing the widths of stencil equations.

- Despite the significant increase in accuracy, the computational costs of the new technique are the same as those for the conventional quadratic isogeometric elements on a given mesh. Because the new approach only changes the values of the coefficients of the stencils equations without changing their widths then all known direct and iterative solvers can be used for the solution of the discrete or semidiscrete equations of the proposed technique.
- It is necessary to mention that for the time dependent heat equation the increase in the order of accuracy of the quadratic isogeometric elements is the same as the increase in the order of the numerical dispersion error for the wave equation with the new technique suggested in our recent papers [23,24]. However, the approach suggested in this paper

and based on the optimization of the local truncation error for high-order stencils is more general and can be used for any order of the time derivative in the heat equation; i.e., it can be directly applied to the wave equation as well. In contrast to our papers [23,24], the results of this paper are also extended to rectangular meshes as well as to a new class of the partial differential equations with non-zero right hand-side function (heat sources).

- For the time independent Poisson equation, the new approach yields a huge increase in the order of accuracy compared with that for the conventional quadratic isogeometric elements. The maximum increase in accuracy by twelve orders can be achieved by the new approach on uniform square meshes. On uniform rectangular meshes the maximum increase in accuracy by ten orders is also very large. This huge increase in accuracy does not require additional computational costs compared with those for the conventional quadratic isogeometric elements. We should mention that for the Poisson equation, the accuracy of the conventional quadratic isogeometric elements on square meshes is also greater (by two orders) than that on rectangular meshes.
- A mesh refinement of square meshes in one direction (i.e., transforming square elements into smaller rectangular elements) for the Poisson equation leads to the decrease in the order of accuracy of the new Q9\_OPT\_2 technique and this should be taken into account at the selection of a refinement strategy.
- Despite a higher accuracy of the conventional quadratic isogeometric elements, the new 25-point stencils with improved accuracy yield much more accurate results compared with those obtained by the conventional quadratic isogeometric elements at the same number of degrees of freedom. Even at a sufficient coarse mesh, the temperature calculated by the new approach is close to the exact solution. Therefore, we hope that the new elements with relatively coarse meshes may be efficient for the numerical analysis of thick and thin structures.
- The 2-D numerical examples are in a good agreement with the theoretical results for the new approach.
- The hybrid methods based on the new 25-point stencils can significantly improve the accuracy of numerical solutions.

Currently, the new technique has been developed for uniform square and rectangular meshes that can be used for rectangular domains. One option to use it for complex geometries is to form a hybrid method with unstructured meshes close to curvilinear boundaries and structured meshes inside the domain; e.g., similar to [31,32] with the finite elements for unstructured meshes and the finite difference method for structured meshes. It was shown in the paper that the new approach can be easily combined with the conventional isogeometric and finite elements in order to form a hybrid method. Similarly, it can be directly used with the overlapping elements (see [33,34]), with the known hybrid schemes (e.g., see [35,36] and many others) or the fictitious domain methods (e.g., see [37–46] and many others) where Cartesian meshes can be used inside irregular domains. However, we plan to extend the new approach for PDEs to complex irregular geometries similar to our technique with simple stencils (that correspond to the linear finite elements) where Cartesian meshes and non-uniform stencils for the grid points close to irregular boundaries are used; see our recent papers [47–49]. The techniques in [47–49] are also based on the minimization of the local truncation error.

The idea of the application of the local truncation error for the analysis and increase in accuracy of the numerical technique used in the paper is general. Its possible application to other cases (other partial differential equations, other numerical techniques, general non-uniform meshes, etc.) will be considered in the future.

#### **Declaration of competing interest**

The authors declare that they have no known competing financial interests or personal relationships that could have appeared to influence the work reported in this paper.

#### Acknowledgements

The research has been supported in part by the NSF grant CMMI-1935452 and by Texas Tech University.

# Appendix A. The structure of the elemental $M^e$ and $K^e$ matrices for the quadratic isogeometric elements on uniform meshes

Here, uniform meshes with uniform spacing in the x and y directions are considered. Fig. 11 shows the spatial locations of 25 degrees of freedom (or more precisely, the basis functions related to the corresponding control variables) for  $3 \times 3 = 9$  neighboring elements contributing to the formation of the 25-point stencil equation for the degree of freedom  $u_{A,B}$  with the conventional quadratic isogeometric elements. For the new 25-point stencils, the form of the stencil equation is the same as that for the conventional quadratic isogeometric elements in [27,30]. To simplify the representation of the elemental  $M^e$  or  $K^e$  matrices, let us use the following order of the degrees of freedom in the local vector of the control variables for any element:  $U = \{u_{A-1,B-1}, u_{A-1,B+1}, u_{A+1,B+1}, u_{A+1,B-1}, u_{A-1,B}, u_{A,B+1}, u_{A+1,B}, u_{A,B-1}, u_{A,B}\}^T$  (here, the degrees of freedom for the central element in Fig. 11 are used). In this case the elemental  $M^e$  or  $K^e$  matrix can be expressed in terms of 17 coefficients  $a_i$  as shown below in Eq. (A.1):

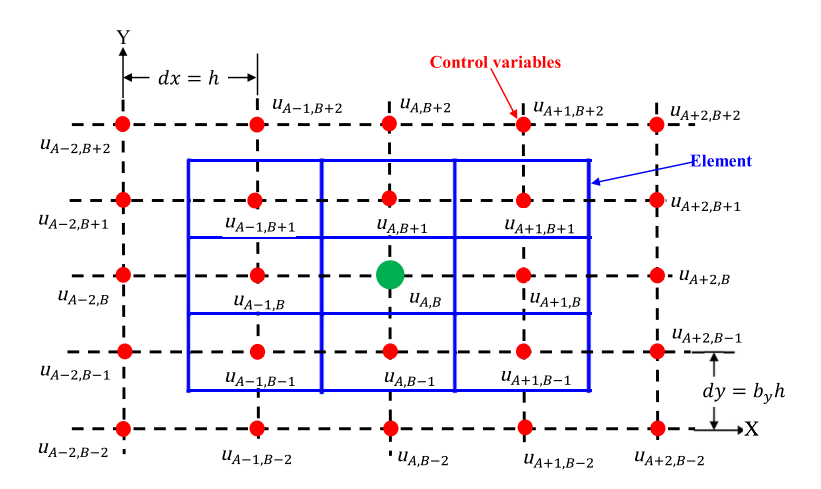


**Fig. 11.** The spatial locations of the degrees of freedom  $u_{i,j}$  (i = A - 2, A - 1, A, A + 1, A + 2 and j = B - 2, B - 1, B, B + 1, B + 2) contributing to the stencil equation for the degree of freedom  $u_{A,B}$  of the new and conventional quadratic isogeometric elements. The nine elements shown are used for the calculation of the stencil equation for the degree of freedom  $u_{A,B}$  according to Eq. (5).

$$\boldsymbol{M}^{e}(\text{or }\boldsymbol{K}^{e}) = \begin{pmatrix} a_{1} & a_{2} & a_{3} & a_{4} & a_{5} & a_{6} & a_{7} & a_{8} & a_{9} \\ a_{2} & a_{1} & a_{4} & a_{3} & a_{5} & a_{8} & a_{7} & a_{6} & a_{9} \\ a_{3} & a_{4} & a_{1} & a_{2} & a_{7} & a_{8} & a_{5} & a_{6} & a_{9} \\ a_{4} & a_{3} & a_{2} & a_{1} & a_{7} & a_{6} & a_{5} & a_{8} & a_{9} \\ a_{5} & a_{5} & a_{7} & a_{7} & a_{10} & a_{11} & a_{12} & a_{11} & a_{13} \\ a_{6} & a_{8} & a_{8} & a_{6} & a_{11} & a_{14} & a_{11} & a_{15} & a_{16} \\ a_{7} & a_{7} & a_{5} & a_{5} & a_{12} & a_{11} & a_{10} & a_{11} & a_{13} \\ a_{8} & a_{6} & a_{6} & a_{8} & a_{11} & a_{15} & a_{11} & a_{14} & a_{16} \\ a_{9} & a_{9} & a_{9} & a_{9} & a_{13} & a_{16} & a_{13} & a_{16} & a_{17} \end{pmatrix}.$$

$$(A.1)$$

Here, the symmetry of matrices  $\mathbf{M}^e$  and  $\mathbf{K}^e$  as well as the symmetry of the location of the first and second four degrees of freedom in vector  $\mathbf{U}$  have been taken into account (therefore the first and second four rows in Eq. (A.1) include the same coefficients). For the implementation of the matrices  $\mathbf{M}^e$  and  $\mathbf{K}^e$  into computer codes, the following order of degrees of freedom in the local vector of the control variables is often used:  $\mathbf{U} = \{u_{A-1,B-1}, u_{A-1,B}, u_{A-1,B+1}, u_{A,B-1}, u$ 

### Appendix B. Non-zero heat source

The inclusion of non-zero heat source f in the partial differential equations, Eqs. (1) and (2), leads to the additional non-zero term  $\bar{f}$  in the stencil equations (15) and (35) (similar to Eq. (7)). The expression for the term  $\bar{f}$  can be calculated from the procedure used for the derivation of the local truncation error in the case of zero heat source. We will show this in more detail for 2-D transient problem and will present the final expressions  $\bar{f}$  for the Poisson equation. In case of non-zero heat source ( $f(x,t) \neq 0$ ), Eqs. (18) and (19) for the exact solution at  $x = x_A$  and  $y = y_B$  can be modified as follows:

$$\frac{\partial u_{A,B}}{\partial t} - a\nabla^2 u_{A,B} = f(x_A, y_B, t), \tag{B.1}$$

$$\frac{\partial^{(2i+2j+1)} u_{A,B}}{\partial x^{2i} \partial y^{2j} \partial t} - a \frac{\partial^{(2i+2j)} \nabla^2 u_{A,B}}{\partial x^{2i} \partial y^{2j}} = \frac{\partial^{(2i+2j)} f(x_A, y_B, t)}{\partial x^{2i} \partial y^{2j}}. \tag{B.2}$$

Then, inserting Eqs. (16), (17), (B.1) and (B.2) with the exact solution to the heat equation, Eq. (1), into the stencil equation, Eq. (15), with non-zero  $\bar{f}$  we will get the following local truncation error in space  $e_f$ :

$$e_{f} = e - \{\bar{f} - [h^{2}f_{A,B}(m_{1} + 2(2m_{2} + m_{3} + 2m_{4} + 2m_{5} + m_{6} + m_{7} + 2m_{8} + m_{9})) + h^{4}(b_{y}^{2} \frac{\partial^{2}f_{A,B}}{\partial y^{2}}(2m_{2} + 8m_{4} + 8m_{5} + m_{7} + 2m_{8} + 4m_{9}) + \frac{\partial^{2}f_{A,B}}{\partial x^{2}}(2m_{2} + m_{3} + 8m_{4} + 2m_{5} + 4m_{6} + 8m_{8})) + \dots]\},$$
 (B.3)

where e is the local truncation error in space given by Eq. (20) for zero heat source,  $f_{A,B}$  in Eq. (B.3) designates function f(x, y, t) and its derivatives calculated at  $x = x_A$  and  $y = y_B$ . Equating to zero the expression in the curly brackets in the right-hand side of Eq. (B.3), we will get the expression for  $\bar{f}$ :

$$\begin{split} \bar{f} &= h^2 f_{A,B} (m_1 + 2(2m_2 + m_3 + 2m_4 + 2m_5 + m_6 + m_7 + 2m_8 + m_9)) \\ h^4 [b_y^2 \frac{\partial^2 f_{A,B}}{\partial y^2} (2m_2 + 8m_4 + 8m_5 + m_7 + 2m_8 + 4m_9) + \frac{\partial^2 f_{A,B}}{\partial x^2} (2m_2 + m_3 + 8m_4 + 2m_5 + 4m_6 + 8m_8)] \\ &+ \frac{h^6}{12} [b_y^4 \frac{\partial^4 f_{A,B}}{\partial y^4} (2m_2 + 32m_4 + 32m_5 + m_7 + 2m_8 + 16m_9) + 12b_y^2 \frac{\partial^4 f_{A,B}}{\partial x^2 \partial y^2} (m_2 + 4(4m_4 + m_5 + m_8)) \\ &+ \frac{\partial^4 f_{A,B}}{\partial x^4} (2m_2 + m_3 + 32m_4 + 2m_5 + 16m_6 + 32m_8)] \\ &+ \frac{h^8}{360} [b_y^6 \frac{\partial^6 f_{A,B}}{\partial y^6} (2m_2 + 128m_4 + 128m_5 + m_7 + 2m_8 + 64m_9) + 30b_y^4 \frac{\partial^6 f_{A,B}}{\partial x^2 \partial y^4} (m_2 + 64m_4 + 16m_5 + 4m_8) \\ &+ 30b_y^2 \frac{\partial^6 f_{A,B}}{\partial x^4 \partial y^2} (m_2 + 64m_4 + 4m_5 + 16m_8) + \frac{\partial^6 f_{A,B}}{\partial x^6} (2m_2 + m_3 + 2(64m_4 + m_5 + 32m_6 + 64m_8))] \\ &+ \frac{h^{10}}{20160} [b_y^8 \frac{\partial^8 f_{A,B}}{\partial y^8} (2m_2 + 512m_4 + 512m_5 + m_7 + 2m_8 + 256m_9) + 56b_y^6 \frac{\partial^8 f_{A,B}}{\partial x^2 \partial y^6} (m_2 + 256m_4 + 64m_5 + 4m_8) + 140b_y^4 \frac{\partial^8 f_{A,B}}{\partial x^4 \partial y^4} (m_2 + 16(16m_4 + m_5 + m_8)) + 56b_y^2 \frac{\partial^8 f_{A,B}}{\partial x^6 \partial y^2} (m_2 + 256m_4 + 4m_5 + 64m_8) + \frac{\partial^8 f_{A,B}}{\partial x^8} (2m_2 + m_3 + 512m_4 + 2m_5 + 256m_6 + 512m_8)] + \dots \end{split}$$
 (B.4)

as well as we will get the same local truncation errors  $e_f = e$  for zero and non-zero heat source. Similar to the 2-D transient problems, the term  $\bar{f}$  can be calculated for the 2-D Poisson equation:

$$\begin{split} \bar{f} &= h^2(2k_2 + k_3 + 8k_4 + 2k_5 + 4k_6 + 8k_8)f_{A,B} \\ &+ \frac{h^4}{12} \big[ \frac{\partial^2 f_{A,B}}{\partial y^2} (b_y^2 (192k_4 + 48k_5 + 48k_8) + 2(6b_y^2 - 1)k_2 - k_3 - 32k_4 - 2k_5 - 16k_6 - 32k_8) \\ &+ \frac{\partial^2 f_{A,B}}{\partial x^2} (2k_2 + k_3 + 32k_4 + 2k_5 + 16k_6 + 32k_8) \big] \\ &+ \frac{h^6}{360} \big[ \frac{\partial^4 f_{A,B}}{\partial y^4} ((30b_y^4 - 30b_y^2 + 2)k_2 + k_3 + 2(b_y^4 (240k_5 + 60k_8) + b_y^2 (-60k_5 - 240k_8) + 64(15b_y^4 - 15b_y^2 + 1)k_4 + k_5 + 32k_6 + 64k_8)) \big] \\ &+ \frac{\partial^4 f_{A,B}}{\partial x^2 \partial y^2} ((30b_y^2 - 2)k_2 - k_3 + 2(b_y^2 (960k_4 + 60k_5 + 240k_8) - 64k_4 - k_5 - 32k_6 - 64k_8)) \big] \\ &+ \frac{h^8}{20160} \big[ \frac{\partial^6 f_{A,B}}{\partial y^6} (b_y^6 (14336k_4 + 3584k_5 + 224k_8) + b_y^4 (-35840k_4 - 2240k_5 - 2240k_5 - 2240k_8) + b_y^2 (14336k_4 + 224k_5 + 3584k_8) \\ &+ 2(28b_y^6 - 70b_y^4 + 28b_y^2 - 1)k_2 - k_3 - 512k_4 - 2k_5 - 256k_6 - 512k_8) \\ &+ \frac{\partial^6 f_{A,B}}{\partial x^2 \partial y^4} (2(70b_y^4 - 28b_y^2 + 1)k_2 + k_3 \\ &+ 2(256(70b_y^4 - 28b_y^2 + 1)k_4 + (1120b_y^4 - 112b_y^2 + 1)k_5 + 32(4k_6 + (35b_y^4 - 56b_y^2 + 8)k_8))) \\ &+ \frac{\partial^6 f_{A,B}}{\partial x^4 \partial y^2} (b_y^2 (56k_2 + 14336k_4 + 224k_5 + 3584k_8) - 2k_2 - k_3 - 512k_4 - 2k_5 - 256k_6 - 512k_8) \\ &+ \frac{\partial^6 f_{A,B}}{\partial x^6 \partial y^2} (2k_2 + k_3 + 512k_4 - 2k_5 - 256k_6 - 512k_8) \\ &+ \frac{\partial^6 f_{A,B}}{\partial x^6 \partial y^2} (2k_2 + k_3 + 512k_4 - 2k_5 - 256k_6 - 512k_8) \\ &+ \frac{\partial^6 f_{A,B}}{\partial x^6 \partial y^2} (2k_2 + k_3 + 512k_4 - 2k_5 - 256k_6 - 512k_8) \\ &+ \frac{\partial^6 f_{A,B}}{\partial x^6} (2k_2 + k_3 + 512k_4 - 2k_5 - 256k_6 - 512k_8) \\ &+ \frac{\partial^6 f_{A,B}}{\partial x^6 \partial y^2} (2k_2 + k_3 + 512k_4 - 2k_5 - 256k_6 - 512k_8) \\ &+ \frac{\partial^6 f_{A,B}}{\partial x^6 \partial y^2} (2k_2 + k_3 + 512k_4 - 2k_5 - 256k_6 - 512k_8) \\ &+ \frac{\partial^6 f_{A,B}}{\partial x^6 \partial y^2} (2k_2 + k_3 + 512k_4 - 2k_5 - 256k_6 - 512k_8) \\ &+ \frac{\partial^6 f_{A,B}}{\partial x^6 \partial y^2} (2k_2 + k_3 + 512k_4 - 2k_5 - 256k_6 - 512k_8) \\ &+ \frac{\partial^6 f_{A,B}}{\partial x^6 \partial y^2} (2k_2 + k_3 + 512k_4 - 2k_5 - 256k_6 - 512k_8) \\ &+ \frac{\partial^6 f_{A,B}}{\partial x^6 \partial y^2} (2k_2 + k_3 + 512k_4 - 2k_5 - 256k_6 - 512k_8) \\ &+ \frac{\partial^6 f_{A,B}}{\partial x^6 \partial y^2} (2k_2 + k_3 + 2(1024(45k_3^8 - 210k_3^6 + 210k_3^6 + 210k_3^6 + 210k_3^6 + 210k$$

$$+3360b_{9}^{4} - 2880b_{2}^{2} + 256)k_{8})) + \frac{3^{8}f_{A,B}}{3x^{2}0y^{6}}(b^{5}(430080k_{4} + 26880k_{5} + 6720k_{8}) + b_{9}^{4}(-430080k_{4} - 6720k_{5} - 26880k_{8}) + b_{2}^{3}(29160k_{4} + 360k_{5} + 23040k_{8}) + (420b_{9}^{6} - 420b_{9}^{4} + 90b_{2}^{3} - 2)k_{2} \\ -k_{3} - 2048k_{4} - 2k_{5} - 1024k_{6} - 2048k_{8}) + \frac{3^{8}f_{A,B}}{3x^{4}\partial^{4}}(b_{9}^{4}(420k_{2} + 430080k_{4} + 6720k_{5} + 26880k_{8}) + b_{2}^{3}(-90k_{2} - 92160k_{4} - 360k_{5} - 23040k_{8}) + 2k_{2} + k_{3} + 2048k_{4} + 2k_{5} + 1024k_{6} \\ + 2048k_{8}) + \frac{3^{8}f_{A,B}}{3x^{8}\partial^{3}y^{2}}(b_{2}^{3}(90k_{2} + 92160k_{4} + 360k_{5} + 23040k_{8}) - 2k_{2} - k_{3} \\ - 2048k_{4} - 2k_{5} - 1024k_{6} - 2048k_{8}) + \frac{3^{8}f_{A,B}}{3x^{8}}(2k_{2} + k_{3} + 2048k_{4} + 2k_{5} + 1024k_{6} + 2048k_{8})] \\ + \frac{h^{12}}{239500800} \left[ \frac{3^{10}f_{A,B}}{3y^{10}}(2(66b_{y}^{10} - 495b_{y}^{8} + 924b_{y}^{6} - 495b_{y}^{4} + 66b_{z}^{2} - 1)k_{2} - k_{3} + 2(4096(66b_{y}^{10} - 495b_{y}^{8} + 924b_{y}^{6} - 495b_{y}^{4} + 66b_{z}^{2} - 1)k_{4} + (67584b_{y}^{10} - 126720b_{y}^{8} + 59136b_{y}^{6} - 7920b_{y}^{4} + 264b_{z}^{2} - 1)k_{5} + 8((33b_{y}^{10} - 990b_{y}^{8} + 7392b_{y}^{6} - 168b_{z}^{2} + 1)k_{2} + k_{3} + 2(4096(495b_{y}^{8} - 924b_{y}^{6} + 495b_{y}^{4} - 66b_{z}^{2} + 1)k_{2} + k_{3} + 2(4096(495b_{y}^{8} - 924b_{y}^{6} + 495b_{y}^{4} - 66b_{z}^{2} + 1)k_{2} + k_{3} + 2(4096(495b_{y}^{8} - 924b_{y}^{6} + 495b_{y}^{4} - 66b_{z}^{2} + 1)k_{2} + k_{3} + 2(4096(495b_{y}^{8} - 924b_{y}^{6} + 495b_{y}^{4} - 66b_{z}^{2} + 1)k_{2} + k_{3} + 2(4096(495b_{y}^{8} - 924b_{y}^{6} + 495b_{y}^{4} - 66b_{z}^{2} + 1)k_{2} + k_{3} + 2(4096(495b_{y}^{8} - 924b_{y}^{6} + 495b_{y}^{4} - 66b_{z}^{2} + 1)k_{2} + k_{3} + 2(4096(495b_{y}^{8} - 924b_{y}^{6} + 495b_{y}^{4} - 4092b_{y}^{4} + 4096k_{y}^{4} + 4024b_{y}^{4} + 256040k_{y}^{4} + 118272k_{y}^{4} + 1$$

$$+\frac{\partial^{12} f_{A,8}}{\partial x^3} y^4 (b_1^4(2002k_2 + 32800768k_4 + 32032k_5 + 2050048k_8) + b_y^2(-182k_2 - 2981888k_4 - 728k_5 - 745472k_8) - 2k_2 + 2k_2 + k_3 + 32768k_4 + 2k_5 + 16384k_6 + 32768k_8) \\ +\frac{\partial^{12} f_{A,8}}{\partial x^{10} \partial y^2} (b_y^2(182k_2 + 2981888k_4 + 728k_5 + 745472k_8) - 2k_2 - k_3 - 32768k_4 - 2k_5 \\ - 16384k_6 - 32768k_8) +\frac{\partial^{12} f_{A,8}}{\partial x^{10}} (2k_2 + k_3 + 32768k_4 + 2k_5 + 16384k_6 + 32768k_8)] \\ +\frac{h^{15}}{10461394944000} [\frac{\partial^{14} f_{A,8}}{\partial x^{10}} (2(210b_y^{14} - 1820(b_y^{12} + b_y^4) + 8008(b_y^{10} + b_y^6)) \\ - 12870b_y^8 + 120b_y^2 - 1)k_2 - k_3 + 2(65536(120b_y^{14} - 1820b_y^{12} + 8008(b_y^{10}b_y^6) + -12870b_y^8 \\ - 1820b_y^4 + 120b_y^2 - 1)k_4 + (1966080b_y^{14} - 7454720b_y^{12} + 8200192b_y^{10} - 3294720b_y^8 \\ + 512512b_y^6 - 29120b_y^4 + 480b_y^2 - 1)k_3 + 32((15b_y^4 - 910b_z^{12} + 16016b_y^{10} - 102960b_y^8 \\ + 526256b_y^6 - 232960b_y^6 + 61440b_y^2 - 2048)k_3 - 1024k_6))) +\frac{\partial^{14} f_{A,8}}{\partial x^2 \partial y^{12}} (2(1820b_y^{12} - 8008b_y^6) \\ + 12870b_y^8 - 8008b_y^6 + 1820b_y^4 - 120b_y^2 + 1)k_2 + k_3 + 2(65536(1820b_y^{12} - 8008b_y^6) \\ + 12870b_y^8 - 8008b_y^6 + 1820b_y^4 - 120b_y^2 + 1)k_4 + (7454720b_y^{12} - 8200192b_y^{10} + 3294720b_y^8 \\ - 512512b_y^6 + 29120b_y^4 - 480b_y^2 + 1)k_5 + 64(512k_6 + (455b_y^2 - 8008b_y^6) + 51480b_y^8 \\ - 128128b_y^6 + 116480b_y^4 - 30720b_y^2 + 1024)k_8))) +\frac{\partial^{14} f_{A,8}}{\partial x^4 \partial y^{10}} (b_y^{10}(16016k_2 + 1049624576k_4 + 1025024k_5 + 16400384k_5) + b_y^6 (16016k_2 + 1049624576k_4 + 1025024k_5 + 16400384k_5) + b_y^6 (16016k_2 + 1049624576k_4 + 1025024k_5 + 16400384k_5) + b_y^6 (-16016k_2 - 1049624576k_4 + 1025024k_5 - 16400384k_5) + b_y^6 (-16016k_2 + 15728640k_4 + 960k_5 + 3932160k_5) - 2k_2 - k_3 \\ - 131072k_4 - 2k_5 - 65536k_6 - 131072k_8) +\frac{\partial^{14} f_{A,8}}{\partial x^6 \partial y^6} (b_y^6) (540k_4 + 58240k_5 + 14909440k_5) + b_y^2 (-240k_2 + 15728640k_4 + 960k_5 + 3932160k_5) - 2k_2 - k_3 \\ - 131072k_4 - 2k_5 - 65536k_6 + 131072k_8) +\frac{\partial^{14} f_{A,8}}{\partial x^{10} \partial y^6} (b_y^6) (540k_2 + 238551040k_4 + 58240k_5 + 14909440k_5) \\ +b$$

$$-190095366_{p}^{6} + 125337600b_{y}^{4} - 2506752b_{y}^{2} + 65536(b_{8})) + \frac{\partial^{16} f_{A,8}}{\partial x^{2} \partial y^{14}} ((6120b_{y}^{14} - 37128b_{y}^{12} - 6120b_{y}^{4} + 306b_{y}^{2} - 2) \lambda_{2} - k_{3} + 2(262144(3060b_{y}^{14} - 18564b_{y}^{12} + 44758b_{y}^{10} - 43758b_{y}^{10} - 43758b_{y}^{10} - 11202048b_{y}^{8} + 1188096b_{y}^{6} - 48960b_{y}^{4} + 612b_{y}^{2} - 1)k_{5} + (50135040b_{y}^{14} - 18564b_{y}^{12} + 24808192b_{y}^{10} - 11202048b_{y}^{8} + 1188096b_{y}^{6} - 48960b_{y}^{4} + 612b_{y}^{2} - 1)k_{5} + (4(1765b_{y}^{14} - 18564b_{y}^{12} + 175032b_{y}^{10} - 700128b_{y}^{8} + 1188096b_{y}^{6} - 783360b_{y}^{4} + 156672b_{y}^{2} - 4096)k_{8} - 2048k_{6})) + \frac{\partial^{16} f_{A,8}}{\partial x^{2} \partial y^{12}} (b_{y}^{12} (37128k_{2} + 9732882432k_{4} + 152076288k_{5} + 2376192k_{8}) + b_{y}^{10} (-87516k_{2} - 22941794304k_{4} - 89616384k_{5} - 22404096k_{8}) + b_{y}^{8} (87516k_{2} + 22941794304k_{4} + 22404096k_{5} + 89616384k_{5} - 22404096k_{5}) + b_{y}^{4} (6120k_{2} + 1604321280k_{4} + 97920k_{5} + 100270080k_{8}) + b_{y}^{4} (-306k_{2} - 80216064k_{4} - 1224k_{5} - 20054016k_{8}) + 2k_{2} + k_{3} + 524288k_{4} + 2k_{5} + 262144k_{6} + 524288k_{8}) + \frac{\partial^{16} f_{A,8}}{\partial x^{2} \partial y^{10}} (b_{y}^{10} (87516k_{2} + 22941794304k_{4} + 289616384k_{5} + 22404096k_{5}) + b_{y}^{6} (-37128k_{2} + 27372882432k_{4} + 2376192k_{5} + 152076288k_{8}) + b_{y}^{4} (-6120k_{2} - 1604321280k_{4} - 97920k_{5} - 100270080k_{8}) + b_{y}^{3} (306k_{2} + 80216064k_{4} + 1224k_{5} + 20054016k_{8}) - 2k_{2} - k_{3} - 524288k_{4} - 2k_{5} - 262144k_{6} - 524288k_{8}) + \frac{\partial^{16} f_{A,8}}{\partial x^{2} \partial y^{3}} (b_{y}^{6} (87516k_{2} + 22941794304k_{4} + 22404096k_{5} + 89616384k_{5}) + \frac{\partial^{16} f_{A,8}}{\partial x^{2} \partial y^{3}} (b_{y}^{6} (37128k_{2} + 2732882432k_{4} - 2376192k_{5} - 1502076288k_{8}) + b_{y}^{4} (6120k_{2} + 1604321280k_{4} + 97920k_{5} + 100270080k_{8}) + b_{y}^{4} (-3628k_{2} + 224884k_{4}) + 2k_{2} - 42884k_{4} + 2k_{2} + 22481944k_{6} + 224288k_{4} + 2k_{5} + 262144k_{6} + 224288k_{8}) + \frac{\partial^{16} f_{A,8}}{\partial x^{10} \partial y^{3}} (b_$$

```
-77520b_{\nu}^{6} + 9690b_{\nu}^{4} - 380b_{\nu}^{2} + 2)k_{2} + k_{3} + 2(1048576(4845b_{\nu}^{16} - 38760b_{\nu}^{14} + 125970b_{\nu}^{12})k_{2} + k_{3} + k
                                +515973120b_{\nu}^{12}-189190144b_{\nu}^{10}+32248320b_{\nu}^{8}-2480640b_{\nu}^{6}+77520b_{\nu}^{4}-760b_{\nu}^{2}+1)k_{5}
                 +16(32768k_6 + (4845b_{\gamma}^{16} - 155040b_{\gamma}^{14} + 2015520b_{\gamma}^{12} - 11824384b_{\gamma}^{10} + 32248320b_{\gamma}^{8} - 39690240b_{\gamma}^{6} + 32248320b_{\gamma}^{8} - 39690240b_{\gamma}^{6} + 32248320b_{\gamma}^{8} - 39690240b_{\gamma}^{8} + 32248320b_{\gamma}^{8} + 32248480b_{\gamma}^{8} + 3224840b_{\gamma}^{8} + 3224840
                                                                                                                  +19845120b_y^4 - 3112960b_y^2 + 65536)k_8))) + \frac{\partial^{18}f_{A,B}}{\partial x^4 \partial y^{14}}(b_y^{14}(77520k_2 + 81285611520k_4)))
 +1270087680k_5 + 4961280k_8) + b_{\nu}^{12}(-251940k_2 - 264178237440k_4 - 1031946240k_5 - 64496640k_8) + b_{\nu}^{12}(-251940k_2 - 264178240k_5 - 64496640k_8) + b_{\nu}^{12}(-251940k_5 - 26417840k_5 - 64496640k_8) + b_{\nu}^{12}(-251940k_5 - 26417840k_5 - 64496k_5 - 
                                                                                                                    +b_{\nu}^{10}(369512k_2+387461414912k_4+378380288k_5+378380288k_8)+b_{\nu}^{8}(-251940k_2)
                           -264178237440k_4 - 64496640k_5 - 1031946240k_8) + b_{\nu}^6 (77520k_2 + 81285611520k_4 + 4961280k_5) + b_{\nu}^6 (77520k_4 + 81285611520k_4 + 4961280k_5) + b_{\nu}^6 (77520k_4 + 81285611520k_4 + 4961280k_5) + b_{\nu}^6 (77520k_4 + 812860k_5) + b_{\nu}^6 (77520k_5 + 812860k_5) + b_{\nu}^6 
                                                                       +1270087680k_8)+b_{\nu}^4(-9690k_2-10160701440k_4-155040k_5-635043840k_8)+b_{\nu}^2(380k_2-10160701440k_4-155040k_5-635043840k_8)+b_{\nu}^2(380k_2-10160701440k_4-155040k_5-635043840k_8)+b_{\nu}^2(380k_2-10160701440k_4-155040k_5-635043840k_8)+b_{\nu}^2(380k_2-10160701440k_4-155040k_5-635043840k_8)+b_{\nu}^2(380k_2-10160701440k_4-155040k_5-635043840k_8)+b_{\nu}^2(380k_2-10160701440k_4-155040k_5-635043840k_8)+b_{\nu}^2(380k_2-10160701440k_4-155040k_5-635043840k_8)+b_{\nu}^2(380k_2-10160701440k_4-155040k_5-635043840k_8)+b_{\nu}^2(380k_2-10160701440k_4-155040k_5-635043840k_8)+b_{\nu}^2(380k_2-10160701440k_4-155040k_5-635043840k_8)+b_{\nu}^2(380k_2-10160701440k_4-155040k_5-635043840k_8)+b_{\nu}^2(380k_2-10160701440k_4-155040k_5-635040k_5-635040k_8)+b_{\nu}^2(380k_2-10160701440k_4-155040k_5-635040k_8)+b_{\nu}^2(380k_2-1016060k_5-635040k_5-635040k_5-635040k_5-635040k_5-635040k_5-635040k_5-635040k_5-635040k_5-635040k_5-635040k_5-635040k_5-635040k_5-635040k_5-635040k_5-635040k_5-635040k_5-635040k_5-635040k_5-635040k_5-635040k_5-635040k_5-635040k_5-635040k_5-635040k_5-635040k_5-635040k_5-635040k_5-635040k_5-635040k_5-635040k_5-636040k_5-636040k_5-636040k_5-636040k_5-636040k_5-636040k_5-636040k_5-636040k_5-636040k_5-636040k_5-636040k_5-636040k_5-636040k_5-636040k_5-636040k_5-636040k_5-636040k_5-636040k_5-636040k_5-636040k_5-636040k_5-636040k_5-636040k_5-636040k_5-636040k_5-636040k_5-636040k_5-636040k_5-636040k_5-636040k_5-636040k_5-636040k_5-636040k_5-636040k_5-636040k_5-636040k_5-636040k_5-636040k_5-636040k_5-636040k_5-636040k_5-636040k_5-636040k_5-636040k_5-636040k_5-636040k_5-636040k_5-636040k_5-636040k_5-636040k_5-636040k_5-636040k_5-636040k_5-636040k_5-636040k_5-636040k_5-636040k_5-636040k_5-636040k_5-636040k_5-636040k_5-636040k_5-636040k_5-636040k_5-636040k_5-636040k_5-636040k_5-636040k_5-636040k_5-636040k_5-636040k_5-636040k_5-636040k_5-636040k_5-636040k_5-636040k_5-636040k_5-636040k_5-636040k_5-636040k_5-636040k_5-636040k_5-636040k_5-636040k_5-636040k_5-636040k_5-636040k_5-636040k_5-636040k_5-636040k_5-636040k_5-636040k_5-636040k_5-636040k_5-
                                                                                                                        +398458880k_4 + 1520k_5 + 99614720k_8) - 2k_2 - k_3 - 2097152k_4 - 2k_5 - 1048576k_6
                                                                   -2097152k_8) + \frac{\partial^{18} f_{A,B}}{\partial x^6 \partial y^{12}} (b_y^{12} (251940k_2 + 264178237440k_4 + 1031946240k_5 + 64496640k_8))
                                                                                                                   +b_{\nu}^{10}(-369512k_2-387461414912k_4-378380288k_5-378380288k_8)+b_{\nu}^{8}(251940k_2)
                                                                                                             +264178237440k_4 + 64496640k_5 + 1031946240k_8) + b_{\nu}^6(-77520k_2 - 81285611520k_4)
                                                                       -4961280k_5 - 1270087680k_8) + b_{\nu}^4 (9690k_2 + 10160701440k_4 + 155040k_5 + 635043840k_8)
                                                                                                                                                                  +b_{\nu}^2(-380k_2-398458880k_4-1520k_5-99614720k_8)+2k_2+k_3+2097152k_4
                                               +2k_5+1048576k_6+2097152k_8)+\frac{\partial^{18}f_{A,B}}{\partial v^8\partial v^{10}}(b_y^{10}(369512k_2+387461414912k_4+378380288k_5))
                                                                                                               +378380288k_8)+b_{\nu}^8(-251940k_2-264178237440k_4-64496640k_5-1031946240k_8)
                                                                                                                                                                      +b_{\nu}^{6}(77520k_{2}+81285611520k_{4}+4961280k_{5}+1270087680k_{8})+b_{\nu}^{4}(-9690k_{2})
                                                                                                                          -10160701440k_4 - 155040k_5 - 635043840k_8) + b_y^2(380k_2 + 398458880k_4 + 1520k_5)
                                                                                                                                                                                                          +99614720k_8) - 2k_2 - k_3 - 2097152k_4 - 2k_5 - 1048576k_6 - 2097152k_8)
                                                           +\frac{\partial^{18} f_{A,B}}{\partial x^{10} \partial x^{8}}(b_{y}^{8}(251940k_{2}+264178237440k_{4}+64496640k_{5}+1031946240k_{8})+b_{y}^{6}(-77520k_{2}+364178237440k_{4}+64496640k_{5}+1031946240k_{8})+b_{y}^{6}(-77520k_{2}+364178237440k_{4}+64496640k_{5}+1031946240k_{8})+b_{y}^{6}(-77520k_{2}+364178237440k_{4}+64496640k_{5}+1031946240k_{8})+b_{y}^{6}(-77520k_{2}+364178237440k_{4}+64496640k_{5}+1031946240k_{8})+b_{y}^{6}(-77520k_{2}+364178237440k_{4}+64496640k_{5}+1031946240k_{8})+b_{y}^{6}(-77520k_{2}+364178237440k_{4}+64496640k_{5}+1031946240k_{8})+b_{y}^{6}(-77520k_{2}+364178237440k_{4}+64496640k_{5}+1031946240k_{8})+b_{y}^{6}(-77520k_{2}+364178237440k_{4}+64496640k_{5}+1031946240k_{8})+b_{y}^{6}(-77520k_{2}+364178237440k_{4}+64496640k_{5}+1031946240k_{8})+b_{y}^{6}(-77520k_{2}+364178237440k_{4}+64496640k_{5}+1031946240k_{8})+b_{y}^{6}(-77520k_{2}+364178237440k_{4}+64496640k_{5}+1031946240k_{8})+b_{y}^{6}(-77520k_{2}+364178237440k_{4}+64496640k_{5}+1031946240k_{8})+b_{y}^{6}(-77520k_{2}+364178237440k_{4}+64496640k_{5}+1031946240k_{8})+b_{y}^{6}(-77520k_{2}+364178237440k_{4}+64496640k_{5}+1031946240k_{8})+b_{y}^{6}(-77520k_{2}+364178237440k_{4}+64496640k_{5}+1031946240k_{8})+b_{y}^{6}(-77520k_{2}+364178237440k_{4}+64496640k_{5}+1031946240k_{8})+b_{y}^{6}(-77520k_{2}+364178240k_{4}+64496640k_{5}+103194640k_{8}+64496640k_{8}+64496640k_{8}+64496640k_{8}+64496640k_{8}+64496640k_{8}+64496640k_{8}+64496640k_{8}+64496640k_{8}+64496640k_{8}+64496640k_{8}+64496640k_{8}+64496640k_{8}+64496640k_{8}+64496640k_{8}+64496640k_{8}+64496640k_{8}+64496640k_{8}+64496640k_{8}+64496640k_{8}+64496640k_{8}+64496640k_{8}+64496640k_{8}+64496640k_{8}+64496640k_{8}+64496640k_{8}+64496640k_{8}+64496640k_{8}+64496640k_{8}+64496640k_{8}+64496640k_{8}+64496640k_{8}+64496640k_{8}+64496640k_{8}+64496640k_{8}+64496640k_{8}+64496640k_{8}+64496640k_{8}+64496640k_{8}+64496640k_{8}+64496640k_{8}+64496640k_{8}+64496640k_{8}+64496640k_{8}+64496640k_{8}+6446640k_{8}+64466640k_{8}+64466640k_{8}+6446640k_{8}+6446640k_{8}+64466640k_{8}+6446640k_{8}+6446640k_{8}+6446640k_{8
                                                                                                                                                     -81285611520k_4 - 4961280k_5 - 1270087680k_8) + b_{\nu}^4(9690k_2 + 10160701440k_4)
                                                                                                                                +155040k_5+635043840k_8)+b_y^2(-380k_2-398458880k_4-1520k_5-99614720k_8)\\
                                                                                                                                             +2k_2+k_3+2097152k_4+2k_5+1048576k_6+2097152k_8)+\frac{\partial^{18}f_{A,B}}{\partial x^{12}\partial x^6}(b_y^6(77520k_2))
                                                                                                                                       +81285611520k_4+4961280k_5+1270087680k_8)+b_y^4(-9690k_2-10160701440k_4)+b_y^4(-9690k_2-10160701440k_4)+b_y^4(-9690k_2-10160701440k_4)+b_y^4(-9690k_2-10160701440k_4)+b_y^4(-9690k_2-10160701440k_4)+b_y^4(-9690k_2-10160701440k_4)+b_y^4(-9690k_2-10160701440k_4)+b_y^4(-9690k_2-10160701440k_4)+b_y^4(-9690k_2-10160701440k_4)+b_y^4(-9690k_2-10160701440k_4)+b_y^4(-9690k_2-10160701440k_4)+b_y^4(-9690k_2-10160701440k_4)+b_y^4(-9690k_2-10160701440k_4)+b_y^4(-9690k_2-10160701440k_4)+b_y^4(-9690k_2-10160701440k_4)+b_y^4(-9690k_2-10160701440k_4)+b_y^4(-9690k_2-10160701440k_4)+b_y^4(-9690k_2-10160701440k_4)+b_y^4(-9690k_2-10160701440k_4)+b_y^4(-9690k_2-10160701440k_4)+b_y^4(-9690k_2-10160701440k_4)+b_y^4(-9690k_2-10160701440k_4)+b_y^4(-9690k_2-10160701440k_4)+b_y^4(-9690k_2-10160701440k_4)+b_y^4(-9690k_2-10160701440k_4)+b_y^4(-9690k_2-10160701440k_4)+b_y^4(-9690k_2-10160701440k_4)+b_y^4(-9690k_2-10160701440k_4)+b_y^4(-9690k_2-10160701440k_4)+b_y^4(-9690k_2-10160701440k_4)+b_y^4(-9690k_2-10160701440k_4)+b_y^4(-9690k_2-10160701440k_4)+b_y^4(-9690k_2-10160701440k_4)+b_y^4(-9690k_2-10160701440k_4)+b_y^4(-960k_2-1016040k_4)+b_y^4(-960k_2-10160k_4)+b_y^4(-960k_2-10160k_4)+b_y^4(-960k_2-10160k_4)+b_y^4(-960k_2-10160k_4)+b_y^4(-960k_2-10160k_4)+b_y^4(-960k_2-10160k_4)+b_y^4(-960k_2-10160k_4)+b_y^4(-960k_2-10160k_4)+b_y^4(-960k_2-10160k_4)+b_y^4(-960k_2-100k_4)+b_y^4(-960k_2-100k_4)+b_y^4(-960k_4-100k_4)+b_y^4(-960k_4-100k_4)+b_y^4(-960k_4-100k_4)+b_y^4(-960k_4-100k_4)+b_y^4(-960k_4-100k_4)+b_y^4(-960k_4-100k_4)+b_y^4(-960k_4-100k_4)+b_y^4(-960k_4-100k_4)+b_y^4(-960k_4-100k_4-100k_4)+b_y^4(-960k_4-100k_4-100k_4)+b_y^4(-960k_4-100k_4-100k_4)+b_y^4(-960k_4-100k_4-100k_4)+b_y^4(-960k_4-100k_4-100k_4)+b_y^4(-960k_4-100k_4-100k_4)+b_y^4(-960k_4-100k_4-100k_4-100k_4)+b_y^4(-960k_4-100k_4-100k_4-100k_4-100k_4-100k_4-100k_4-100k_4-100k_4-100k_4-100k_4-100k_4-100k_4-100k_4-100k_4-100k_4-100k_4-100k_4-100k_4-100k_4-100k_4-100k_4-100k_4-100k_4-100k_4-100k_4-100k_4-100k_4-100k_4-100k_4-100k_4-100k_4-100k_4-100k_4-100k_4-100k_4-100k_4-100k_4-100
                                                                                                                                              -155040k_5 - 635043840k_8) + b_y^2(380k_2 + 398458880k_4 + 1520k_5 + 99614720k_8)
                                                                                        -2k_2-k_3-2097152k_4-2k_5-1048576k_6-2097152k_8)+\frac{\partial^{18}f_{A,B}}{\partial x^{14}\partial x^4}(b_y^4(9690k_2))
                                               +10160701440k_4 + 155040k_5 + 635043840k_8) + b_v^2(-380k_2 - 398458880k_4 - 1520k_5)
                                                                                                                                             -99614720k_8) + 2k_2 + k_3 + 2097152k_4 + 2k_5 + 1048576k_6 + 2097152k_8)
+\frac{\partial^{18} f_{A,B}}{\partial \mathbf{v}^{16} \partial \mathbf{v}^{2}} (b_{y}^{2} (380 k_{2} + 398458880 k_{4} + 1520 k_{5} + 99614720 k_{8}) - 2 k_{2} - k_{3} - 2097152 k_{4} - 2 k_{5} + 2 k_
                                                                                                                                                                                         -1048576k_6 - 2097152k_8) + \frac{\partial^{18} f_{A,B}}{\partial x^{18}} (2k_2 + k_3 + 2097152k_4 + 2k_5)
                                                                                                                                                                                                                                                                                                                                                                                                                                                                                                                                                                                                                                                                                                                                                                                                (B.5)
```

The coefficients  $m_i$  and  $k_i$  (i = 1, 2, 3, ..., 9) in Eqs. (B.4)-(B.5) are given by Eqs. (21), (40) and Eq. (46) (see also Table 1 for the conventional elements) for the corresponding techniques with zero heat source.

We should mention that in the calculation of  $\bar{f}$  with the help of Eqs. (B.4)-(B.5) we need to include the terms with the maximum power of h equal to 4, 6, 8, 12, 14 and 18 for the 4th, 6th, 8th, 12th, 14th and 18th orders of the local truncation

error, respectively (according to the order of accuracy of the corresponding technique with zero heat source). As can be also seen,  $\bar{f}$  is directly calculated in terms of the heat source f at the points with the coordinates  $x_A$  and  $y_A$  with the help of Eqs. (B.4)-(B.5) (similar to the introduction of the concentrated forces in the FEM).

# Appendix C. The coefficients $b_p$ in Eq. (20)

```
b_1 = (k_1 + 2(2k_2 + k_3 + 2k_4 + 2k_5 + k_6 + k_7 + 2k_8 + k_9)).
         b_2 = 12(2k_2 + k_3 + 8k_4 + 2k_5 + 4k_6 + 8k_8 + m_1 + 4m_2 + 2m_3)
                              +4m_4 + 4m_5 + 2m_6 + 2m_7 + 4m_8 + 2m_9),
                    b_3 = 12(b_y^2(2k_2 + 8k_4 + 8k_5 + k_7 + 2k_8 + 4k_9) + m_1
                 +2(2m_2+m_3+2m_4+2m_5+m_6+m_7+2m_8+m_9)),
                     b_4 = (2k_2 + k_3 + 2(16k_4 + k_5 + 8k_6 + 16k_8 + 12m_2)
                               +6m_3 + 48m_4 + 12m_5 + 24m_6 + 48m_8)).
                      b_5 = b_y^2 (b_y^2 (2k_2 + 32k_4 + 32k_5 + k_7 + 2k_8 + 16k_9))
                           +12(2m_2+8m_4+8m_5+m_7+2m_8+4m_9)),
  b_6 = 12(2m_2 + m_3 + 8m_4 + 2m_5 + 4m_6 + 8m_8 + b_v^2(k_2 + 16k_4 + 4k_5)
                        +4k_8 + 2m_2 + 8m_4 + 8m_5 + m_7 + 2m_8 + 4m_9)),
          b_7 = (2k_2 + k_3 + 2(64k_4 + k_5 + 32k_6 + 64k_8 + 30m_2 + 15m_3)
                                   +480m_4 + 30m_5 + 240m_6 + 480m_8)
                   b_8 = b_y^4 (b_y^2 (2k_2 + 128k_4 + 128k_5 + k_7 + 2k_8 + 64k_9)
                       +30(2m_2+32m_4+32m_5+m_7+2m_8+16m_9)),
                      b_9 = 30(2m_2 + m_3 + 32m_4 + 2m_5 + 16m_6 + 32m_8
       +b_{\nu}^{2}(k_{2}+4(16k_{4}+k_{5}+4k_{8}+3m_{2}+48m_{4}+12m_{5}+12m_{8})))
b_{10} = 30b_{\nu}^{2}(12(m_{2} + 4(4m_{4} + m_{5} + m_{8})) + b_{\nu}^{2}(k_{2} + 64k_{4} + 16k_{5} + 4k_{8}))
                           +2m_2 + 32m_4 + 32m_5 + m_7 + 2m_8 + 16m_9)
                                       b_{11} = (2k_2 + k_3 + 2(256k_4 + k_5 + 4(32k_6 + 64k_8)))
                                    +7(2m_2+m_3+2(64m_4+m_5+32m_6+64m_8)))),
                                b_{12} = b_{y}^{6}(b_{y}^{2}(2k_{2} + 512k_{4} + 512k_{5} + k_{7} + 2k_{8} + 256k_{9})
                                   +56(2m_2+128m_4+128m_5+m_7+2m_8+64m_9)),
                                 b_{13} = 56(2m_2 + m_3 + 128m_4 + 2m_5 + 64m_6 + 128m_8
               +b_{\nu}^{2}(k_{2}+256k_{4}+4k_{5}+64k_{8}+30m_{2}+1920m_{4}+120m_{5}+480m_{8})),
                        b_{14} = 140b_{\nu}^{2}(12(m_{2} + 4(16m_{4} + m_{5} + 4m_{8})) + b_{\nu}^{2}(k_{2} + 4(64k_{4} + m_{5} + 4m_{8})))
                                        +4k_5+4k_8+3m_2+192m_4+48m_5+12m_8))),
                                           b_{15} = 56(b_{\nu}^4)(30(m_2 + 4(16m_4 + 4m_5 + m_8))
     +b_{v}^{2}(k_{2}+256k_{4}+64k_{5}+4k_{8}+2m_{2}+128m_{4}+128m_{5}+m_{7}+2m_{8}+64m_{9})),
                  b_{16} = (2k_2 + k_3 + 2(1024k_4 + k_5 + 512k_6 + 1024k_8 + 90m_2 + 45m_3)
                                          +23040m_4 + 90m_5 + 11520m_6 + 23040m_8),
                            b_{17} = b_y^8 (b_y^2 (2k_2 + 2048k_4 + 2048k_5 + k_7 + 2k_8 + 1024k_9))
                                  +90(2m_2+512m_4+512m_5+m_7+2m_8+256m_9))
                                b_{18} = 90(2m_2 + m_3 + 512m_4 + 2m_5 + 256m_6 + 512m_8
               +b_{\nu}^{2}(k_{2}+4(256k_{4}+k_{5}+64k_{8}+14m_{2}+3584m_{4}+56m_{5}+896m_{8}))),
b_{19} = 420(b_y^2)(b_y^2(k_2 + 1024k_4 + 16k_5 + 64k_8 + 30m_2 + 7680m_4 + 480m_5 + 480m_8)
```

$$\begin{aligned} &+12(m_2+4(64m_4+m_5+16m_8)))\,,\\ b_{20}&=420b_y^4(30(m_2+16(16m_4+m_5+m_8))\\ &+b_y^2(k_2+4(256k_4+16k_5+4k_8+3m_2+768m_4+192m_5+12m_8)))\,,\\ b_{21}&=90(b_y^6)(56(m_2+4(64m_4+16m_5+m_8))\\ &+b_y^2(k_2+1024k_4+256k_5+4k_8+2m_2+512m_4+512m_5+m_7+2m_8+256m_9))\,. \end{aligned} \tag{C.1}$$

# Appendix D. The coefficients $d_j$ and $f_j$ in Eqs. (26) and (27) for the new Q 9\_0 PT stencils

$$d_1 = \frac{1}{4}(\frac{1}{5x_1}|b_y^4(2220a_1 - 4677a_2 + 4016a_3) - 5b_y^2(2334a_1 - 3537a_2 + 596a_3) + 2850a_1] - a_{11} \\ -2a_4 - 2a_8), \qquad d_2 = \frac{1}{2}[a_1 - a_9], \\ d_3 = \frac{1}{180x_1}[b_y^4(2220a_1 + 69a_2 - 832a_3) + b_y^2(-11670a_1 + 1011a_2 + 92a_3) + 2850a_1], \\ d_4 = \frac{1}{2}[a_1 - a_6], \\ d_5 = \frac{1}{4}(\frac{1}{10x_1}|b_y^4(-2960a_1 - 2397a_2 + 5416a_3) + b_y^2(15560a_1 + 3537a_2 - 1736a_3) - 3800a_1] - 2a_{10}), \\ d_6 = \frac{1}{360x_1}[b_y^4(-8880a_1 - 1311a_2 + 2488a_3) + 5b_y^2(9336a_1 + 543a_2 - 184a_3) - 11400a_1], \\ d_7 = \frac{1}{360x_1}[b_y^4(-8880a_1 - 1311a_2 + 2488a_3) + 5b_y^2(9336a_1 + 543a_2 - 184a_3) - 11400a_1], \\ d_8 = \frac{1}{4}(\frac{1}{10x_1}|b_y^4(-2960a_1 - 2397a_2 + 5416a_3) + b_y^2(15560a_1 + 3537a_2 - 1736a_3) - 3800a_1] - 2a_7), \\ d_9 = \frac{1}{90x_1}[120x_1a_1 - b_y^2(87(41b_y^2 - 221)a_2 + 8(53b_y^2 + 257)a_3)] - a_5, \\ d_{10} = a_4, \quad d_{11} = a_5, \quad d_{12} = a_6, \quad d_{13} = a_7, \\ d_{14} = a_8, \quad d_{15} = a_9, \quad d_{16} = a_{10}, \quad d_{17} = a_{11}. \\ f_1 = \frac{1}{10x_1}[b_y^4(-370a_{16} - 2367a_2 - 174a_3) + b_y^2(1945a_{16} + 7335a_2 + 2295a_3) + 5x_1(a_{14} + 2a_{15}) \\ -475a_{16} + 21222a_2 - 3291a_3], \\ f_2 = \frac{1}{10x_1}[b_y^4(370(a_{14} + a_{16}) + 2321a_2 - 258a_3) + b_y^2(-1945(a_{14} + a_{16}) - 1224a_2 + 873a_3], \\ f_3 = \frac{(b_y^2 + 1)((46b_y^2 - 341)a_2 + (62b_y^2 + 23)a_3)}{10x_1}, \quad f_4 = \frac{a_3 - a_{14}}{2}, \\ f_5 = -\frac{1}{10x_1}[b_y^4(370(a_{14} + a_{15}) - 23a_2 - 216a_3) + b_y^2(-1945(a_{14} + a_{15}) + 845a_2) + 5x_1(a_{12} + 2a_{13}) \\ +475(a_{14} + a_{15}) - 1922a_2 + 216a_3], \\ f_6 = \frac{a_2}{2}, \quad f_7 = \frac{1}{10x_1}[a_1(a_2(-23b_y^4 + 845b_y^2 - 1922) - 216a_3(b_y^4 - 1)], \\ f_8 = \frac{1}{10x_1}[4b_y^4(370(a_{14} + a_{15}) - 12a_2 + 166a_3) + b_y^2(-1945(a_{14} + a_{15}) - 9920a_2 + 2560a_3) \\ +5x_1(a_{12} + 4a_{13}) + 475(a_{14} + a_{16}) - 11632a_2 + 896a_3], \\ f_{16} = \frac{1}{5x_1}[b_y^4(370(a_{14} + a_{15}) + 2296a_2 - 1088a_3) + b_y^2(-1945(a_{14} + a_{16}) - 10720a_2 + 4160a_3) \\ +5x_1(a_{12} + 4a_{13}) + 475(a_{14} + a_{16}) - 10720a_2 + 4160a_3)$$

$$+5x_{1}(a_{12}+2a_{13})+475(a_{14}+a_{15})-1496a_{2}-512a_{3}],$$

$$f_{17}=-\frac{1}{x_{1}}[2(x_{1}a_{12}+x_{1}a_{14}+2(96(-4a_{3}b_{y}^{2}+3(b_{y}^{2}-3)a_{2}+2a_{3})b_{y}^{2}+x_{1}a_{15}))].$$
(D.2)

In Eqs. (D.1) and (D.2)  $a_j$  (j = 1, 2, ..., 16) are sixteen arbitrary coefficients and  $x_1 = 74b_y^4 - 389b_y^2 + 95$ .

# Appendix E. The coefficients $b_p$ in Eqs. (39)

```
b_1 = (k_1 + 2(2k_2 + k_3 + 2k_4 + 2k_5 + k_6 + k_7 + 2k_8 + k_9)),
b_2 = (2(-1+b_v^2)k_2 - k_3 - 8k_4 + 8b_v^2k_4 - 2k_5 + 8b_v^2k_5 - 4k_6 + b_v^2k_7 - 8k_8 + 2b_v^2k_8 + 4b_v^2k_9),
           b_3 = (2(1 - 6b_v^2 + b_v^4)k_2 + k_3 + 32k_4 - 192b_v^2k_4 + 32b_v^4k_4 + 2k_5 - 48b_v^2k_5 + 32b_v^4k_5 + 16k_6 + b_v^4k_7)
                                                                                                                                                                                                                    +32k_8-48b_y^2k_8+2b_y^4k_8+16b_y^4k_9,
b_4 = (2(-1 + 15b_y^2 - 15b_y^4 + b_y^6)k_2 - k_3 - 128k_4 + 1920b_y^2k_4 - 1920b_y^4k_4 + 128b_y^6k_4 - 2k_5 + 120b_y^2k_5 + 
                                                   -480b_{\nu}^4k_5+128b_{\nu}^6k_5-64k_6+b_{\nu}^6k_7-128k_8+480b_{\nu}^2k_8-120b_{\nu}^4k_8+2b_{\nu}^6k_8+64b_{\nu}^6k_9)\,,
                      b_5 = (2(1 - 28b_v^2 + 70b_v^4 - 28b_v^6 + b_v^8)k_2 + k_3 + 512k_4 - 14336b_v^2k_4 + 35840b_v^4k_4 - 14336b_v^6k_4
                                                                                 +512b_{\nu}^{8}k_{4}+2k_{5}-224b_{\nu}^{2}k_{5}+2240b_{\nu}^{4}k_{5}-3584b_{\nu}^{6}k_{5}+512b_{\nu}^{8}k_{5}+256k_{6}+b_{\nu}^{8}k_{7}
                                                                                                                  +512k_8-3584b_{\nu}^2k_8+2240b_{\nu}^4k_8-224b_{\nu}^6k_8+2b_{\nu}^8k_8+256b_{\nu}^8k_9)\,,
                b_6 = (2(-1+45b_v^2-210b_v^4+210b_v^6-45b_v^8+b_v^{10})k_2 - k_3 - 2048k_4 + 92160b_v^2k_4 - 430080b_v^4k_4
                 +430080b_{\nu}^{6}k_{4}-92160b_{\nu}^{8}k_{4}+2048b_{\nu}^{10}k_{4}-2k_{5}+360b_{\nu}^{2}k_{5}-6720b_{\nu}^{4}k_{5}+26880b_{\nu}^{6}k_{5}-23040b_{\nu}^{8}k_{5}
                                                                               +2048b_{\nu}^{10}k_{5}-1024k_{6}+b_{\nu}^{10}k_{7}-2048k_{8}+23040b_{\gamma}^{2}k_{8}-26880b_{\gamma}^{4}k_{8}+6720b_{\gamma}^{6}k_{8}
                                                                                                                                                                                                                              -360b_{\nu}^{8}k_{8}+2b_{\nu}^{10}k_{8}+1024b_{\nu}^{10}k_{9},
                                    b_7 = (2(1 - 66b_v^2 + 495b_v^4 - 924b_v^6 + 495b_v^8 - 66b_v^{10} + b_v^{12})k_2 + k_3 + 8192k_4 - 540672b_v^2k_4
                                                                       +4055040b_{\nu}^{4}k_{4}-7569408b_{\nu}^{6}k_{4}+4055040b_{\nu}^{8}k_{4}-540672b_{\nu}^{10}k_{4}+8192b_{\nu}^{12}k_{4}+2k_{5}
                                     -528b_{\nu}^2k_5 + 15840b_{\nu}^4k_5 - 118272b_{\nu}^6k_5 + 253440b_{\nu}^8k_5 - 135168b_{\nu}^{10}k_5 + 8192b_{\nu}^{12}k_5 + 4096k_6
                                                                                                                                              +b_{\nu}^{12}k_7 + 8192k_8 - 135168b_{\nu}^2k_8 + 253440b_{\nu}^4k_8 - 118272b_{\nu}^6k_8
                                                                                                                                                                           +15840b_{\nu}^{8}k_{8}-528b_{\nu}^{10}k_{8}+2b_{\nu}^{12}k_{8}+4096b_{\nu}^{12}k_{9},
                          b_8 = (2(-1+91b_{\nu}^2-1001b_{\nu}^4+3003b_{\nu}^6-3003b_{\nu}^8+1001b_{\nu}^{10}-91b_{\nu}^{12}+b_{\nu}^{14})k_2-k_3-32768k_4
 +2981888b_{\nu}^{2}k_{4}-32800768b_{\nu}^{4}k_{4}+98402304b_{\nu}^{6}k_{4}-98402304b_{\nu}^{8}k_{4}+32800768b_{\nu}^{10}k_{4}-2981888b_{\nu}^{12}k_{4}
                                    +32768b_{\nu}^{14}k_4-2k_5+728b_{\nu}^2k_5-32032b_{\nu}^4k_5+384384b_{\nu}^6k_5-1537536b_{\nu}^8k_5+2050048b_{\nu}^{10}k_5
                                                                                                  -745472b_{\nu}^{12}k_5 + 32768b_{\nu}^{14}k_5 - 16384k_6 + b_{\nu}^{14}k_7 - 32768k_8 + 745472b_{\nu}^2k_8
                                                                                                          -2050048b_{\nu}^{4}k_{8}+1537536b_{\nu}^{6}k_{8}-384384b_{\nu}^{8}k_{8}+32032b_{\nu}^{10}k_{8}-728b_{\nu}^{12}k_{8}
                                                                                                                                                                                                                                                              +2b_{\nu}^{14}k_8+16384b_{\nu}^{14}k_9),
                                                                     b_9 = (2(1 - 120b_v^2 + 1820b_v^4 - 8008b_v^6 + 12870b_v^8 - 8008b_v^{10} + 1820b_v^{12} - 120b_v^{14})
                                                                          +b_{\nu}^{16})k_2+k_3+131072k_4-15728640b_{\nu}^2k_4+238551040b_{\nu}^4k_4-1049624576b_{\nu}^6k_4
             +1686896640b_{\nu}^{8}k_{4}-1049624576b_{\nu}^{10}k_{4}+238551040b_{\nu}^{12}k_{4}-15728640b_{\nu}^{14}k_{4}+131072b_{\nu}^{16}k_{4}+2k_{5}k_{5}+1686896640b_{\nu}^{14}k_{5}+1686896640b_{\nu}^{14}k_{5}+1686896640b_{\nu}^{14}k_{5}+1686896640b_{\nu}^{14}k_{5}+1686896640b_{\nu}^{14}k_{5}+1686896640b_{\nu}^{14}k_{5}+1686896640b_{\nu}^{14}k_{5}+1686896640b_{\nu}^{14}k_{5}+1686896640b_{\nu}^{14}k_{5}+1686896640b_{\nu}^{14}k_{5}+1686896640b_{\nu}^{14}k_{5}+1686896640b_{\nu}^{14}k_{5}+1686896640b_{\nu}^{14}k_{5}+1686896640b_{\nu}^{14}k_{5}+1686896640b_{\nu}^{14}k_{5}+1686896640b_{\nu}^{14}k_{5}+1686896640b_{\nu}^{14}k_{5}+1686896640b_{\nu}^{14}k_{5}+1686896640b_{\nu}^{14}k_{5}+1686896640b_{\nu}^{14}k_{5}+1686896640b_{\nu}^{14}k_{5}+1686896640b_{\nu}^{14}k_{5}+1686896640b_{\nu}^{14}k_{5}+1686896640b_{\nu}^{14}k_{5}+1686896640b_{\nu}^{14}k_{5}+1686896640b_{\nu}^{14}k_{5}+1686896640b_{\nu}^{14}k_{5}+1686896640b_{\nu}^{14}k_{5}+1686896640b_{\nu}^{14}k_{5}+1686896640b_{\nu}^{14}k_{5}+1686896640b_{\nu}^{14}k_{5}+1686896640b_{\nu}^{14}k_{5}+168686640b_{\nu}^{14}k_{5}+16868640b_{\nu}^{14}k_{5}+16868640b_{\nu}^{14}k_{5}+16868640b_{\nu}^{14}k_{5}+16868640b_{\nu}^{14}k_{5}+16868640b_{\nu}^{14}k_{5}+16868640b_{\nu}^{14}k_{5}+16868640b_{\nu}^{14}k_{5}+16868640b_{\nu}^{14}k_{5}+16868640b_{\nu}^{14}k_{5}+16868640b_{\nu}^{14}k_{5}+16868640b_{\nu}^{14}k_{5}+1686640b_{\nu}^{14}k_{5}+1686640b_{\nu}^{14}k_{5}+1686640b_{\nu}^{14}k_{5}+1686640b_{\nu}^{14}k_{5}+1686640b_{\nu}^{14}k_{5}+1686640b_{\nu}^{14}k_{5}+1686640b_{\nu}^{14}k_{5}+1686640b_{\nu}^{14}k_{5}+1686640b_{\nu}^{14}k_{5}+1686640b_{\nu}^{14}k_{5}+1686640b_{\nu}^{14}k_{5}+1686640b_{\nu}^{14}k_{5}+1686640b_{\nu}^{14}k_{5}+1686640b_{\nu}^{14}k_{5}+1686640b_{\nu}^{14}k_{5}+1686640b_{\nu}^{14}k_{5}+1686640b_{\nu}^{14}k_{5}+1686640b_{\nu}^{14}k_{5}+1686640b_{\nu}^{14}k_{5}+1686640b_{\nu}^{14}k_{5}+1686640b_{\nu}^{14}k_{5}+1686640b_{\nu}^{14}k_{5}+1686640b_{\nu}^{14}k_{5}+1686640b_{\nu}^{14}k_{5}+1686640b_{\nu}^{14}k_{5}+1686640b_{\nu}^{14}k_{5}+1686640b_{\nu}^{14}k_{5}+1686640b_{\nu}^{14}k_{5}+1686640b_{\nu}^{14}k_{5}+1686640b_{\nu}^{14}k_{5}+1686640b_{\nu}^{14}k_{5}+1686640b_{\nu}^{14}k_{5}+1686640b_{\nu}^{14}k_{5}+1686640b_{\nu}^{14}k_{5}+168664
                                     -960b_{\nu}^2k_5 + 58240b_{\nu}^4k_5 - 1025024b_{\nu}^6k_5 + 6589440b_{\nu}^8k_5 - 16400384b_{\nu}^{10}k_5 + 14909440b_{\nu}^{12}k_5
                    -3932160b_{y}^{14}k_{5}+131072b_{y}^{16}k_{5}+65536k_{6}+b_{y}^{16}k_{7}+131072k_{8}-3932160b_{y}^{2}k_{8}+14909440b_{y}^{4}k_{8}
                                                                                              -16400384b_{\nu}^{6}k_{8}+6589440b_{\nu}^{8}k_{8}-1025024b_{\nu}^{10}k_{8}+58240b_{\nu}^{12}k_{8}-960b_{\nu}^{14}k_{8}
                                                                                                                                                                                                                                                               +2b_{\nu}^{16}k_{8}+65536b_{\nu}^{16}k_{9}),
                                         b_{10} = (2(-1+153b_y^2-3060b_y^4+18564b_y^6-43758b_y^8+43758b_y^{10}-18564b_y^{12}+3060b_y^{14}+3060b_y^{14}+3060b_y^{14}+3060b_y^{14}+3060b_y^{14}+3060b_y^{14}+3060b_y^{14}+3060b_y^{14}+3060b_y^{14}+3060b_y^{14}+3060b_y^{14}+3060b_y^{14}+3060b_y^{14}+3060b_y^{14}+3060b_y^{14}+3060b_y^{14}+3060b_y^{14}+3060b_y^{14}+3060b_y^{14}+3060b_y^{14}+3060b_y^{14}+3060b_y^{14}+3060b_y^{14}+3060b_y^{14}+3060b_y^{14}+3060b_y^{14}+3060b_y^{14}+3060b_y^{14}+3060b_y^{14}+3060b_y^{14}+3060b_y^{14}+3060b_y^{14}+3060b_y^{14}+3060b_y^{14}+3060b_y^{14}+3060b_y^{14}+3060b_y^{14}+3060b_y^{14}+3060b_y^{14}+3060b_y^{14}+3060b_y^{14}+3060b_y^{14}+3060b_y^{14}+3060b_y^{14}+3060b_y^{14}+3060b_y^{14}+3060b_y^{14}+3060b_y^{14}+3060b_y^{14}+3060b_y^{14}+3060b_y^{14}+3060b_y^{14}+3060b_y^{14}+3060b_y^{14}+3060b_y^{14}+3060b_y^{14}+3060b_y^{14}+3060b_y^{14}+3060b_y^{14}+3060b_y^{14}+3060b_y^{14}+3060b_y^{14}+3060b_y^{14}+3060b_y^{14}+3060b_y^{14}+3060b_y^{14}+3060b_y^{14}+3060b_y^{14}+3060b_y^{14}+3060b_y^{14}+3060b_y^{14}+3060b_y^{14}+3060b_y^{14}+3060b_y^{14}+3060b_y^{14}+3060b_y^{14}+3060b_y^{14}+3060b_y^{14}+3060b_y^{14}+3060b_y^{14}+3060b_y^{14}+3060b_y^{14}+3060b_y^{14}+3060b_y^{14}+3060b_y^{14}+3060b_y^{14}+3060b_y^{14}+3060b_y^{14}+3060b_y^{14}+3060b_y^{14}+3060b_y^{14}+3060b_y^{14}+3060b_y^{14}+3060b_y^{14}+3060b_y^{14}+3060b_y^{14}+3060b_y^{14}+3060b_y^{14}+3060b_y^{14}+3060b_y^{14}+3060b_y^{14}+3060b_y^{14}+3060b_y^{14}+3060b_y^{14}+3060b_y^{14}+3060b_y^{14}+3060b_y^{14}+3060b_y^{14}+3060b_y^{14}+3060b_y^{14}+3060b_y^{14}+3060b_y^{14}+3060b_y^{14}+3060b_y^{14}+3060b_y^{14}+3060b_y^{14}+3060b_y^{14}+3060b_y^{14}+3060b_y^{14}+3060b_y^{14}+3060b_y^{14}+3060b_y^{14}+3060b_y^{14}+3060b_y^{14}+3060b_y^{14}+3060b_y^{14}+3060b_y^{14}+3060b_y^{14}+3060b_y^{14}+3060b_y^{14}+3060b_y^{14}+3060b_y^{14}+3060b_y^{14}+3060b_y^{14}+3060b_y^{14}+3060b_y^{14}+3060b_y^{14}+3060b_y^{14}+3060b_y^{14}+3060b_y^{14}+3060b_y^{14}+3060b_y^{14}+3060b_y^{14}+3060b_y^{14}+3060b_y^{14}+3060b_y^{14}+3060b_y^{14}+3060b_y^{14}+3060b_y^{14}+3060b_y^{14}+3060b_y^{1
                                    -153b_{v}^{16}+b_{v}^{18})k_{2}-k_{3}-524288k_{4}+80216064b_{v}^{2}k_{4}-1604321280b_{v}^{4}k_{4}+9732882432b_{v}^{6}k_{4}
     -22941794304b_{\nu}^{8}k_{4}+22941794304b_{\nu}^{10}k_{4}-9732882432b_{\nu}^{12}k_{4}+1604321280b_{\nu}^{14}k_{4}-80216064b_{\nu}^{16}k_{4}
              +524288b_{\nu}^{18}k_4-2k_5+1224b_{\nu}^2k_5-97920b_{\nu}^4k_5+2376192b_{\nu}^6k_5-22404096b_{\nu}^8k_5+89616384b_{\nu}^{10}k_5
```

$$-152076288b_{y}^{12}k_{5}+100270080b_{y}^{14}k_{5}-20054016b_{y}^{16}k_{5}+524288b_{y}^{18}k_{5}-262144k_{6}+b_{y}^{18}k_{7}\\ -524288k_{8}+20054016b_{y}^{2}k_{8}-100270080b_{y}^{4}k_{8}+152076288b_{y}^{6}k_{8}-89616384b_{y}^{8}k_{8}+22404096b_{y}^{10}k_{8}\\ -2376192b_{y}^{12}k_{8}+97920b_{y}^{14}k_{8}-1224b_{y}^{16}k_{8}+2b_{y}^{18}k_{8}+262144b_{y}^{18}k_{9})\,,\\ b_{11}=(2(1-190b_{y}^{2}+4845b_{y}^{4}-38760b_{y}^{6}+125970b_{y}^{8}-184756b_{y}^{10}+125970b_{y}^{12}-38760b_{y}^{14}\\ +4845b_{y}^{16}-190b_{y}^{18}+b_{y}^{20})k_{2}+k_{3}+2097152k_{4}-398458880b_{y}^{2}k_{4}+10160701440b_{y}^{4}k_{4}\\ -81285611520b_{y}^{6}k_{4}+264178237440b_{y}^{8}k_{4}-387461414912b_{y}^{10}k_{4}+264178237440b_{y}^{12}k_{4}\\ -81285611520b_{y}^{14}k_{4}+10160701440b_{y}^{16}k_{4}-398458880b_{y}^{18}k_{4}+2097152b_{y}^{20}k_{4}+2k_{5}-1520b_{y}^{2}k_{5}\\ +155040b_{y}^{4}k_{5}-4961280b_{y}^{6}k_{5}+64496640b_{y}^{8}k_{5}-378380288b_{y}^{10}k_{5}+1031946240b_{y}^{12}k_{5}\\ -1270087680b_{y}^{14}k_{5}+635043840b_{y}^{16}k_{5}-99614720b_{y}^{18}k_{5}+2097152b_{y}^{20}k_{5}+1048576k_{6}\\ +b_{y}^{20}k_{7}+2097152k_{8}-99614720b_{y}^{2}k_{8}+635043840b_{y}^{16}k_{5}-1270087680b_{y}^{6}k_{8}+1031946240b_{y}^{8}k_{8}\\ -378380288b_{y}^{10}k_{8}+64496640b_{y}^{12}k_{8}-4961280b_{y}^{14}k_{8}+155040b_{y}^{16}k_{8}-1520b_{y}^{18}k_{8}\\ +2b_{y}^{20}k_{8}+1048576b_{y}^{20}k_{9})\,. \tag{E.1}$$

# Appendix F. The coefficients $f_i$ in Eqs. (27) for the new Q 9\_0 PT\_1 stencils

$$\begin{split} f_1 &= \frac{1}{36y_1} [7(13993904b_y^{16} + 165087200b_y^{14} - 1044338491b_y^{12} - 56494700b_y^{10} + 6943474174b_y^8 \\ &-56494700b_y^6 - 1044338491b_y^4 + 165087200b_y^2 + 13993904)a_1 + 9y_1(8a_2 + 2(a_3 + a_4) - a_6)], \\ &f_2 &= \frac{1}{12y_1} [(58288976b_y^{16} - 481727600b_y^{14} + 1456399991b_y^{12} - 1756955850b_y^{10} \\ &+ 1159844496b_y^8 - 441576750b_y^6 + 83309881b_y^4 - 4919800b_y^2 + 176656)a_1 - 6a_4y_1], \\ &f_3 &= \frac{(b_y^2 + 1)^2(b_y^2 + 4)(4b_y^2 + 1)a_1}{36y_1} [44164b_y^8 - 234075b_y^6 + 379522b_y^4 - 234075b_y^2 + 44164], \\ &f_4 &= \frac{1}{12y_1} [(176656b_y^{16} - 4919800b_y^{14} + 83309881b_y^{12} - 441576750b_y^{10} + 1159844496b_y^8 \\ &- 1756955850b_y^6 + 1456399991b_y^4 - 481727600b_y^2 + 58288976)a_1 - 6a_3y_1], \\ &f_5 &= -\frac{2(b_y^2 + 1)(b_y^2 + 4)a_1}{3y_1} [14572244b_y^{12} - 105226995b_y^{10} + 247191783b_y^8 - 129893985b_y^6 \\ &+ 30238377b_y^4 - 4502520b_y^2 + 598096] - \frac{a_5}{2}, \\ &f_6 &= -\frac{2(b_y^2 + 1)(4b_y^2 + 1)a_1}{9y_1} [598096b_y^{12} - 4480120b_y^{10} + 12056297b_y^8 \\ &- 12208585b_y^6 + 5767943b_y^4 - 1132795b_y^2 + 44164], \\ &f_7 &= -\frac{2(b_y^2 + 1)(b_y^2 + 4)a_1}{9y_1} [44164b_y^1 - 1132795b_y^{10} + 5767943b_y^8 - 12208585b_y^6 \\ &+ 12056297b_y^4 - 4480120b_y^2 + 598096], \\ &f_8 &= \frac{8(4b_y^2 + 1)}{36y_1} [598096b_y^{14} - 3882024b_y^{12} - 73487183b_y^{10} + 526759552b_y^8 - 1006418222b_y^6 \\ &- 33540332b_y^4 + 173697309b_y^2 - 34147196)a_1 - 9y_1(4a_2 - 2a_5 - a_6)], \\ &f_9 &= \frac{8(b_y^2 + 4)(4b_y^2 + 1)a_1}{9y_1} [598096b_y^{12} - 6291208b_y^{10} + 26094929b_y^8 - 47431534b_y^6 \\ &+ 26094929b_y^4 - 6291208b_y^2 + 598096] - a_2, \\ &f_{10} &= \frac{32(b_y^2 + 4)}{18y_1} [13332608b_y^{14} - 92829957b_y^{12} + 205720886b_y^{10} - 77268019b_y^8 - 17831596b_y^6 \\ \end{cases}$$

$$+22126034b_{y}^{4} - 7797648b_{y}^{2} + 1196192)a_{1} - 9y_{1}(8a_{2} + 2a_{3} - 4a_{5} - a_{6})],$$

$$f_{11} = a_{2}, \qquad f_{12} = a_{3},$$

$$f_{13} = \frac{1}{18y_{1}}[9y_{1}(4a_{2} - 2a_{5} - a_{6}) - 32(b_{y}^{2} + 4)(4b_{y}^{2} + 1)(598096b_{y}^{12} - 6291208b_{y}^{10} + 26094929b_{y}^{8} - 47431534b_{y}^{6} + 26094929b_{y}^{4} - 6291208b_{y}^{2} + 598096)a_{1}],$$

$$f_{14} = \frac{1}{2y_{1}}[1120(4b_{y}^{2} + 1)(64336b_{y}^{10} - 418184b_{y}^{8} + 793633b_{y}^{6} + 30298b_{y}^{4} - 138719b_{y}^{2} + 27136)a_{1} - y_{1}(2a_{4} + 4a_{5} + a_{6}],$$

$$f_{15} = a_{4}, \qquad f_{16} = a_{5}, \qquad f_{17} = a_{6}$$
(F.2)

with  $y_1$  defined by Eq. (41).  $a_j$  (j = 1, 2, ..., 6) are six arbitrary coefficients.

### Appendix G. The coefficients $f_i$ in Eqs. (27) for the new Q 9\_0 PT\_2 stencils

$$\begin{split} f_1 &= \frac{1}{36y_3} [7(401399984b_y^{20} + 2972658592b_y^{18} - 41060434627b_y^{16} + 84142306982b_y^{14} + 175854264643b_y^{12} \\ & - 478641391148b_y^{10} + 175854264643b_y^{8} + 84142306982b_y^{6} - 41060434627b_y^{4} \\ & + 2972658592b_y^{2} + 401399984b_{11} + 9y_3(8a_2 + 2(a_3 + a_4) - a_6)], \\ f_2 &= \frac{1}{12} (\frac{1}{y_3} [(1521978576b_y^{20} - 17351608272b_y^{18} + 76872755327b_y^{16} - 164715787152b_y^{14} \\ & + 193939316847b_y^{12} - 137578948912b_y^{10} + 60627164237b_y^{8} - 15793920632b_y^{6} \\ & + 2089789797b_y^{4} - 107855032b_y^{2} + 3115216)a_{1}] - 6a_4), \\ f_3 &= \frac{1}{36y_3} [(b_y^{2} + 1)^{2}(b_y^{2} + 4)(4b_y^{2} + 1)(778804b_y^{12} - 6705623b_y^{10} + 20440296b_y^{8} \\ & - 29052954b_y^{6} + 20440296b_y^{4} - 6705623b_y^{2} + 778804)a_{1}], \\ f_4 &= \frac{1}{12} (\frac{1}{y_3} [(3115216b_y^{20} - 107855032b_y^{18} + 2089789797b_y^{16} - 15793920632b_y^{14} + 60627164237b_y^{12} \\ & - 137578948912b_y^{10} + 193939316847b_y^{8} - 164715787152b_y^{6} + 76872755327b_y^{4} \\ & - 17351608272b_y^{2} + 1521978576)a_{1}] - 6a_3), \\ f_5 &= -\frac{1}{3y_3} [2(b_y^{2} + 1)(b_y^{2} + 4)(380494644b_y^{16} - 3950564583b_y^{14} + 15033132452b_y^{12} - 24170522596b_y^{10} \\ & + 17293159050b_y^{8} - 5959344309b_y^{6} + 1165078718b_y^{4} - 158704512b_y^{2} + 13671136)a_{1}] - \frac{a_5}{2}, \\ f_6 &= -\frac{2(b_y^{2} + 1)(4b_y^{2} + 1)}{9y_3} a_{1} [13671136b_y^{16} - 146695872b_y^{14} + 602568798b_y^{12} - 1172018969b_y^{10} \\ & + 1186108650b_y^{8} - 654628796b_y^{6} + 190632612b_y^{4} - 24576363b_y^{2} + 778804], \\ f_7 &= -\frac{2(b_y^{2} + 1)(b_y^{2} + 4)}{9y_3} a_{1} [778804b_y^{16} - 24576363b_y^{14} + 190632612b_y^{12} - 654628796b_y^{10} \\ & + 1186108650b_y^{8} - 1172018969b_y^{6} + 602568798b_y^{4} - 146695872b_y^{2} + 13671136], \\ f_8 &= \frac{1}{36y_3} [8(4b_y^{2} + 1)(13671136b_y^{18} - 133024736b_y^{16} - 1610446434b_y^{14} + 19467493189b_y^{12} \\ & - 67752177839b_y^{10} + 82726410574b_y^{8} - 20590969064b_y^{6} - 15810053271b_y^{4} \\ & + 7617442201b_y^{2} - 922745756)a_1 - 9y_3(4a_2 - 2a_5 - a_6)], \\ f_9 &= \frac{1}{9y_3} [16(b_y$$

$$f_{10} = \frac{1}{18y_3} [128(b_y^2 + 4)(85062557b_y^{18} - 864173437b_y^{16} + 3178213137b_y^{14} - 4742456632b_y^{12} + 2624606822b_y^{10} + 16550018b_y^8 - 616721908b_y^6 + 305229483b_y^4 - 71015608b_y^2 + 6835568)a_1 - 9y_3(8a_2 + 2a_3 - 4a_5 - a_6)],$$

$$f_{11} = a_2, \qquad f_{12} = a_3,$$

$$f_{13} = \frac{1}{18y_3} [9y_3(4a_2 - 2a_5 - a_6) - 64(b_y^2 + 4)(4b_y^2 + 1)(6835568b_y^{16} - 98357880b_y^{14} + 569516043b_y^{12} - 1642477120b_y^{10} + 2351066778b_y^8 - 1642477120b_y^6 + 569516043b_y^4 - 98357880b_y^2 + 6835568)a_1],$$

$$f_{14} = \frac{1}{2y_3} [4480(4b_y^2 + 1)(409984b_y^{14} - 3975584b_y^{12} + 13445688b_y^{10} - 16308518b_y^8 + 3993447b_y^6 + 3169863b_y^4 - 1516119b_y^2 + 183239)a_1 - y_3(2a_4 + 4a_5 + a_6)],$$

$$f_{15} = a_4, \qquad f_{16} = a_5, \qquad f_{17} = a_6$$
(G.1)

with  $y_3$  defined by Eq. (47).  $a_i$  (j = 1, 2, ..., 6) are six arbitrary coefficients.

#### Appendix H. Supplementary material

Supplementary material related to this article can be found online at https://doi.org/10.1016/j.jcp.2020.109640.

#### References

- [1] S. Ji, Y. Yang, G. Pang, X. Antoine, Accurate artificial boundary conditions for the semi-discretized linear Schrodinger and heat equations on rectangular domains, Comput. Phys. Commun. 222 (2018) 84–93.
- [2] S.-ichi Satake, H. Yoshimori, T. Suzuki, Optimizations of a GPU accelerated heat conduction equation by a programming of CUDA Fortran from an analysis of a PTX file, Comput. Phys. Commun. 183 (11) (2012) 2376–2385.
- [3] M. Held, M. Wiesenberger, A. Stegmeir, Three discontinuous Galerkin schemes for the anisotropic heat conduction equation on non-aligned grids, Comput. Phys. Commun. 199 (2016) 29–39.
- [4] S. Lin, J. Smith, W.K. Liu, G.J. Wagner, An energetically consistent concurrent multiscale method for heterogeneous heat transfer and phase transition applications, Comput. Methods Appl. Mech. Eng. 315 (2017) 100–120.
- [5] B. Szabo, I. Babuska, Introduction to Finite Element Analysis: Formulation, Verification and Validation, John Wiley and Sons, Ltd, 2011.
- [6] T.J.R. Hughes, The Finite Element Method: Linear Static and Dynamic Finite Element Analysis, Prentice-Hall, Englewood Cliffs, NJ, 1987.
- [7] K.J. Bathe, Finite Element Procedures, Prentice-Hall Inc., Upper Saddle River, New Jersey, 1996.
- [8] S. Krenk, Dispersion-corrected explicit integration of the wave equation, Comput. Methods Appl. Mech. Eng. 191 (2001) 975–987.
- [9] K.J. Marfurt, Accuracy of finite difference and finite element modeling of the scalar and elastic wave equation, Geophysics 49 (1984) 533-549.
- [10] R. Mullen, T. Belytschko, Dispersion analysis of finite element semidiscretizations of the two-dimensional wave equation, Int. J. Numer. Methods Eng. 18 (1982) 11–29.
- [11] G. Seriani, S.P. Oliveira, Optimal blended spectral-element operators for acoustic wave modeling, Geophysics 72 (5) (2007) 95-106.
- [12] B. Yue, M.N. Guddati, Dispersion-reducing finite elements for transient acoustics, J. Acoust. Soc. Am. 118 (4) (2005) 2132-2141.
- [13] V. Gyrya, K. Lipnikov, M-adaptation method for acoustic wave equation on square meshes, J. Comput. Acoust. 20 (2012) 1250022.
- [14] V. Bokil, N. Gibson, V. Gyrya, D. McGregor, Dispersion reducing methods for edge discretizations of the electric vector wave equation, J. Comput. Phys. 287 (2015) 88–109.
- [15] A. Tkachuk, M. Bischoff, Direct and sparse construction of consistent inverse mass matrices: general variational formulation and application to selective mass scaling, Int. J. Numer. Methods Eng. 101 (6) (2015) 435–469.
- [16] M. Ainsworth, H.A. Wajid, Optimally blended spectral-finite element scheme for wave propagation and nonstandard reduced integration, SIAM J. Numer. Anal. 48 (1) (2010) 346–371.
- [17] D. Wang, W. Liu, H. Zhang, Novel higher order mass matrices for isogeometric structural vibration analysis, Comput. Methods Appl. Mech. Eng. 260 (2013) 92–108.
- [18] D. Wang, W. Liu, H. Zhang, Superconvergent isogeometric free vibration analysis of Euler-Bernoulli beams and Kirchhoff plates with new higher order mass matrices, Comput. Methods Appl. Mech. Eng. 286 (2015) 230–267.
- [19] D. Wang, Q. Liang, J. Wu, A quadrature-based superconvergent isogeometric frequency analysis with macro-integration cells and quadratic splines, Comput. Methods Appl. Mech. Eng. 320 (2017) 712–744.
- [20] V. Puzyrev, Q. Deng, V. Calo, Dispersion-optimized quadrature rules for isogeometric analysis: modified inner products, their dispersion properties, and optimally blended schemes, Comput. Methods Appl. Mech. Eng. 320 (2017) 421–443.
- [21] V. Puzyrev, Q. Deng, V. Calo, Spectral approximation properties of isogeometric analysis with variable continuity, Comput. Methods Appl. Mech. Eng. 334 (2018) 22–39.
- [22] V. Calo, Q. Deng, V. Puzyrev, Dispersion optimized quadratures for isogeometric analysis, J. Comput. Appl. Math. 355 (2019) 283-300.
- [23] A.V. Idesman, Optimal reduction of numerical dispersion for wave propagation problems. Part 1: application to 1-d isogeometric elements, Comput. Methods Appl. Mech. Eng. 317 (2017) 970–992.
- [24] A. Idesman, B. Dey, Optimal reduction of numerical dispersion for wave propagation problems. Part 2: application to 2-d isogeometric elements, Comput. Methods Appl. Mech. Eng. 321 (2017) 235–268.
- [25] A. Idesman, B. Dey, The use of the local truncation error for the increase in accuracy of the linear finite elements for heat transfer problems, Comput. Methods Appl. Mech. Eng. 319 (2017) 52–82.
- [26] A. Idesman, The use of the local truncation error to improve arbitrary-order finite elements for the linear wave and heat equations, Comput. Methods Appl. Mech. Eng. 334 (2018) 268–312.

- [27] T. Hughes, A. Reali, G. Sangalli, Duality and unified analysis of discrete approximations in structural dynamics and wave propagation: comparison of p-method finite elements with k-method NURBS, Comput. Methods Appl. Mech. Eng. 197 (49–50) (2008) 4104–4124.
- [28] C. Pozrikidis, Introduction to Finite and Spectral Element Methods Using MATLAB, CRC Press, 2005.
- [29] O.C. Zienkiewicz, R.L. Taylor, The Finite Element Method, Butterworth-Heinemann, Oxford, UK, 2000.
- [30] J. Cottrell, A. Reali, Y. Bazilevs, T. Hughes, Isogeometric analysis of structural vibrations, Comput. Methods Appl. Mech. Eng. 195 (41–43) (2006) 5257–5296.
- [31] T. Rylander, A. Bondeson, Stable fem-fdtd hybrid method for Maxwell's equations, Comput. Phys. Commun. 125 (1) (2000) 75-82.
- [32] A. Monorchio, A.R. Bretones, R. Mittra, G. Manara, R.G. Martin, A hybrid time-domain technique that combines the finite element, finite difference and method of moment techniques to solve complex electromagnetic problems, IEEE Trans. Antennas Propag. 52 (10) (2004) 2666–2674.
- [33] K.-J. Bathe, L. Zhang, The finite element method with overlapping elements a new paradigm for cad driven simulations, Comput. Struct. 182 (2017) 526–539.
- [34] J. Huang, K.-J. Bathe, Quadrilateral overlapping elements and their use in the AMORE paradigm, Comput. Struct. 222 (2019) 25-35.
- [35] V. Arias, D. Bochkov, F. Gibou, Poisson equations in irregular domains with Robin boundary conditions solver with second-order accurate gradients, J. Comput. Phys. 365 (2018) 1–6.
- [36] S. Britt, S. Tsynkov, E. Turkel, Numerical solution of the wave equation with variable wave speed on nonconforming domains by high-order difference potentials, J. Comput. Phys. 354 (2018) 26–42.
- [37] K. Singh, J. Williams, A parallel fictitious domain multigrid preconditioner for the solution of Poisson's equation in complex geometries, Comput. Methods Appl. Mech. Eng. 194 (45–47) (2005) 4845–4860.
- [38] P. Vos, R. van Loon, S. Sherwin, A comparison of fictitious domain methods appropriate for spectral/hp element discretisations, Comput. Methods Appl. Mech. Eng. 197 (25–28) (2008) 2275–2289.
- [39] E. Burman, P. Hansbo, Fictitious domain finite element methods using cut elements: I. A stabilized Lagrange multiplier method, Comput. Methods Appl. Mech. Eng. 199 (41–44) (2010) 2680–2686.
- [40] E. Rank, S. Kollmannsberger, C. Sorger, A. Duster, Shell finite cell method: a high order fictitious domain approach for thin-walled structures, Comput. Methods Appl. Mech. Eng. 200 (45–46) (2011) 3200–3209.
- [41] T. Hoang, C.V. Verhoosel, F. Auricchio, E.H. van Brummelen, A. Reali, Mixed isogeometric finite cell methods for the Stokes problem, Comput. Methods Appl. Mech. Eng. 316 (2017) 400–423.
- [42] S. May, M. Berger, An explicit implicit scheme for cut cells in embedded boundary meshes, J. Sci. Comput. 71 (3) (2017) 919-943.
- [43] S. Krenk, State-space time integration with energy control and fourth-order accuracy for linear dynamic systems, Int. J. Numer. Methods Eng. 65 (5) (2006) 595–619.
- [44] Z. Jomaa, C. Macaskill, The embedded finite difference method for the Poisson equation in a domain with an irregular boundary and Dirichlet boundary conditions, J. Comput. Phys. 202 (2) (2005) 488–506.
- [45] J.L. Hellrung Jr., L. Wang, E. Sifakis, J.M. Teran, A second order virtual node method for elliptic problems with interfaces and irregular domains in three dimensions, J. Comput. Phys. 231 (4) (2012) 2015–2048.
- [46] J. Bedrossian, J.H. von Brecht, S. Zhu, E. Sifakis, J.M. Teran, A second order virtual node method for elliptic problems with interfaces and irregular domains, J. Comput. Phys. 229 (18) (2010) 6405–6426.
- [47] A. Idesman, B. Dey, A 3-D new numerical approach to the solution of PDEs with optimal accuracy on irregular domains and Cartesian meshes, Comput. Methods Appl. Mech. Eng. 354 (2019) 568–592.
- [48] A. Idesman, B. Dey, The treatment of the Neumann boundary conditions for a new numerical approach to the solution of PDEs with optimal accuracy on irregular domains and Cartesian meshes, Comput. Methods Appl. Mech. Eng. 365 (2020) 112985.
- [49] A. Idesman, B. Dey, A new numerical approach to the solution of the 2-D Helmholtz equation with optimal accuracy on irregular domains and Cartesian meshes, Comput. Mech. 65 (2020) 1189–1204.